



**A MODEL TO PREDICT DIFFRACTION ATTENUATION  
RESULTING FROM SIGNAL PROPAGATION OVER TERRAIN IN  
LOW EARTH ORBIT SATELLITE SYSTEMS**

**THESIS**

**20010706 167**

**Peter Pollock, Squadron Leader, RAAF**

**AFIT/GSO/ENG/01M-01**

**DEPARTMENT OF THE AIR FORCE  
AIR UNIVERSITY**

**AIR FORCE INSTITUTE OF TECHNOLOGY**

---

---

**Wright-Patterson Air Force Base, Ohio**

**APPROVED FOR PUBLIC RELEASE; DISTRIBUTION UNLIMITED**

AFIT/GSO/ENG/01M-01

A Model to Predict Diffraction Attenuation Resulting From  
Signal Propagation Over Terrain in Low Earth Orbit Satellite Systems

THESIS

Peter R. Pollock

Squadron Leader, Royal Australian Air Force

AFIT/GSO/ENG/01M-01

Approved for public release; distribution unlimited

The views expressed in this document are those of the author and do not reflect the official policy or position of the U.S. Department of Defense or the U.S. Government, or the Government of the Commonwealth of Australia.

AFIT/GSO/ENG/01M-01

**A Model to Predict Diffraction Attenuation Resulting From  
Signal Propagation Over Terrain in Low Earth Orbit Satellite Systems**

**THESIS**

**Presented to the faculty of the Graduate School of Engineering**

**Of the Air Force Institute of Technology**

**Air University**

**Air Education and Training Command**

**In Partial Fulfillment of the Requirements for the**

**Degree of Master of Science in Space Operations**

**Peter R. Pollock**

**Squadron Leader, Royal Australian Air Force**

**March, 2001**

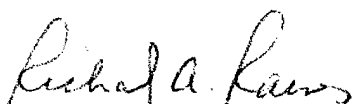
**Approved for public release; distribution unlimited**

A Model to Predict Diffraction Attenuation Resulting From  
Signal Propagation Over Terrain in Low Earth Orbit Satellite Systems

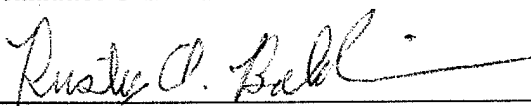
Peter R. Pollock, Master of Science in Space Operations

Squadron Leader, Royal Australian Air Force

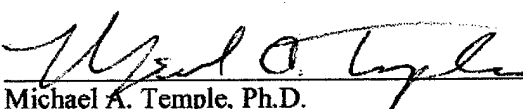
Approved:

  
Richard A. Raines, Ph.D., Major, USAF  
Committee Chairman

1 Mar 01  
date

  
Rusty O. Baldwin, Ph.D., Major, USAF  
Committee Member

1 Mar 01  
date

  
Michael A. Temple, Ph.D.  
Committee Member

1 Mar 01  
date

## ACKNOWLEDGEMENTS

I would like to express my sincere appreciation to my thesis advisor, Major Richard Raines for his support and encouragement over the course of my studies. After supervising two Australian students over the past three years he has developed a fine understanding of the Australian psyche and language and has been very patient with the constant spelling conversions. I would also like to thank my committee members, Major Rusty Baldwin and Dr. Michael Temple, for their guidance and advice. I have relied heavily upon the support provided by each of the committee members. I would also like to acknowledge the contribution made to my work by Major Kelce Wilson, who provided the terrain data and interpolation files referenced throughout this thesis.

I am very grateful to the Royal Australian Air Force for giving me the opportunity to study at AFIT and experience, for twenty months, American life and culture. While studying has been a privilege for me, my fondest memories will be of the people, social events and places. I must extend a special thank you to . and . in the International Students Office for their untiring efforts in support of the international families.

To my wife, , and children, , I can only say 'thanks, I love you, and pleased to meet you, again'.

# TABLE OF CONTENTS

<b>ACKNOWLEDGEMENTS</b>	<b>V</b>
<b>TABLE OF CONTENTS</b>	<b>VI</b>
<b>LIST OF FIGURES</b>	<b>IX</b>
<b>LIST OF TABLES</b>	<b>XI</b>
<b>ABSTRACT</b>	<b>XII</b>
<b>CHAPTER 1 INTRODUCTION</b>	<b>1</b>
1.1 RESEARCH OBJECTIVES	2
1.2 MOTIVATION	2
1.3 SUMMARY	4
<b>CHAPTER 2 BACKGROUND AND LITERATURE REVIEW</b>	<b>5</b>
2.1 INTRODUCTION	5
2.2 INTRODUCTION TO MULTIPATH COMMUNICATIONS	6
2.3 MULTIPATH PROPAGATION MECHANISMS	6
2.3.1 Refraction	6
2.3.2 Reflection	6
2.3.3 Diffraction	7
2.4 PRIMARY CAUSES OF MULTIPATH COMMUNICATIONS	9
2.4.1 Scintillation	9
2.4.2 Elevation Angle	10
2.4.3 Antenna Design	10
2.4.4 Frequency	11
2.5 CHARACTERIZING THE EFFECTS OF MULTIPATH COMMUNICATIONS	11
2.5.1 Amplitude and Phase	11
2.5.2 Depolarization	12
2.5.3 Bandwidth.	13
2.5.4 Angle-of-arrival	13
2.6 MODELING TERRAIN DIFFRACTION USING GEOMETRIC THEORY OF DIFFRACTION	14
2.6.1 Diffraction Over Terrain Modeled as Knife Edges	14
2.6.1.1 The Effect of Multiple Diffraction Points.	16
2.6.1.2 Real Terrain Diffraction Model	16
2.6.2 Diffraction Over Terrain Modeled as Rounded Obstacles	17
2.7 MODELING TERRAIN DIFFRACTION USING PROBABILITY DISTRIBUTION MODELS	19
2.7.1 Rayleigh Distribution	20
2.7.2 Ricean Distribution	21
2.7.3 Nakagami Distribution	22
2.8 MODELING TERRAIN DIFFRACTION USING EMPIRICAL REGRESSION MODELS	23
2.9 REPRESENTATIVE SATELLITE CONSTELLATIONS	24
2.9.1 Iridium	24
2.9.1.1 Operational Overview	24
2.9.1.2 The Constellation	25
2.9.1.3 Footprint	25
2.9.1.4 In-View Times and Orbital Period	26
2.9.1.5 Links to Users	27

2.9.2 Globalstar	27
2.9.2.1 The Constellation	27
2.9.2.2 In-View Times and Orbital Period	28
2.9.2.3 Links to Users	28
2.9.3 Orbcomm	29
2.9.3.1 The Constellation and Ground Segment	29
2.9.3.2 In-View Times and Orbital Period	30
2.9.3.3 Links to Users	30
2.10 THE TERRAIN DATA SOURCES	31
2.11 REVIEW OF RELEVANT LITERATURE	33
<b>CHAPTER 3 ANALYSIS AND MODELING METHODOLOGIES</b>	<b>34</b>
3.1 INTRODUCTION	34
3.2 REQUIRED OUTPUTS	34
3.3 METHOD OF ANALYSIS	35
3.4 OVERVIEW OF THE PROCESS	36
3.5 MODEL PARAMETERS AND ASSUMPTIONS	37
3.5.1 The Notional Terrain	37
3.5.1.1 The 100 Meter Data Set	38
3.5.1.2 The Condensed Data Set	39
3.5.1.3 Approximating the Curvature of the Dominant Feature	41
3.5.2 The User Sites	43
3.5.3 The Constellations	43
3.5.4 Period of Simulation	44
3.5.5 The Sampling Interval	45
3.6 ESTABLISHING THE BASELINE	46
3.6.1 Generating the Initial SOAP Observation Reports	47
3.6.1.1 The Samples Report	47
3.6.1.2 The Observations Report	48
3.6.1.3 Analyzing the Observations	48
3.7 MODELING TERRAIN DIFFRACTION EFFECTS WITH KNIFE-EDGE OBSTACLES	49
3.8 MODELING TERRAIN DIFFRACTION EFFECTS WITH ROUNDED OBSTACLES	51
3.9 VERIFICATION AND VALIDATION	53
3.10 SUMMARY	54
<b>CHAPTER 4 ANALYSIS AND PRESENTATION OF RESULTS</b>	<b>55</b>
4.1 INTRODUCTION	55
4.2 THE NEED FOR DEFINED PERFORMANCE MEASURES AND SIMULATIONS	56
4.2.1 Required Inputs to the Simulations	56
4.2.2 Performance Measures	57
4.2.3 Iridium	57
4.2.3.1 Theoretical Performance Analysis	57
4.2.3.2 Ideal Terrain Environment Simulation Performance Analysis	58
4.2.3.3 Predictions Drawn From the Observation Data	59
4.2.4 Globalstar	60
4.2.4.1 Theoretical Performance Analysis	60
4.2.4.2 Ideal Terrain Environment Simulation Performance Analysis	61
4.2.4.3 Predictions Drawn From the Observation Data	62
4.2.5 Orbcomm	64
4.2.5.1 Theoretical Performance Analysis	64



4.2.5.2 Ideal Terrain Environment Simulation Performance Analysis	66
4.2.5.3 Predictions Drawn From the Observation Data	67
4.3 THE NOTIONAL TERRAIN PROFILE APPLIED IN THE SIMULATIONS	69
4.4 CHARACTERIZING THE TRANSMISSION PATHS OVER THE NOTIONAL TERRAIN	70
4.4.1 Iridium	70
4.4.2 Globalstar	72
4.4.3 Orbcomm	75
4.5 CHARACTERIZING THE INFLUENCE OF THE NOTIONAL TERRAIN ON THE RESULTS	76
4.6 SUMMARY	82
<b>CHAPTER 5 SUMMARY AND CONCLUSIONS</b>	<b>83</b>
5.1 SUMMARY	83
5.1.1 Ideal Terrain Environment Performance	84
5.1.2 Notional Terrain Environment Performance	85
5.1.3 The Significance of the Notional Terrain Landscape	86
5.2 CONCLUSIONS	87
5.3 RECOMMENDATIONS	88
<b>APPENDIX A: MATLAB PROGRAM LISTINGS</b>	<b>89</b>
<b>BIBLIOGRAPHY</b>	<b>111</b>
<b>VITA</b>	<b>113</b>

## LIST OF FIGURES

FIGURE 2-1: LIT DIFFRACTION CALCULATION GEOMETRY	15
FIGURE 2-2: ATTENUATION DUE TO KNIFE-EDGE DIFFRACTION AS A FUNCTION OF $N^{1/2}$ (WHERE $N^{1/2} = H_c/F_1$ ) [Flo87]	16
FIGURE 2-3: ATTENUATION DUE TO ROUNDED OBSTACLE DIFFRACTION AS A FUNCTION OF $H/F_1$ OR $H/R$ [Flo87]	18
FIGURE 2-4: RAYLEIGH PROBABILITY DENSITY FUNCTION [Rap96]	20
FIGURE 2-5: RICEAN PROBABILITY DENSITY FUNCTIONS [Rap96]	21
FIGURE 2-6: NAKAGAMI PROBABILITY DENSITY FUNCTION [Pro95]	23
FIGURE 2-7: THE IRIDIUM SATELLITE ORBITS [Llo00]	26
FIGURE 2-8: THE GLOBALSTAR SATELLITE ORBITS [Llo00]	28
FIGURE 2-9: THE ORBCOMM SATELLITE ORBITS [Llo00]	30
FIGURE 2-10: EXAMPLE TERRAIN MESH AND TERRAIN IMAGE PLOTS PRODUCED FROM THE NIMA DATA [Jan97]	32
FIGURE 3-1: ANALYSIS PROCESS FLOWCHART	36
FIGURE 3-2: THE NOTIONAL TERRAIN SURFACE	38
FIGURE 3-3: THE NOTIONAL TERRAIN CONTOUR PROFILE	39
FIGURE 3-4: RELEVANCE OF GRID DIMENSIONS TO AZIMUTHAL RESOLUTION	40
FIGURE 3-5: CURVATURE CONSIDERATIONS WITH A FINE TERRAIN GRID	42
FIGURE 3-6: CURVATURE CONSIDERATIONS WITH A COARSE TERRAIN GRID	42
FIGURE 3-7: THE PROCESS USED TO ESTABLISH THE BASELINE	46
FIGURE 3-8: THE PROCESS USED TO MODEL TERRAIN AS KNIFE-EDGE OBSTACLES	49
FIGURE 3-9: SATELLITE OBSERVATION CATEGORIZATION REGIONS APPLIED IN THE MODEL	50
FIGURE 3-10: THE PROCESS USED TO MODEL TERRAIN AS ROUNDED OBSTACLES	52
FIGURE 4-1: THE IRIDIUM ORBITS (INSTANTANEOUS VIEW)	57
FIGURE 4-2: IRIDIUM SATELLITE OBSERVATIONS MADE OVER THE TWO-DAY SIMULATION PERIOD	59
FIGURE 4-3: PDFS OF IRIDIUM ELEVATION ANGLES (EQUATOR TO 60 DEGREES LATITUDE) [Cro99]	60
FIGURE 4-4: THE GLOBALSTAR ORBITS (INSTANTANEOUS VIEW)	61
FIGURE 4-5: GLOBALSTAR SATELLITE OBSERVATIONS MADE OVER THE TWO-DAY SIMULATION PERIOD	63
FIGURE 4-6: PDF OF GLOBALSTAR PATH ELEVATION ANGLES [Cro99]	63
FIGURE 4-7: ORBCOMM SATELLITE SPACING	64
FIGURE 4-8: THE ORBCOMM ORBITS (INSTANTANEOUS VIEW)	65
FIGURE 4-9: ORBCOMM SATELLITE OBSERVATIONS MADE OVER THE TWO-DAY SIMULATION PERIOD	68
FIGURE 4-10: SIGNIFICANT TERRAIN FEATURE ELEVATIONS PROFILE	69
FIGURE 4-11: A COMPARISON OF THE GLOBALSTAR AND IRIDIUM SATELLITE OBSERVATIONS MADE AT ANCHORAGE	74
FIGURE 4-12: ATTENUATION PREDICTIONS FOR USERS OF IRIDIUM AT PANAMA	77
FIGURE 4-13: ATTENUATION PREDICTIONS FOR USERS OF GLOBALSTAR AT PANAMA	77

FIGURE 4-14: ATTENUATION PREDICTIONS FOR USERS OF ORBCOMM AT PANAMA	78
FIGURE 4-15: VIEW OF THE SOUTHWEST CORNER OF THE NOTIONAL TERRAIN SURFACE	80
FIGURE 4-16: DISTRIBUTION OF DOMINANT FEATURE PEAK CURVATURE VALUES	81

## LIST OF TABLES

TABLE 3-1: COMMUNICATIONS PARAMETERS FOR THE THREE CONSTELLATIONS	44
TABLE 3-2: THE SAMPLES REPORT FORMAT	47
TABLE 3-3: THE OBSERVATIONS REPORT FORMAT	48
TABLE 4-1: IDEAL ENVIRONMENT SIMULATION RESULTS FOR THE IRIIDIUM CONSTELLATION	58
TABLE 4-2: IDEAL ENVIRONMENT SIMULATION RESULTS FOR THE GLOBALSTAR CONSTELLATION	61
TABLE 4-3: IDEAL ENVIRONMENT SIMULATION RESULTS FOR THE ORBCOMM CONSTELLATION	66
TABLE 4-4: IRIIDIUM CONSTELLATION PERFORMANCE IN A TERRAIN DIFFRACTION ENVIRONMENT	71
TABLE 4-5: GLOBALSTAR CONSTELLATION PERFORMANCE IN A TERRAIN DIFFRACTION ENVIRONMENT	72
TABLE 4-6: ORBCOMM CONSTELLATION PERFORMANCE IN A TERRAIN DIFFRACTION ENVIRONMENT	75
TABLE 4-7: A SUMMARY OF THE ATTENUATION DISTRIBUTIONS	78
TABLE 4-8: AVAILABILITY REDUCTIONS ATTRIBUTABLE TO BLOCKAGE AND DIFFRACTION	79

## **ABSTRACT**

A critical issue for designers of communication systems is the characterization of the communication channel. The free-space propagation model does not adequately predict the mean path loss in space-to-ground communication systems. Traditional methods for predicting the effect of terrain impacting the path of propagating signals focus on statistical or empirical models, which can not always be extrapolated to model prevailing physical conditions.

This study focuses instead on the development and application of knife-edge and rounded obstacle terrain models. The models are based on the geometric theory of diffraction and predict the attenuation affects due to diffraction caused by signal propagation over terrain. Previous work undertaken by Jang [Jan97] on terrain diffraction effects in a ground-to-ground communications environment is used as the basis for model development.

Three satellite constellations, being representative of modern low earth orbit (LEO) satellite communication system designs, are defined and considered in the model simulations. These are based on the Iridium®, Globalstar® and Orbcomm® implementations. Simulated users are located at Anchorage, Killeen and Panama, providing a spread of latitudes for consideration in the simulation results. A notional terrain is also defined and applied at of these sites, providing the basis for a comparative analysis of each system's performance in both the ideal (featureless) and notional terrain environments.

The comparisons show that the Orbcomm communication system is most affected by terrain diffraction. This primarily results from fewer satellites being available to users at the

sites chosen for this study and a majority of observations being made to satellites that are at elevation angles considerably lower than those of the Iridium and Globalstar systems.

The simulation results also confirm that the Iridium system performance is optimized for users located at higher latitudes, while Globalstar is optimized for users located at middle latitudes. Within the scope of this research, Globalstar consistently achieved higher availability reports than Iridium or Orbcomm even though the terrain impact was evident in the results for each system. This robustness is due to a higher average number of in-view satellites available to users of the Globalstar system and a greater proportion of observations being made to higher elevation satellites.

<sup>1</sup> Iridium is a registered trademark and service mark of Iridium LLC

<sup>2</sup> Globalstar is a trademark of Globalstar, L.P.

<sup>3</sup> Orbcomm is a trademark of Orbcomm, L.P.

# **CHAPTER 1**

## **INTRODUCTION**

Traditionally, commercial satellite systems, such as Iridium, Globalstar, and Orbcomm have been considered a tool of corporate organizations and private enterprise. Each system provides mobile communication services to users, and the quality of that service is dependent on the choices made during the design process. Indeed, the system architectures reflect the customer base being targeted, and ensure the commercial viability of the respective companies that develop and operate the systems. A critical issue that designers have to contend with is the characterization of the communication channel, as this impacts other design considerations such as transmit and receive power requirements and the coverage afforded by the system.

This study extended the work of Crowe in 1999 [Cro99] on performance characterization of the Iridium and Globalstar systems. While Crowe focused on atmospheric and ionospheric impairments to the LEOSAT communications channel, this research focuses on terrain multipath propagation affects. In addition, the research develops and applies a terrain diffraction model to the space-to-ground communications channel. The analysis was broadened beyond Crowe's work to include a third LEOSAT communication system, Orbcomm.

The primary objective of this research is the production of a reliable transmission path model that efficiently calculates terrain diffraction effects. Model results are used as the basis for comparing the performance of various LEOSAT communication systems.

## **1.1 Research Objectives**

The research objectives of this thesis are as follows:

- Compare the performance of the Iridium, Globalstar, and Orbcomm constellations in an ideal (or featureless) terrain environment. Performance comparisons are made using measures such as the average number of satellites in-view, the number and duration of outages, and the overall availability achieved.
- Develop and implement a terrain diffraction model utilising, to the extent possible, actual terrain data to model the features of the earth surface.
- Contrast the performance of each system in a full-feature terrain environment with that of an ideal environment.

The analysis is intended to provide a basis for further development of a transmission path model for analysing the performance of mobile satellite communication systems. A thorough understanding of the LEOSAT transmission path and its impact on communication systems such as Iridium, Globalstar, and Orbcomm may assist potential users understand the operational strengths and performance limitations associated with each system.

## **1.2 Motivation**

In recent years, Australian defence and civil protection agencies have been involved in an increasing number of deployments in support of humanitarian relief and United Nations peace-keeping efforts. Deployments have occurred to Somalia, the Middle East, Bougainville, Cambodia, Papua New-Guinea, East Timor, and within Australia itself. Many of these countries are without basic communication services in the regions where the support is required.



Installation of a communications backbone, in a timely manner, contributes to the safety and effective command and control of the deployed forces. LEOSAT communication systems represent a viable means of establishing voice and low speed data communications without the installation time and cost overhead associated with implementing a terrestrial cable network. The 'global' nature of the coverage afforded by these systems and the ease with which connections to the public switched telephone network can be established also increase their appeal over traditional ground-to-ground communication system alternatives that operate in the UHF, VHF, and HF bands. As such, LEOSAT systems are particularly suitable for providing, quickly and efficiently, a basic communications infrastructure in remote areas.

The ability to distinguish between the many options for setting up a satellite communications network, including both commercial and military alternatives, would be of considerable advantage to planners. Such an analysis should include a technical comparison of the performance of each system being considered based on measures such as the average number of satellites in-view, the likely number and duration of outages and the overall system availability in the area of operations. However, there is no tool currently available to perform such a comparison or, more generally, to predict the relative performance of LEOSAT communication systems for users located at any point of the earth surface. Therefore, the process used to select the most appropriate satellite system is unlikely to adequately consider all of the technical information currently available on those systems and the regions of interest.

Crowe's [Cro99] model of the atmospheric and ionospheric impediments to LEOSAT transmission paths was the first step in creating such a tool. The next step is to broaden the analysis to include terrain multipath propagation effects, commencing with terrain diffraction

as addressed in this study. Eventually, a model package could be available that predicts the performance of any LEOSAT system for users located at any point on the earth surface, giving consideration to a variety of technical and non-technical planning issues. Such a tool would be invaluable to the planners and commanders of Australian deployments.

### **1.3 Summary**

This chapter defined the goals for conducting the research and described the motivation leading to the selection of those goals. Chapter 2 provides the background necessary to support the research and presents a review of relevant literature in the areas of multipath propagation mechanisms, traditional approaches to modelling terrain diffraction, and on the LEOSAT communication system implementations. Chapter 3 explains the methodology used to model the terrain diffraction effects and presents the assumptions and limitations of the modelling process. Chapter 4 presents the results of the analyses and provides a performance comparison of the three LEOSAT systems to verify the functionality of the terrain models. Chapter 5 contains conclusions from the research and recommendations for further research.

## **CHAPTER 2**

### **BACKGROUND AND LITERATURE REVIEW**

#### **2.1 Introduction**

The radio channel places fundamental performance limitations on users of wireless communications systems. The transmission path between the transmitter and receiver can vary from simple line-of-sight to one that is strongly influenced by obstacles such as mountains, man-made structures, or the composition of the atmosphere. In low earth orbit satellite (LEOSAT) systems, even the relative speed between the transmitter and receiver can impact the quality of the received signal. Modeling the dynamic nature of such radio channels is very difficult and typically requires statistical techniques, based on measurements made for specific applications or spectrum allocations [Rap96].

The propagation mechanisms and primary causes of multipath communications are discussed in this chapter in the context of a LEOSAT communications environment. Modeling techniques commonly used to predict propagation losses due to multipath and terrain diffraction are reviewed and a methodology selected for application within this thesis.

Also provided are operational overviews and constellation design summaries of the Iridium, Globalstar and Orbcomm LEOSAT systems. Quantification of the performance of each of these systems, in the context of a terrain diffraction environment, and characterization of the propagation path is the primary output from this thesis.

## **2.2 Introduction to Multipath Communications**

Multipath communications occur when propagation conditions allow, or force, a transmitted radio wave to reach the receiving antenna by two or more propagation paths. There are three primary mechanisms by which multipath communications can occur; refraction, reflection, and diffraction. Each of these mechanisms can occur when a propagating radio wave encounters refractive index irregularities in the earth's atmosphere or structural and terrain obstructions on the surface of the earth.

## **2.3 Multipath Propagation Mechanisms**

### **2.3.1 Refraction**

Refraction occurs when the refractive index through which an electromagnetic wave is propagating varies. This variation results in a change in the direction of propagation of all or part of the wave, causing the wave to bend by increasing amounts, toward the region of higher refractive index [All89].

Changes in the refractive index of the earth's atmosphere are mostly gradual since the density of air increases with height above the earth's surface at an approximately uniform rate. However, in practice, the amount of path curvature varies with time due to changes in atmospheric temperature, pressure, humidity, total electron content, and atmospheric turbulence [All89].

### **2.3.2 Reflection**

Reflection occurs when a propagating electromagnetic wave impinges upon an object or region that has very large physical dimensions relative to the wavelength of the

propagating wave. For example, if the wave is incident on a perfect dielectric, part of the energy is reflected back into the first medium and part of the energy is transmitted into the second medium and there is no absorption loss. If the second medium is a perfect conductor, then all of the energy is reflected back into the first medium without loss of energy. In practice, neither a perfect conductor nor a dielectric is possible and reflections from surfaces can generally be classified as one of the following:

**2.3.2.1 Specular.** Specular reflections occur from surfaces or objects that are smooth with respect to the wavelength of the incident wave. Scattered energy is contained within a cone, close to the direction for which the angle of reflection is equal to the angle of incidence. The phase is coherent which means that its mean value can be determined for any point in space. The specular components result from the re-radiation of energy from points on a Fresnel ellipsoid, which gives rise to equal phase at the receiver.

**2.3.2.2 Diffuse.** The diffuse component has little directivity, originates over a larger area of the incident surface than that of the specular component, and has large amplitude fluctuations. The phase, unlike the specular component, is incoherent and has equal probability of having any value at any point in space. If the surface appears very rough to the incident energy, there will be no specular component and the diffuse component will be uniformly distributed in all directions [Rap96] [Tow88].

### **2.3.3 Diffraction**

Diffraction of radio waves is the bending of waves around objects or through a restricted aperture. The amount of bending increases as the object diameter is increased and also as the wavelength increases.

The diffraction phenomena can be explained by Huygen's principle which states that all points on a wave can be considered as point sources for the production of secondary wavelets and that these wavelets combine to produce a new wave front in the direction of propagation. Simply, diffraction is the propagation of secondary wavelets into shadowed regions [Rap96].

The field strength of a diffracted wave in the shadowed region is the complex vector sum of all the electric field components of the secondary wavelets in the space around the obstacle. If a diffracted wave travels one half of a carrier wavelength more than the primary wave in reaching the receiver, the two signals will tend to cancel each other, causing signal fade. While such destructive interference also occurs when diffracted wavelets travel an integer multiple of half wavelengths further to the receiver than the primary wave, the contribution is insignificant due to the reduced signal power contained in them [Rap96].

Any obstruction between the transmitter and receiver causes additional loss over that of the free-space path conditions. This is defined as either shadow or lit diffraction losses. Shadow diffraction losses ( $L_{\text{shadow}}$ ) occur when there is no direct line-of-sight between the transmitter and receiver. Lit diffraction losses ( $L_{\text{lit}}$ ) occur when a line-of-sight path exists between the transmitter and receiver, as well as a diffracted signal due to the obstruction [Jan97][Ass71].

Shadow diffraction losses can be a significant and variable propagation factor in ground-to-ground mobile communications systems. In such systems, high transmitter output power levels, coupled with relatively short propagation distances, can result in viable signals reaching the receiver, despite the absence of a direct line-of-sight communications path. Mobile satellite communications systems are usually power limited because it is impractical

and expensive to operate high power transmitters and high gain antennas in space. Such systems function with relatively low fade margins at, or near, the line-of-sight signal level and require a line-of-sight path to exist between the transmitter and receiver. Consequently, only the calculation of  $L_{lit}$  is required to determine if a viable path exists in a mobile satellite communications environment [Gol92].

## **2.4 Primary Causes of Multipath Communications**

### **2.4.1 Scintillation**

Scintillation describes the rapid fluctuations in the characteristics of a radio wave caused by time dependent and small-scale irregularities in the transmission path. Scintillation effects can be produced in the ionospheric and tropospheric regions of the earth's atmosphere [Tas94].

**2.4.1.1 Ionospheric.** Ionospheric scintillation is produced by electron density fluctuation in the ionosphere, the most significant of which occurs at the F2 Layer peak at an altitude of 225 to 400 km above the earth's surface. The varying electron densities cause fluctuations in the scatter, refraction, and diffraction effects experienced by transiting electromagnetic waves. These variations may result in signal cancellation or reinforcement, which is observed as rapid changes in the characteristics of the received signal. Factors influencing the severity of ionospheric scintillation include the time of year, local time of day, the level of solar activity, level of geomagnetic activity, earth station latitude, and satellite height [Tas94].

**2.4.1.2 Tropospheric.** Tropospheric scintillations are produced when transiting radio waves pass through regions of the atmosphere that are subject to refractive index fluctuations

with time and height. These fluctuations are caused by high humidity gradients and temperature inversion layers and generally occur in the first few kilometers of altitude above the earth's surface. The effects are strongly correlated with season, local time of day, and with local climate and latitude [Cro99].

#### **2.4.2 Elevation Angle**

The elevation angle is that angle between the earth local horizon and the straight-line path between a user and a particular satellite. The severity of multipath effects tend to be related to the transmission path elevation angle for the following reasons:

- a. Reflective and diffractive effects are likely to increase at low elevation angles as the ground station antenna 'sees' more of the natural terrain and man-made obstructions, in the path between the ground station and the LEOSAT.
- b. Refractive effects associated with atmospheric composition are, in general, increased at low elevation angles, as the signal passes through more of the atmosphere in completing the transmitter to receiver link [Cro99].

#### **2.4.3 Antenna Design**

Unlike geostationary satellite communications, the paths to satellites in a LEO constellation continuously change in azimuth, elevation, and range continuously. Consequently, the antenna of the Satellite Personal Communications Services (S-PCS) handset is necessarily omni-directional, providing the user with the ability to communicate with fast moving satellites. The design trade-off for having small antennas with wide beamwidths is that the system is especially prone to multipath communication problems [All89].



#### **2.4.4 Frequency**

Variations in the selected frequency of operation can have a marked effect on the overall system performance. Relevant parameters that vary with frequency selection include:

- a. The half-power beamwidth of an earth station antenna is inversely proportional to the carrier frequency. Multipath communication effects are reduced as the beamwidth is reduced, as the system is less susceptible to reflections, primarily from the earth surface [Rod96].
- b. Electron density irregularities in the ionosphere can affect frequencies up to about 6 GHz, while refractive index irregularities in the troposphere have significant effect on frequencies above about 3 GHz [Ipp86].

### **2.5 Characterizing the Effects of Multipath Communications**

Each of the propagating mechanisms can be present along the transmission path at the same time and it is very difficult to identify the particular mechanism, or mechanisms, that produce a change in the characteristics of a transmitted signal. The parameters that can be measured or observed on a typical link are amplitude and phase, polarization, frequency, bandwidth and angle-of-arrival. Each of the propagating mechanisms, if present along the path, can affect one or more of the signal parameters [Ipp86].

#### **2.5.1 Amplitude and Phase**

Whenever multipath conditions occur, more than one transmission path exists between the transmitter and receiver resulting in the interference of two (or more) waves. The observed effect is that the received signal varies in amplitude, although this variation

may actually be caused by phase variations in the received signals. While variations in the other parameters may or may not be observed on a multipath link, amplitude and phase variations always occur when more than one path is present [Rap96].

### **2.5.2 Depolarization**

Radio wave depolarization is characterized by the presence of an anisotropic propagation medium, which produces different attenuation and phase shifts on radio waves with different polarizations. In effect, a depolarized radio wave has its polarization state altered such that power is transferred from the desired polarization to an undesired polarization (orthogonal), resulting in interference or cross talk between the orthogonally polarized channels. Depolarization is particularly important in the design of frequency reuse systems employing dual, independent, orthogonally polarized channels in the same frequency band to increase channel capacity. Multipath depolarization is generally limited to very low elevation angles ( $< 10^\circ$ ) or where the transmission frequency is less than 3 GHz [All89].

Multipath depolarization effects can be further classified, according to the primary source or origin (atmospheric or antenna design). Atmospheric depolarization processes include [Ipp86]:

- a. depolarization of the direct co-polarized signal by tropospheric turbulence along the path,
- b. depolarization of an indirect component of the co-polarized signal due to reflection from an atmospheric layer,
- c. depolarization of an indirect component of the co-polarized signal due to scattering or reflection from land or water surfaces along the path, or

- d. depolarization of a direct component of the wave due to refractive bending.

Antenna depolarization processes include [Ipp86]:

- a. coupling of an indirect component of the signal reflected from (or refracted through) an atmospheric layer via the cross-polarized pattern of the antennas,
- b. coupling of an indirect component of the signal via the cross-polarized antenna pattern due to reflection from land or water surfaces, or
- c. coupling of an indirect component of the signal via the cross-polarized antenna pattern due to multiple reflections between the ground and the atmosphere.

### **2.5.3 Bandwidth.**

Coherence bandwidth is the upper limit on the information bandwidth or channel capacity that can be supported by a radio channel. This upper limit is set by the dispersive properties of the atmosphere or by multipath propagation. In effect, coherence bandwidth is a statistical measure of how 'flat' the channel is with respect to the spectral components of interest. In practice, spectral analysis techniques and simulation are required to determine the impact that time varying multipath has on a particular signal. When the information bandwidth is approximately less than one percent of the carrier frequency the effects are minimal [Ipp86].

### **2.5.4 Angle-of-arrival**

Angle-of-arrival fluctuations can be considered as a single ray that has deviated from its normal path. This deviation is caused by refractive index changes in the atmosphere. In some situations, several possible paths can exist simultaneously between the transmitter and

receiver. The rays traveling the various paths arrive at the receiver with different amplitudes and phase, which results in interference. On satellite to ground paths above an angle of elevation of  $10^\circ$ , angle-of-arrival variations are virtually non-existent. If the elevation angle is low enough, destructive interference due to reflections from the ground can also occur [Ipp86].

## **2.6 Modeling Terrain Diffraction Using Geometric Theory of Diffraction**

Many models, including McNamara's knife-edge and Balanis' wedge diffraction models, have been derived to compute the electric field phase contributions of the diffracted signals at a receiver. As the signal power is related to the electric field strength, an expression for received signal power can also be derived from such an analysis. Jang provided a comprehensive treatment of this derivation including the mathematical basis [Jan97].

The problem of determining phase contributions from diffracted signals is, however, computationally intensive. Only recently have computer technology improvements made the application of numerical modeling methods to such an analysis problem practical [Jan97].

### **2.6.1 Diffraction Over Terrain Modeled as Knife Edges**

When an obstruction is modeled as a single knife-edge, the resultant lit diffraction can be expressed as a function of the ratio of the path clearance and the first Fresnel zone radius [Dey66]. Figure 2-1 shows how real terrain can be modeled for the purposes of lit diffraction calculations. The parameters in Figure 2-1 are defined as follows:

- $h_c$ : Height difference or path clearance between the line-of-sight path and the terrain point closest to the line-of-sight path.
- $d_T$ : Distance between the transmitter and the point that is closest to the line-of-sight path.
- $d_R$ : Distance between the diffraction point and the receiver.

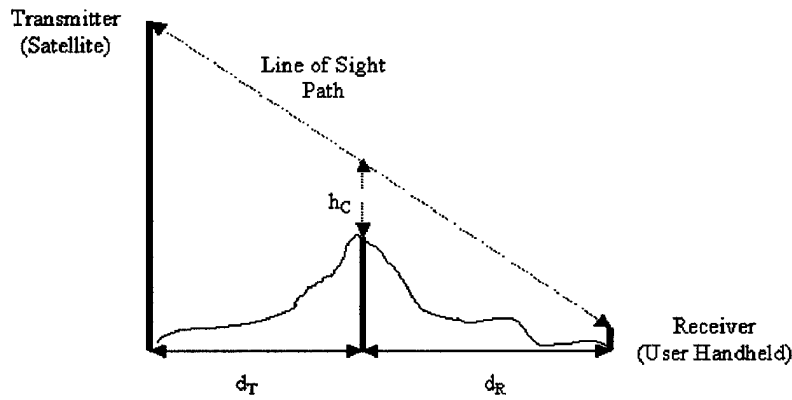


*Figure 2-1: Lit Diffraction Calculation Geometry*

The first Fresnel radius,  $F_1$ , can be expressed in terms of these parameters and the propagating signal wavelength,  $\lambda$ , as follows:

$$F_1 = \sqrt{\frac{\lambda \cdot d_T \cdot d_R}{(d_T + d_R)}} \quad (\text{Equation 2-1})$$

In the case of LEOSAT communications systems, where  $d_T$  is approximately equal to  $(d_T + d_R)$ , the expression becomes [Flo87]:

$$F_1 = \sqrt{\lambda \cdot d_R} \quad (\text{Equation 2-2})$$

The resultant attenuation due to knife-edge diffraction, can be expressed as [Flo87]:

$$\text{Attenuation} = \sqrt{2} \cdot \left( \frac{h_c}{F_1} \right) \quad (\text{Equation 2-3})$$

The attenuation as a function of  $h_c/F_1$  (or  $n^{1/2}$ ) is depicted in Figure 2-2. If the edge of the knife-edge obstruction is at the line-of-sight, a loss of 6dB is encountered. To avoid significant attenuation, a clearance of about 0.6 ( $F_1$ ) is required [Flo87].

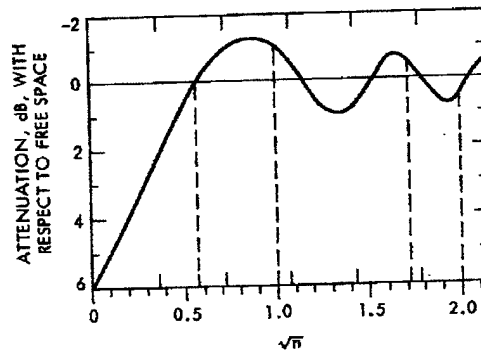


Figure 2-2: Attenuation Due to Knife-Edge Diffraction as a Function of  $n^{1/2}$  (where  $n^{1/2} = h_c/F_1$ ) [Flo87]

#### 2.6.1.1 The Effect of Multiple Diffraction Points.

For multiple obstacles, only the obstacle edge that is closest to the line-of-sight path needs to be considered and the effects of all other obstacles can be ignored [Dey66].

#### 2.6.1.2 Real Terrain Diffraction Model

Jang implemented a knife-edge diffraction model based on the geometric theory of diffraction calculations [Jan97]. The model predicts the propagation effects in ground-to-ground and air-to-ground communication systems but could be modified to address the specific requirements of the LEOSAT communications environment and also form the

basis of a rounded obstacle diffraction algorithm. A complete description of the model, algorithms, and code are given in [Jan97].

## 2.6.2 Diffraction Over Terrain Modeled as Rounded Obstacles

Another method used to predict the diffraction effects of terrain assumes that the obstacles are cylindrical, with the parameter of interest being the radius of curvature at the obstacle top [Ass71]. The loss due to lit diffraction in this case can be as high as 20 dB, an increase of 14 dB over that of the knife-edge diffraction model. The latter value corresponds with the smooth earth value proposed by Bullington in 1977 [Flo87]. The calculations required in the case of rounded obstacles are as follows [Flo87]:

$$R = \sqrt{\frac{\lambda \cdot d_T \cdot d_R}{d_T + d_R}} \quad (\text{Equation 2-4})$$

$$\alpha = \frac{\lambda^{\frac{2}{3}} \cdot r^{\frac{1}{3}}}{R} \quad (\text{Equation 2-5})$$

$$\text{Attenuation} = \sqrt{2} \cdot \left( \frac{H}{R} \right) \quad (\text{Equation 2-6})$$

The parameters of interest in the model calculations are:

- H: Height difference between the line-of-sight path and the terrain point closest to the line-of-site path.
- $d_T$ : Distance between the transmitter and the point that is closest to the line-of-sight path.

- $d_R$ : Distance between the diffraction point and the receiver.
- $R$ : First Fresnel zone Radius.
- $r$ : Obstacle radius of curvature in the vicinity of the feature peak.
- $\lambda$ : Wavelength.
- $\alpha$ : Curvature index [Flo87].

The losses for single and multiple diffraction points are calculated in the same manner as that for the knife-edge terrain model. The resultant curves depicting the losses due to diffraction are presented in Figure 2-3. Of note, the curve for  $\alpha = 0$  is equivalent to the resultant curve in the knife-edge diffraction model [Flo87].

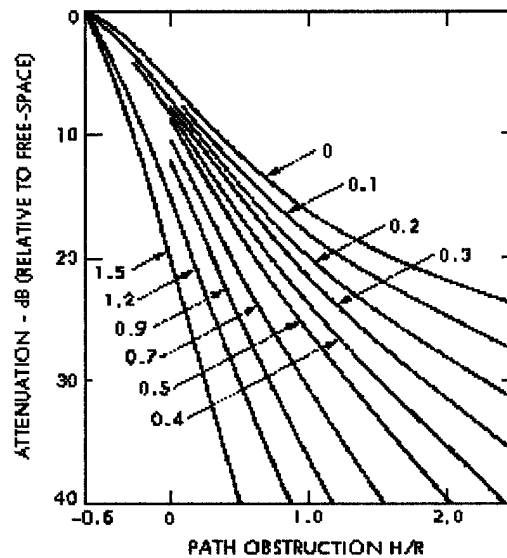


*Figure 2-3: Attenuation Due to Rounded Obstacle Diffraction as a Function of  $H/F_1$  or  $H/R$  [Flo87]*



## 2.7 Modeling Terrain Diffraction Using Probability Distribution Models

Probability distribution models can accurately describe the effect of terrain diffraction and other phenomena in particular situations. The following describes types of fading that can affect the communications channel.

**Flat Fading.** When a radio channel has a constant gain and linear phase response over a bandwidth that is greater than the bandwidth of the transmitted signal, the received signal will undergo flat fading. For this type of fading, the spectral characteristics of the transmitted signal are preserved at the receiver, but the strength of the received signal will vary with time due to fluctuations in the gain caused by the multipath channel. The Rayleigh, Ricean, and Nakagami models are all commonly used to predict the performance of flat fading channels [Rap96].

**Selective Fading.** If the channel possesses a constant gain and linear phase response over a bandwidth that is smaller than the bandwidth of the transmitted signal, then frequency selective fading will occur. When this happens, the received signal includes multiple versions of the transmitted signal that are attenuated and delayed in time and hence the received signal is distorted. Frequency selective fading induces inter-symbol interference or a smearing of the signal. This type of fade is more difficult to model and wideband measurements are often required to assist in the development of models, particular to a given channel. The Rayleigh and Nakagami models can be adapted to suit such an analysis [Rap96].

### 2.7.1 Rayleigh Distribution

The Rayleigh distribution is commonly used to describe the statistical time-varying nature of the received envelope of a flat fading signal, or the envelope of an individual fading component. The distribution is also known to effectively model the summation envelope of two quadrature Gaussian noise signals. This means that the distribution is most effective when modeling a channel where no single component dominates the received signal. The Rayleigh probability density function is given by [Rap96]:

$$p(r) = \frac{r}{\sigma^2} \cdot e^{\left(\frac{-r^2}{2\sigma^2}\right)} \quad 0 \leq r \leq \infty \quad (\text{Equation 2-7})$$

where  $\sigma$  is the rms value of the received signal voltage before envelope detection, and  $\sigma^2$  is the time average power of the received signal before envelope detection. Figure 2-4 shows a typical Rayleigh probability density function.

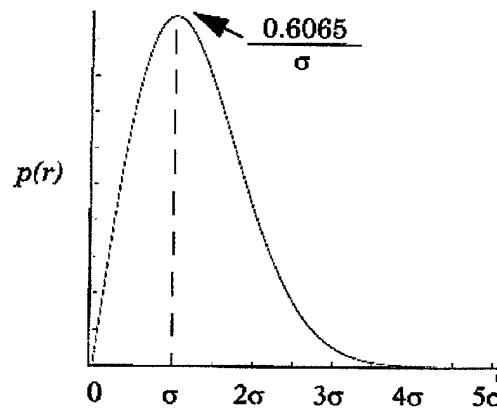


Figure 2-4: Rayleigh Probability Density Function [Rap96]

### 2.7.2 Ricean Distribution

When there is a dominant stationary (non-fading) signal component present in the received signal, such as a direct line-of-sight propagation path, the small scale fading envelope distribution is Ricean. In such situations, random multipath components arriving at different angles are superimposed on a stationary dominant signal. At the output of an envelope detector this has the effect of adding a DC component to the random multipath signal. As the dominant signal becomes weaker, the composite signal resembles a noise signal, which has an envelope that is Rayleigh distributed. Consequently, the Ricean distribution degenerates to a Rayleigh distribution when the dominant component fades away. The Ricean distribution is given by [Rap96]:

$$p(r) = \frac{r}{\sigma^2} \cdot e^{\left[ \frac{-(r^2 + A^2)}{2\sigma^2} \right]} \cdot I_0 \left( \frac{A \cdot r}{\sigma^2} \right) \quad (A \geq 0, r \geq 0) \quad (\text{Equation 2-8})$$

where  $A$  denotes the peak amplitude of the dominant signal and  $I_0(\ )$  is the modified Zero-order Bessel function of the first kind. The Ricean distribution is often described in terms of the parameter  $K$  which is defined as  $K = A^2/(2\sigma^2)$ . Figure 2-5 shows typical Ricean probability density functions for two values of the parameter  $K$  [Rap96].

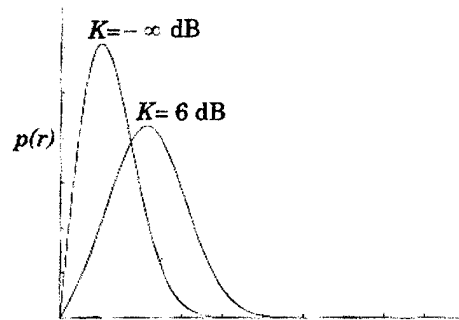


Figure 2-5: Ricean Probability Density Functions [Rap96]

### 2.7.3 Nakagami Distribution

The Nakagami distribution, also known as the ‘m distribution’, offers greater flexibility in predicting channel performance in a variety of fading environments. Experimental results have shown that the Nakagami distribution fits experimental data collected in a variety of fading environments, better than the Rayleigh or Ricean distributions.

The Nakagami distribution spans from the one-sided Gaussian distribution, with  $m = 0.5$ , to the non-fading channel case, where  $m = \text{infinity}$ . The distribution contains Rayleigh fading ( $m = 1$ ) as a special case, along with fades that are more severe ( $0.5 < m < 1$ ) and those that are less severe than Rayleigh fades ( $m > 1$ ). The Nakagami distributions can also be used to approximate the Lognormal and Ricean distributions for a certain range of average signal-to-noise ratio [Pol99]. The probability density function for the Nakagami distribution is given as:

$$p_{\alpha}(r) = \frac{2}{\Gamma(m)} \cdot \left(\frac{m}{\Omega}\right)^m \cdot r^{2 \cdot m - 1} \cdot e^{-\frac{m \cdot r^2}{\Omega}} \quad \text{where} \quad \left(m = \frac{\Omega^2}{\text{Var}(\alpha^2)}\right) \geq \frac{1}{2} \quad (\text{Equation 2-9})$$
$$\Omega = E(\alpha^2)$$
$$\alpha \geq 0$$

The parameter  $m$  is referred to as the ratio of moments or the fading figure. Figure 2-6 shows a Nakagami probability density function for varying values of the parameter  $m$ .

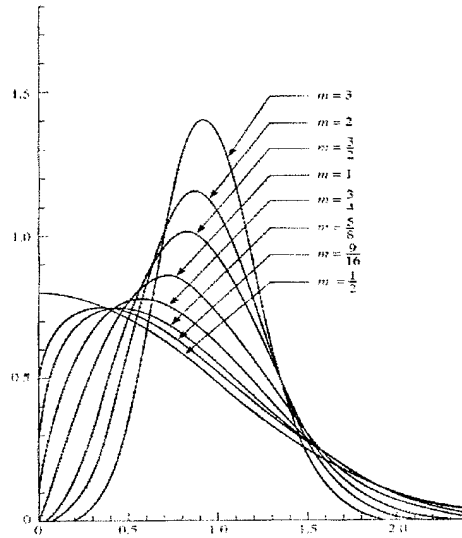


Figure 2-6: Nakagami Probability Density Function [Pro95]

## 2.8 Modeling Terrain Diffraction Using Empirical Regression Models

Empirical regression models correspond to fade distributions derived from experimental measurements at different frequencies, elevation angles, terrain and vegetation types, and the extent of shadowing. The models have the benefit of being based on actual data and can be used with a degree of confidence for the prediction of fade distributions over regions or terrain similar to those for which the measurements were recorded [Gol92].

A common disadvantage of these models is that experimental results often can't be extrapolated to model prevailing physical conditions. For example, carrier frequency changes and micro-variations in the physical environment pose extrapolation difficulties due to their stochastic nature [Gol92]. For this reason, these models have not been considered for implementation in this thesis.

## **2.9 Representative Satellite Constellations**

Traditionally, constellations comprising as few as three satellites in geostationary earth orbit (GEO) have been used to provide global communications to the world (or at least coverage of 70% of the earth's lower latitudes). The limitations of this approach include a one-way propagation delay of 120 ms and a requirement for large antennas to establish effective links (the most recent user terminal design for INMARSAT, a typical GEO communications system is suitcase-sized).

Satellite constellations have recently been launched into low and mid earth orbits (LEO and MEO) that purport to provide continuous global communications coverage, even to the polar-regions. Such systems include Iridium, Globalstar, and Orbcomm. Each of these systems are modeled as part of this thesis, and are indicative of modern-technology LEOSAT communication system alternatives.

### **2.9.1 Iridium**

#### ***2.9.1.1 Operational Overview***

Conceived in 1987, Motorola's Iridium system is based on an Adams-Rider design and was fully deployed in May 1998, claiming to provide global voice, data, fax, and paging capabilities [Rod96]. Financial difficulties have undermined the effectiveness and compromised the operation of the system.

The Iridium communication system comprises the satellites, gateways, and user handsets. The satellites utilize inter-satellite links to route traffic and relay data/voice either directly to an Iridium handset or terminal or to one of 15 tracking ground stations (gateways) that are located in strategic, high traffic density locations. The gateways provide a link

between the satellite constellation and the public switched telephone network (PSTN). The final component, the dual mode user handset, allows users to access both the Iridium and compatible cellular phone networks [Cro99]

#### ***2.9.1.2 The Constellation***

The original configuration was based on a 77-satellite constellation, which was the basis for the name 'Iridium' as the 77<sup>th</sup> element of the periodic table. The constellation was later reduced to 66 satellites in an effort to reduce system costs [Rod96].

The constellation of 66 satellites is contained within six planes, each plane containing 11 satellites. The satellites are located at an altitude of 780 km in near circular orbits at an inclination of 86°. The co-rotating planes, two through five, are spaced 31.6° apart and the counter rotating planes, one and six, are spaced 22° apart to give 360° coverage of the earth (i.e.,  $31.6^\circ \times 5 + 22^\circ \times 1 = 180^\circ$ ). The nominal spacing between satellites in each plane is 32.7° and there is one 'spare' satellite located within each plane orbiting 130 km below the operational satellites [Rod96]. Figure 2-7 depicts the Iridium constellation, which was derived from the North American Aerospace Defense Command (NORAD) two-line element set [Llo00].

#### ***2.9.1.3 Footprint***

Each satellite in the Iridium constellation communicates with ground-based users via three antennas which form a honeycomb pattern of 48 beams on the earth's surface below each satellite. The beam pattern covers an area of approximately 15.3 million km<sup>2</sup>, which equates to a footprint radius of 2210 km. As the satellite footprint moves over the ground, the subscriber signal is switched from one beam to the next similar to the concept employed

in terrestrial cellular systems where the roaming user often moves between stationary adjacent cells. As the satellites approach the poles, their footprints converge and the beams overlap. Outer beams are then turned off to eliminate this overlap and to conserve spacecraft power [Rod96].

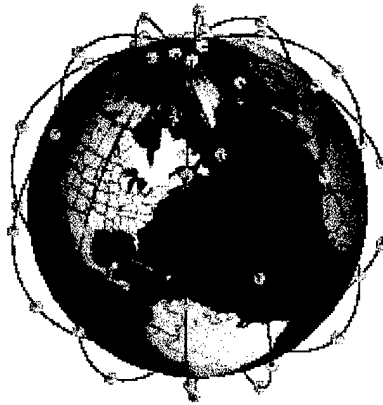


*Figure 2-7: The Iridium Satellite Orbits [Llo00]*

#### **2.9.1.4 In-View Times and Orbital Period**

The earth-relative velocity of a LEO satellite at 780 km altitude is 0.00104 rad/s. The period, or time for each satellite to complete a single orbit is 6019 seconds (or 100 minutes 16.9 seconds) [Cro99].

Given the minimum elevation required for a user to ‘see’ each satellite is specified as being  $8.2^\circ$  for the Iridium system, the expected in-view time for each satellite can be calculated as being approximately 10 minutes. This small in-view time means that users will experience a rapid procession through the various beams that constitute the footprint during each call. Consequently, tracking and hand-off procedures are required to process calls and maintain network awareness between each satellite in the constellation. This represents a



considerable increase in design complexity over that required in achieving communications with a GEO satellite based communication systems [Cro99].

#### ***2.9.1.5 Links to Users***

The links between the Iridium satellites and each user are established using frequencies in the L-band (1.616 – 1.6265 GHz). A combination of time and frequency division multiple access (TDMA and FDMA) signal multiplexing is utilized to divide the available spectrum into 3840 carrier channels, each approximately 2800 Hz wide. Voice signals from each user handset are modulated onto the carrier using a quadrature phase shift key (QPSK) modulation scheme and transmitted at 2400 bps using right-hand circular polarization. Each subscriber unit is capable of transmitting 3.7 W of power with a gain of 1 dBi and operates on receive power levels around  $10^{-15}$  W [Rod96].

#### **2.9.2 Globalstar**

Globalstar is a satellite based wireless telecommunications system designed to provide world-wide telephone, facsimile, paging, position location, and data transmission services [Llo00].

##### ***2.9.2.1 The Constellation***

The Globalstar system features a constellation deployed in a T/P/F = 48/8/6 Walker ‘delta’ pattern. This means that there are  $T = 48$  satellites, in eight orbit planes with six satellites per plane. Each orbit plane is inclined at  $52^\circ$ , providing a notional communications coverage to  $\pm 70^\circ$  latitudes. This ensures that the Globalstar system will be accessible to approximately 98% of the world’s population [Pri93] including multiple satellite coverage in

highly populated areas such as the United States, Europe and China. Figure 2-8 depicts the Globalstar constellation and was derived from the NORAD two-line element set [Llo00].

#### ***2.9.2.2 In-View Times and Orbital Period***

The satellites are located in circular orbits 1410 km above the earth's surface. From this altitude, a satellite can provide coverage to a region 4800 km in diameter. The orbit period for each satellite is 114 minutes and each satellite has a maximum in-view time of approximately 16.5 minutes. The minimum elevation angle for a mobile user or an earth station is stipulated as being  $10^{\circ}$ , and the maximum slant range is 3503 km [Wer99].

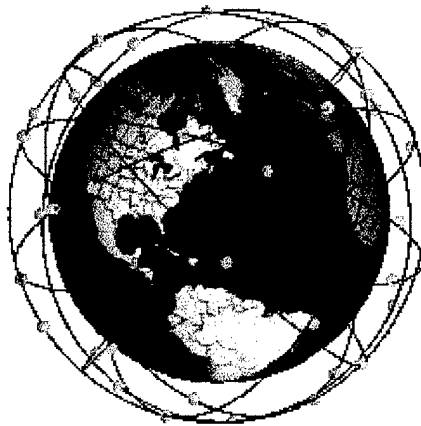


*Figure 2-8: The Globalstar Satellite Orbits [Llo00]*

#### ***2.9.2.3 Links to Users***

The user terminal-to-satellite uplink operates in the L-Band from 1610 MHz to 1626.5 MHz. The satellite to user terminal downlink operates in the S-Band from 2483.5 to 2500 MHz. Both gateway links operate in the C-Band, the uplink in the range 5091 to 5250 MHz and the downlink in the range 6875 to 7055 MHz. The communications system provides adaptive data rates up to 9600 bps for voice transmission and 7200 bps sustained for

data transfer. A quaternary phase shift keying modulation system is used, allowing more efficient use of the allotted bandwidth [Llo00].

Each satellite supports up to 3000 voice circuits at any one time. Connections are established via one of the system gateways, which can route calls via the public switched telephone network (PSTN) or through any in-view Globalstar satellite. Consequently, the satellites provide a bent-pipe communication function and have no inherent ability to route calls as in the Iridium design. Globalstar documentation estimates the number of gateways required to service the earth at 60 [Llo00].

### **2.9.3 Orbcomm**

The Orbital Communications Corporation (Orbcomm) system is a LEO satellite system also intended to provide two way message and data communications as well as position determination services [Rod96].

#### ***2.9.3.1 The Constellation and Ground Segment***

There are four main orbital planes. The first plane, inclined at  $7^\circ$ , contains seven satellites spaced approximately  $52^\circ \pm 8^\circ$ . Planes two through four are inclined at  $45^\circ$  and contain eight satellites spaced from each other by  $45^\circ \pm 5^\circ$ . Two supplemental orbits have also been provided, each containing two satellites. The first of these, Plane 5, is inclined at  $70^\circ$  and Plane six is inclined at  $108^\circ$ . The latter two planes are intended to provide enhanced polar coverage. Each satellite is located in circular orbit at an altitude of 775 km. Figure 2-9 depicts the Orbcomm constellation as derived from the NORAD two-line element set [Llo00].

The ground segment consists of the subscribers, gateway earth stations that provide access to the PSTN and other mobile services, a network control center (NCC) and a satellite control center (SCC). The NCC and SCC are located in Dulles, Virginia and the four gateway services for US operations are located near the corners of contiguous USA [Rod96].

### ***2.9.3.2 In-View Times and Orbital Period***

The satellites are located in circular orbits 775 km above the earth's surface. From this altitude a satellite can provide coverage to a region approximately 4400 km in diameter. The orbital period for each satellite is 100 minutes and each satellite has a maximum in-view time of approximately 12.5 minutes. The minimum elevation angle for a mobile user or an earth station is stipulated as being  $5^\circ$  and the maximum slant range is 2700 km [Llo00].

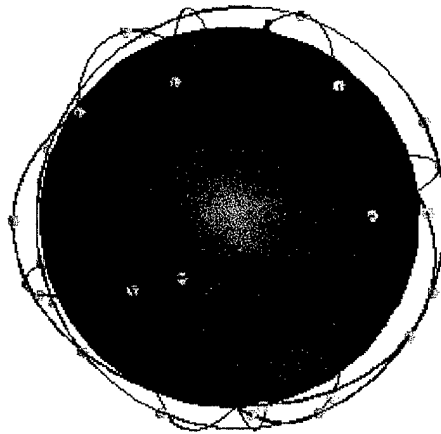


*Figure 2-9: The Orbcomm Satellite Orbits [Llo00]*

### ***2.9.3.3 Links to Users***

The message and data channels are located in the VHF Band. Satellites receive in the 148 to 149.9 MHz range and transmit in the 138 to 139 MHz range. Circular polarization is employed on all channels and the uplink channels utilize a dynamic channel activity assignment system. This system uses a scanning receiver aboard the satellite to measure the

interference received in small bandwidths and scans the entire band every five seconds. Using this data, the satellite receiver compiles a list of available channels (out of a total 760 channels) and prioritizes those according to the interference levels expected. A supplementary transmission beacon at 400.1 MHz is used to assist position determination and to correct for errors in timing introduced by the ionosphere [Rod96].

## **2.10 The Terrain Data Sources**

**The National Imagery and Mapping Agency (NIMA).** The mission of the NIMA is to provide timely, relevant, and accurate imagery, imagery intelligence, and geospatial information in support of US national security objectives. In support of military applications the agency has developed a standard digital data set, the Digital Terrain Elevation Data (DTED) Level 0, which may be of value to scientific, and technical communities. This data set allows a gross representation of the Earth's surface for general modeling and assessment and can be freely copied and used with other geo-spatial information as desired [Nim00].

**Digital Terrain Elevation Data.** The DTED product is a matrix of terrain elevation values, which provide basic quantitative data about terrain elevation, slope, and surface roughness. One matrix file represents a 30 arc second (nominally one kilometer square) area of the earth surface. A separate binary file provides minimum, maximum, and mean elevation values computed for each 30 arc second square area. Finally, DTED Level 0 contains the NIMA Digital Mean Elevation Data (DMED) providing minimum, maximum, and mean elevation values as well as standard deviations for each 15-minute x 15-minute area in a one-degree cell. A typical terrain data file and the interpretation of that file via a mesh plot are shown at Figure 2-10.

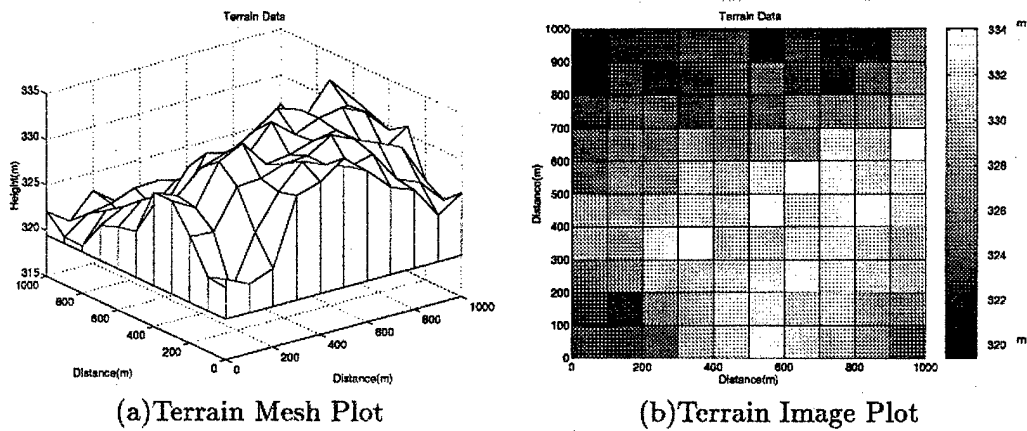


Figure 2-10: Example Terrain Mesh and Terrain Image Plots Produced from the NIMA Data [Jan97]

**Data Interpolation.** DTED elevation points are evenly spaced when expressed in arc second units, but this is not the case when the files are converted into meter units. Wilson developed an interpolation methodology that converted the DTED 30 arc second, non-uniform data files into a uniform data set with reporting posts spaced every 100 m. Appropriate terrain files were created using code provided by Wilson and these have been used throughout this thesis to model a notional terrain around the selected sites [Wil98].

Wilson's interpolation also provided a cubic equation or representation of the earth's surface within each grid square. The coefficients of this cubic equation can be used to approximate the radius of curvature at any given point, using a relationship based on the terrain feature height (y) and location (x) [Wer99]:

$$\text{Curvature} = \frac{\left( \frac{d^2}{dx^2} y \right)}{\left[ 1 + \left( \frac{d}{dx} y \right)^2 \right]^{\frac{3}{2}}} \quad (\text{Equation 2-10})$$

$$\text{Radius} = |\text{Curvature}| \quad (\text{Equation 2-11})$$

## 2.11 Review of Relevant Literature

The focus of this study is the application of the GTD to predict terrain diffraction effects in a LEOSAT communications environment. A review of the available literature indicated that many similar studies have been undertaken with regard to ground-to-ground communications systems. Most of these studies assume that the location of the transmitter and receiver remains relatively constant and therefore, the number of computations required to implement an effective model are small. Analysis of mobile satellite communications links have traditionally focused on the application of statistical and empirical models to predict the combined attenuation effects due to diffraction, reflection, and refraction.

Only one other study was found to have applied a geometric theory of diffraction to predict diffraction effects due to transmission path obstacles in a mobile satellite communications environment. In [TIR98], Tirkas, Wangsvick, and Balanis developed a propagation model to account for building blockage in an urban environment. The study focuses on verifying the feasibility of applying a knife-edge diffraction model to the case of a roaming user in a high-rise environment. No consideration was afforded the rounded obstacle model or the development of a practical tool to predict the performance in any given city or for any satellite constellation [Tir98].

## **CHAPTER 3**

### **ANALYSIS AND MODELING METHODOLOGIES**

#### **3.1 Introduction**

The purpose of this chapter is to describe and support the methods used to achieve the objectives of the research and to properly define the scope and limitations of the methods chosen. In Section 3.2, the outputs required from the research are defined followed by an overview of the method used to meet the objectives. In Section 3.5 the assumptions and restrictions needed to establish a workable baseline for the analyses are defined. Section 3.6 describes the baseline scenario and how the ideal terrain environment was created and analyzed. Sections 3.7 and 3.8 present the methods used to analyze the performance of the LEOSAT constellations in a notional terrain environment modeled using knife-edged and rounded obstacles. Section 3.9 describes the processing methods used to obtain and present the results, followed by a discussion on the verification process followed.

#### **3.2 Required Outputs**

The intent of this thesis is to characterize the impact of attenuation due to terrain diffraction in a LEOSAT communications environment. The following data is required to complete the research:

- Definition and modeling of representative LEOSAT communication systems. The elevation angle, azimuth, and range to each visible satellite from the selected user sites must be determined as transmission path calculations are based on these factors.



The performance of each system, in both the ideal (rounded earth) and notional terrain environments, is required.

- Selection of appropriate user sites. The sites chosen should assist characterization of each LEOSAT communication system's performance as a function of latitude.
- Definition of a notional terrain data set. The notional terrain selected should ensure terrain diffraction is a significant factor in transmission path calculations at each of the user sites.
- Characterization of the transmission path including the number of satellites in-view, number and duration of outages, system availability, and the distribution of elevation angles to in-view satellites for the selected constellations.
- Presentations, including relevant tables and plots, to support conclusions drawn from the analysis work.

### **3.3 Method of Analysis**

Both direct measurement and simulation can be used to generate the data required to satisfy the requirements of the research. However, there are considerable difficulties associated with measuring the received signal from a LEOSAT system and determining the amount of attenuation due solely to terrain diffraction effects. The time and cost associated with procuring the necessary equipment and materials and undertaking the measurements would be significant. Alternatively, simulation is a relatively straightforward option as software packages exist (such as SOAP and STK) that can be used to model the selected constellations and communication paths and many physical effects peculiar to the space-to-earth communications channel. Other packages, such as MATLAB and

MATHCAD, are also available to implement the two geometrical models of diffraction discussed in Chapter 2.

Given that simulation is the most appropriate method for conducting the analysis, the selection of the most appropriate software packages was based on several factors. The availability of standard and tailorable reports within each of the packages, the user interface provided by each application, and the format of relevant research work undertaken by other students (and applicable to this thesis) all influenced the selection of simulation packages.

### 3.4 Overview of the Process

Figure 3-1 describes the processes used to achieve the objectives of the study.

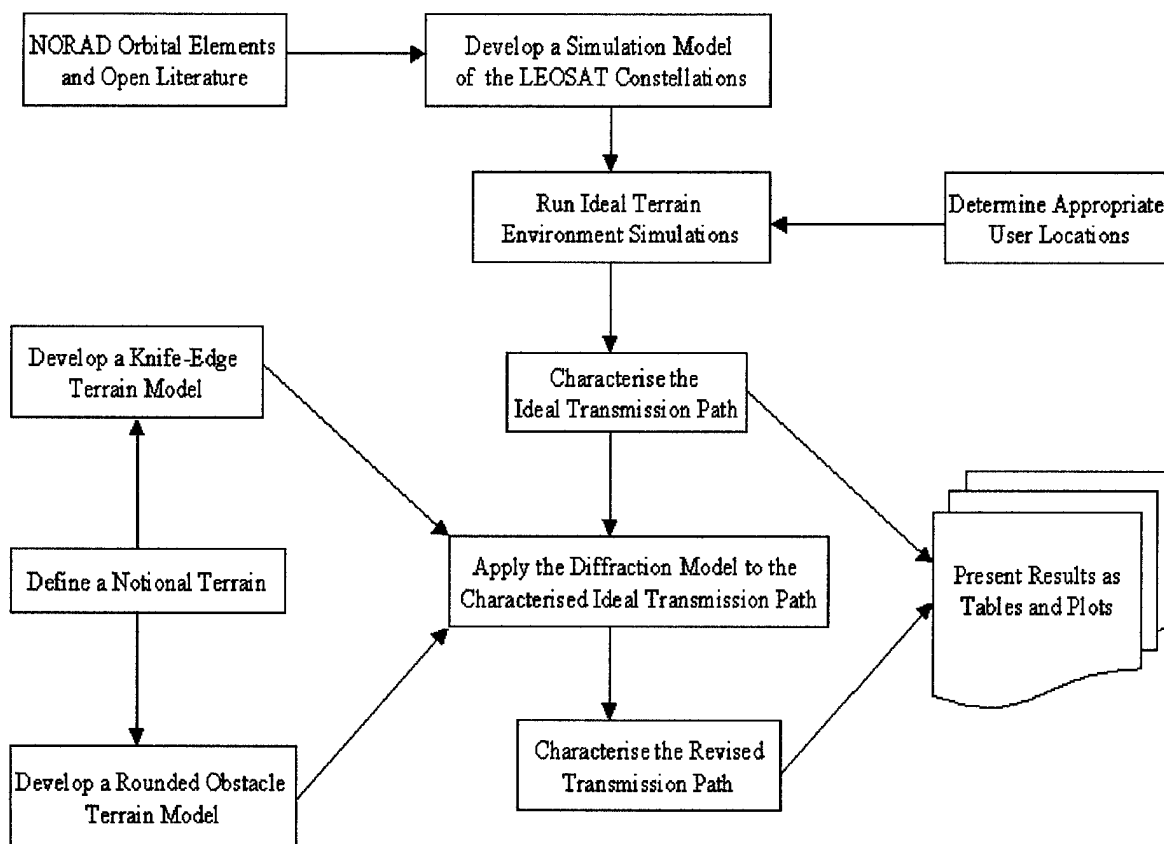


Figure 3-1: Analysis Process Flowchart

The commercial orbital simulation package, Satellite Orbit Analysis Program (SOAP) was used to create the LEOSAT constellations and identify the location of each satellite over the simulation period. MATLAB routines were written to determine the following:

- a. The free-space path loss and corresponding in-view times for each satellite. Based on this information a figure for the system availability was determined corresponding to the case of an ideal, rounded earth.
- b. The expected losses due to blockage and terrain diffraction associated with the presence of a notional terrain. The availability statistics were revised based on this information and conclusions were drawn about the performance of each constellation when operating in a terrain diffraction environment.

### **3.5 Model Parameters and Assumptions**

#### **3.5.1 The Notional Terrain**

The choice to model a notional rather than an actual terrain environment was driven by the access limitations placed on NIMA data files. Data files consisting of terrain height information at one meter spacing have restrictions on accessibility. These files could have been used in the analysis on the proviso that the thesis be placed on limited distribution. To ensure the research undertaken was available to all interested parties in the future, a decision was made to limit the analysis to an unclassified NIMA data set. This data set is based on the Killeen area of Texas and contains terrain height information at 100 meter spacing. Most importantly, the routines and processes developed for use in the analysis can be applied to any NIMA data set, regardless of the resolution of the data files.

### 3.5.1.1 The 100 Meter Data Set

The area of Texas, centered on Killeen (31° N, 97° W), provides a relatively flat landscape. However, the data set for this area is unclassified and was able to be applied without restriction in this thesis. In order to define a notional terrain that could be a significant influence in the diffraction analysis, each feature height had to be multiplied by a factor of 20. This reduced the time required to produce a notional terrain data set and ensured the analysis methods remained compatible with the NIMA data formats should follow-on work be considered in the future. Other multiplication factors were considered (10, 15 and 30) but these either provided insufficient or too much opportunity for terrain blockage and diffraction. Two different views of the notional terrain applied throughout the analysis are depicted in Figure 3-2 (surface) and Figure 3-3 (contour).

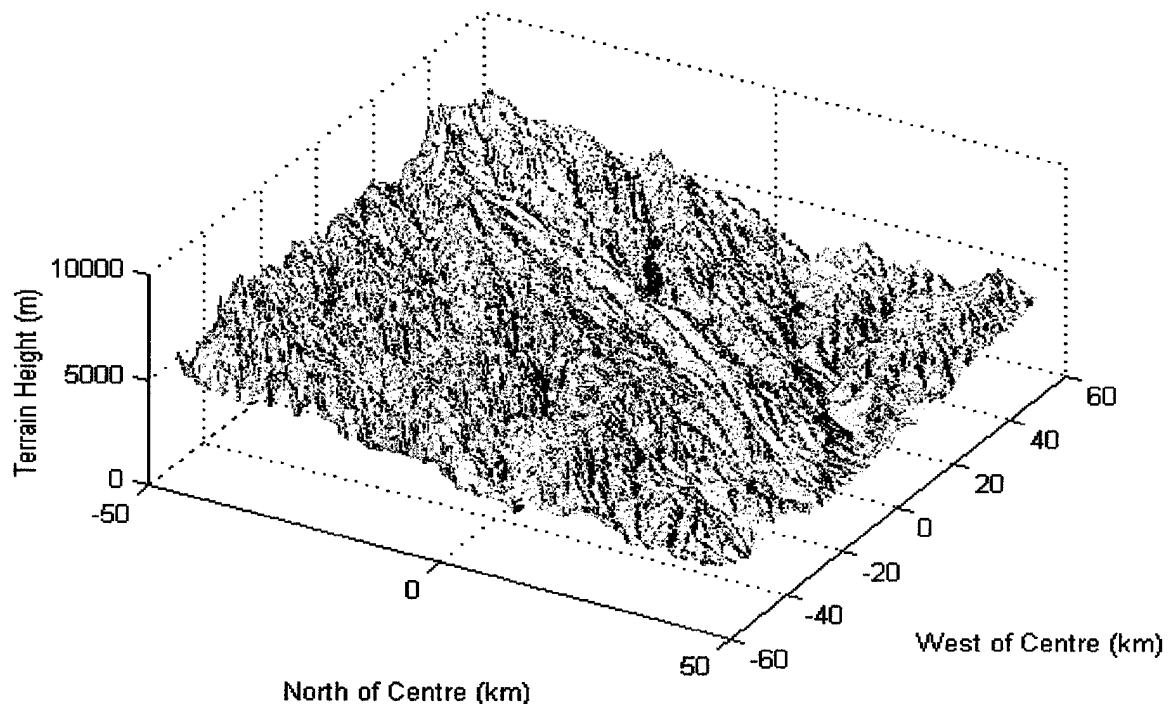
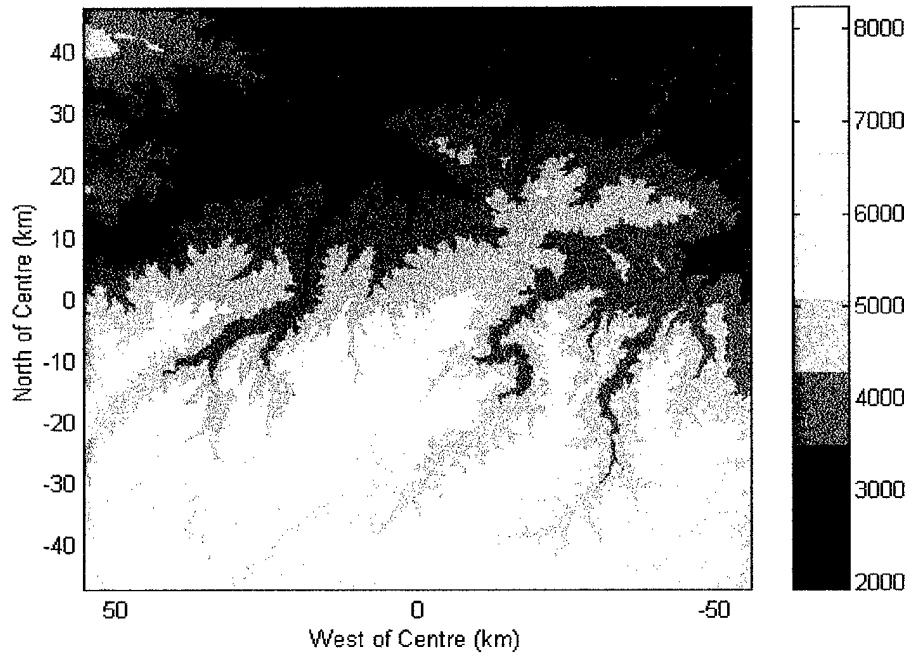


Figure 3-2: The Notional Terrain Surface



*Figure 3-3: The Notional Terrain Contour Profile*

The data set contains terrain height information for an area of land approximately 100 km x 100 km in size, represented by a grid matrix where each grid square represents a 100 m x 100 m portion of land. One height measurement is recorded for each grid square. This is the height of the terrain feature at the bottom left corner of each square.

#### ***3.5.1.2 The Condensed Data Set***

An analysis could have been undertaken using this notional terrain format. However, given the size of the terrain data file (12 Mbytes), simulations were expected to take considerable time and processor resources to complete. To reduce the size of the terrain data file and the processing requirements for each simulation, the data file was pre-processed. The following reasoning was applied based on the theory presented in Chapter 2 in developing a simplified notional terrain format for use in the analysis:

- a. Only one of the terrain features, the dominant feature, contributes to the diffraction calculations along any given line-of-sight between the satellite and the receiver.
- b. The dominant feature along any given line-of-sight is that feature causing the greatest look angle (angle of elevation) between the receiver and the feature peak.
- c. The azimuth resolution required is a function of the grid spacing and the dimensions of the land area being considered, as depicted in Figure 3-4. The best azimuthal resolution able to be obtained between adjacent line-of-sight paths about a receiver located at the center of the Killeen data set is approximately  $0.11^\circ$ .

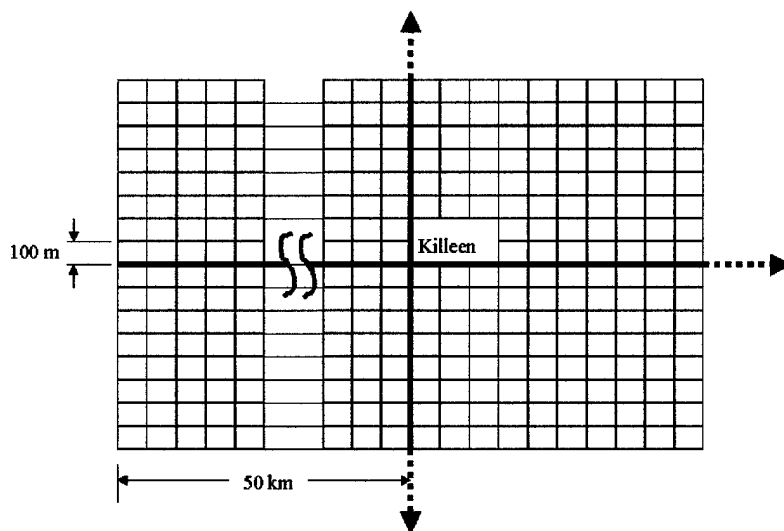


*Figure 3-4: Relevance of Grid Dimensions to Azimuthal Resolution*

- d. The notional terrain can be 'sampled' at azimuth intervals of  $0.1^\circ$  without losing terrain feature details.
- e. A MATLAB routine was written to perform the required sampling, from which a condensed notional terrain file was produced. The resulting file contained 3600

samples (360 / 0.1), representing the height of the dominant feature each 0.1° in azimuth about the receiver and the cell reference of that feature.

- f. The reduction in the size of the condensed notional terrain file, to 125 Kbytes, significantly reduced the file handling and processor requirements during the simulations that followed.

#### ***3.5.1.3 Approximating the Curvature of the Dominant Feature***

The calculations required to determine the curvature at the top of the dominant features were discussed in Chapter 2. The cubic equations developed from Wilson's interpolation [Wil98] approximated the shape of the surface within each grid square. These equations could have been used as the basis to approximate the surface curvature in any given direction of propagation, between the satellite and the receiver. On initial inspection, such an approach appears to offer an accurate method for determining the curvature of the dominant feature peak. However, further scrutiny shows that the accuracy of the approximation is related to the interaction of two elements:

- a. The granularity of the terrain samples (100m in the notional terrain),
- b. The regularity of the terrain surface.

The terrain scenarios depicted in Figure 3-5 and Figure 3-6 were chosen to illustrate circumstances where a rigorous mathematical treatment of the terrain surface would not provide an accurate approximation for the actual curvature of interest. In the first case, the granularity of a terrain data file is too fine. The feature of interest is the cliff, with a curvature very closely resembling a knife-edge. The calculated curvature, using the approximation derived from Wilson's interpolation, would yield an approximation equal to

the curvature of the knoll at the feature peak. The second case describes a situation where the granularity of the terrain data file is too coarse. The actual feature of interest is again the cliff face, but the calculated curvature, an average value, would yield an approximation equal to the slope of the dotted line.

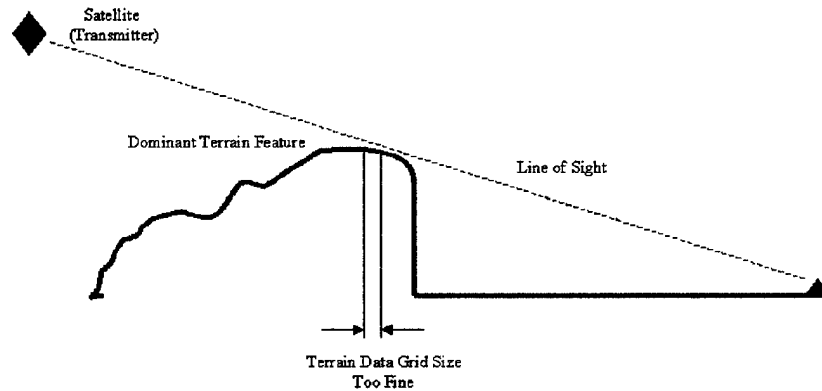


*Figure 3-5: Curvature Considerations With a Fine Terrain Grid*

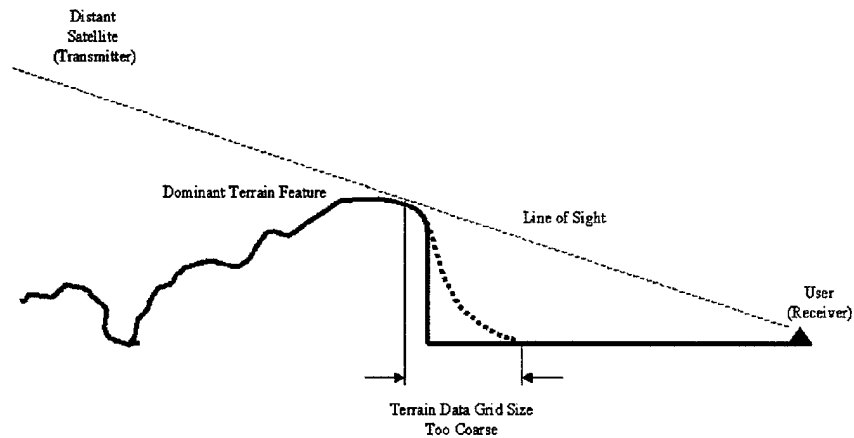


*Figure 3-6: Curvature Considerations with a Coarse Terrain Grid*

A compromise solution is implemented based on comments contained in [Ass71]. Assis states that the rounded obstacle model need only approximate the curvature of the dominant feature ‘in the vicinity of the feature peak’ and not necessarily in the direction of



signal propagation. Calculation of the curvature in the northerly and easterly directions is derived, relatively simply, from Wilson's interpolation. The larger of these two values is then assumed to be the curvature of the feature, yielding an approximation for the worst-case terrain diffraction.

### **3.5.2 The User Sites**

Simulations are conducted for users located at Panama (8°58' N, 79°33' W), Killen (31° N, 97° W), and Anchorage (61°13' N, 149°54' W). These sites are chosen to ensure the performance of the constellations can be evaluated in areas where research suggests performance changes might occur. Varying the location of a user between the 0° and 70° latitudes is considered critical to the performance evaluations. The selection of user location is also a valuable consideration from both a commercially viable and practical point of view. The period of simulation selected ensures that the analysis is insensitive to a user's longitude.

### **3.5.3 The Constellations**

Current satellite position information, derived from the NORAD two line element sets for each of the constellations, are downloaded from [Nor00] and imported directly into SOAP. Only the unique NORAD identifier field for each satellite, or satellite name, is changed prior to importing the data. This allows for a simplified naming scheme to be used throughout the simulation process. Communications parameters are then defined and assigned to each satellite based on the research presented in Chapter 2 and in [Glo01]. The required parameters are summarized in Table 3-1.

*Table 3-1: Communications Parameters for the Three Constellations*

	<b>Iridium</b>	<b>Globalstar</b>	<b>Orbcomm</b>
Half Cone Angle (Degrees)	62	53	67.1
Transmit Frequency (GHz)	1.6	2.46	0.1375
Maximum Transmitted EIRP (dBW)	15.7	2.8	12.5
Required Received EIRP (dBW)	- 151.5	-171.4	- 143.8

### **3.5.4 Period of Simulation**

With the constellation model in place, a period of simulation must be selected to correctly represent all relevant characteristics and events. The ideal situation is to determine the period for the constellation to repeat, or the time required for each satellite to return to the same point in the sky at the same time of day. This occurs when an integer number of satellite orbits coincides with an integer number of sidereal days.

Using Iridium as an example, the constellation is at an altitude of 785 km and the period of each orbit is approximately 6021 seconds. The number of orbits required to get each Iridium satellite within 500 seconds of their original starting point above the earth surface would be 2467, which is the equivalent of 171 days 23 hours and 40 minutes of simulation time. Simulations for durations such as these are beyond the capabilities of the software packages and would require an inordinate amount of processing time and disk space to complete. Instead, a representative simulation period can be determined and analyzed.

The statistical analysis conducted by Crowe [Cro99] demonstrated that a 24-hour simulation period was adequate to represent the performance of the Iridium constellation.

Based on these results, a simulation period of 48 hours or 172,800 seconds is selected. Several sample periods are used to determine the optimum number of observations for each visible satellite. The results of this analysis are presented in Chapter 4.

### **3.5.5 The Sampling Interval**

The following reasoning is applied for selecting a suitable interval for sampling the location of satellites in each constellation:

- a. The sample interval chosen should seek to provide a balance between the resolution achieved and the resource requirements produced by a corresponding simulation.
- b. The solution also needs to consider the resolution limitations imposed by the use of the notional terrain data set. The azimuthal resolution of the data set is  $0.1^\circ$ .
- c. The interval should be based on the requirements of the fastest moving satellites, those contained in the Orbcomm constellation. At an altitude of 775 km, these satellites travel at approximately 7.46 km/s [Wer99].
- d. The slant range to a satellite in the Orbcomm constellation, at low elevation, is approximately 3240 km [Wer99]. At this range, the satellites could travel 6.480 km between samples and achieve a  $0.1^\circ$  azimuth resolution. The time taken for a satellite to transit 6.480 km is approximately 0.9 seconds.
- e. If a sample interval of one second is chosen, approximately 1 Gbyte of data is required to represent the Iridium constellation over a two-day simulation period. Resourcing these simulations poses considerable concerns and limits the effectiveness of the method as a planning tool in a tactical environment.

- f. A sample interval of five seconds is therefore chosen, primarily to avoid considerable data storage and processing overheads, while providing a reasonable azimuthal resolution. The azimuthal resolution achieved between samples for the constellation is approximately  $0.5^\circ$ .

### 3.6 Establishing the Baseline

Figure 3-7 describes the process used to establish the baseline propagation information.

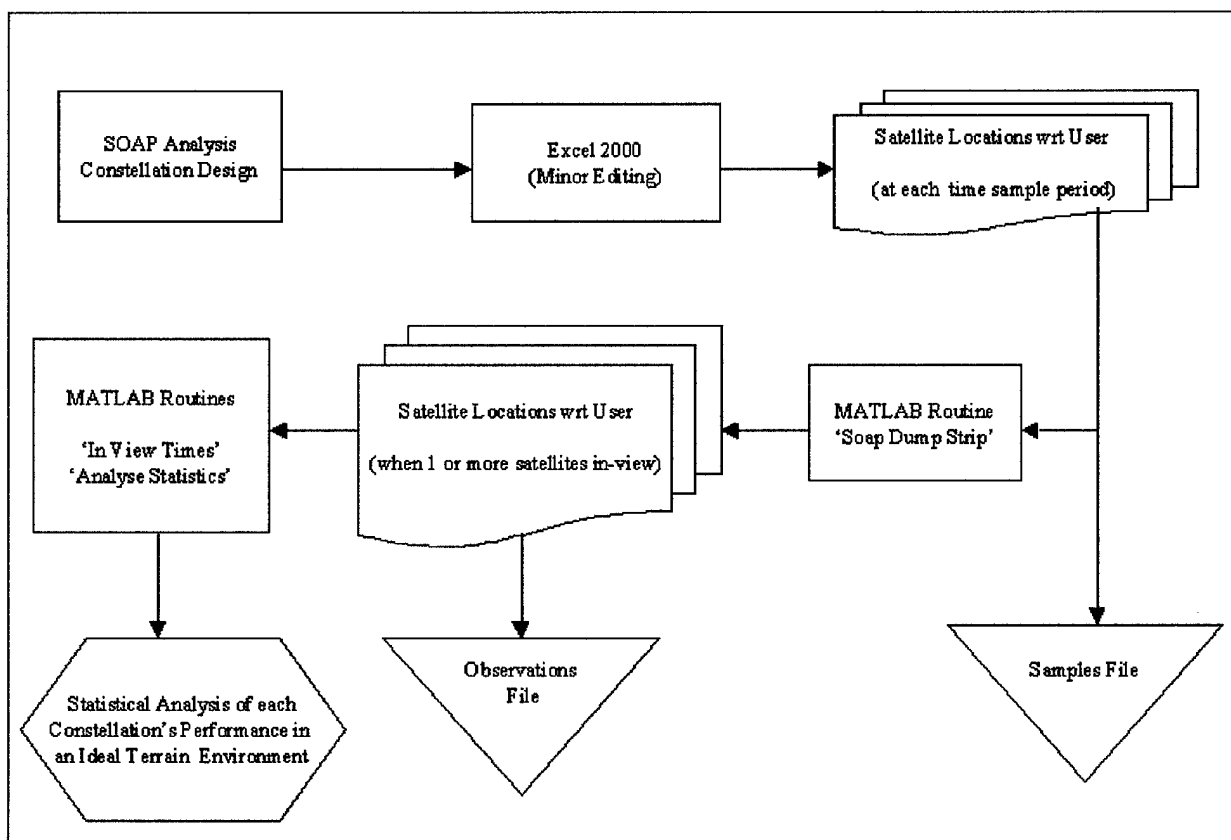


*Figure 3-7: The Process Used to Establish the Baseline*

### 3.6.1 Generating the Initial SOAP Observation Reports

The SOAP package is configured to generate path geometry reports for use as an input to the routines used later in the simulation process. The analysis identifies the location of each satellite in a given plane at five-second intervals and whether a user at the selected site has satellite visibility. Note that all of the satellite observations are given with respect to the position of the user.

#### 3.6.1.1 The Samples Report

Sample reports are limited to a single plane rather than the entire constellation. This reduces the size of the output file being handled at each simulation stage. A typical report for one of the six Iridium planes covering observations made every five seconds over a two-day simulation period contained over 30 Mbytes of data. Minor formatting changes are made to this baseline data set using tools available in EXCEL 2000. This ensures that the files can be directly imported into MATLAB. The changes include the removal of title and column headings, and the conversion of observation values to a Boolean format (i.e., '1' if in-view and '0' otherwise). The format of this 'samples' report is shown in the example provided at Table 3-2, based on the first five entries for the satellites in Orbcomm Plane number five.

Table 3-2: The Samples Report Format

Sample Time (Seconds)	Sample Data for Satellite 1				Sample Data for Satellite 2			
	In-View (Boolean)	Azimuth (Degrees)	Elevation (Degrees)	Range (Km)	In-View (Boolean)	Azimuth (Degrees)	Elevation (Degrees)	Range (Km)
0	0	356.40	-33.36	8393	0	173.47	-52.91	11150
5	0	356.53	-33.51	8418	0	173.61	-52.76	11132
10	0	356.66	-33.67	8443	0	173.75	-52.61	11114
15	0	356.79	-33.83	8468	0	173.89	-52.46	11095
20	0	356.92	-33.99	8493	0	174.03	-52.31	11077

### 3.6.1.2 The Observations Report

A MATLAB routine, 'Soap\_Dump\_Strip', scans the SOAP output file and extracts range, azimuth, and elevation data for those satellites that are in-view of the selected receive site, as well as the time of each observation. The file format is then changed so that observations are only recorded at times when at least one satellite is in view of the receiver. If no satellite is in view at a particular time no entry is made in the file. When at least one satellite is in-view the observation details and time are recorded to file. This change in file format reduces the average size of an output file to 1 Mbytes. This simplifies file-handling procedures while retaining all of the observation data about the constellations. An example of the abbreviated 'observations' report, based on the first five entries for the satellites in Orbcomm Plane number 5, is provided at Table 3-3.

Table 3-3: The Observations Report Format

Observation Time (Seconds)	Observation Data for Satellite 1			Observation Data for Satellite 2		
	Azimuth (Degrees)	Elevation (Degrees)	Range (Km)	Azimuth (Degrees)	Elevation (Degrees)	Range (Km)
1685	0	0	0	250.17	0.016	3399
1690	0	0	0	250.76	0.13	3387
1695	0	0	0	251.35	0.25	3374
1700	0	0	0	251.96	0.36	3363
1705	0	0	0	252.56	0.471	3351

### 3.6.1.3 Analyzing the Observations

A final MATLAB routine, 'Analyze Statistics', scans the observation data and produces a number of reports that summarize the performance of the constellations in this

idealized terrain environment. These reports provide a baseline against which variations in availability and other statistics, associated with the application of the notional terrain, can later be compared. The statistics compiled and conclusions drawn from the analysis are provided at Chapter 4.

### 3.7 Modeling Terrain Diffraction Effects with Knife-Edge Obstacles

Figure 3-8 describes the process used to model the diffraction effects from terrain modeled as knife-edges.

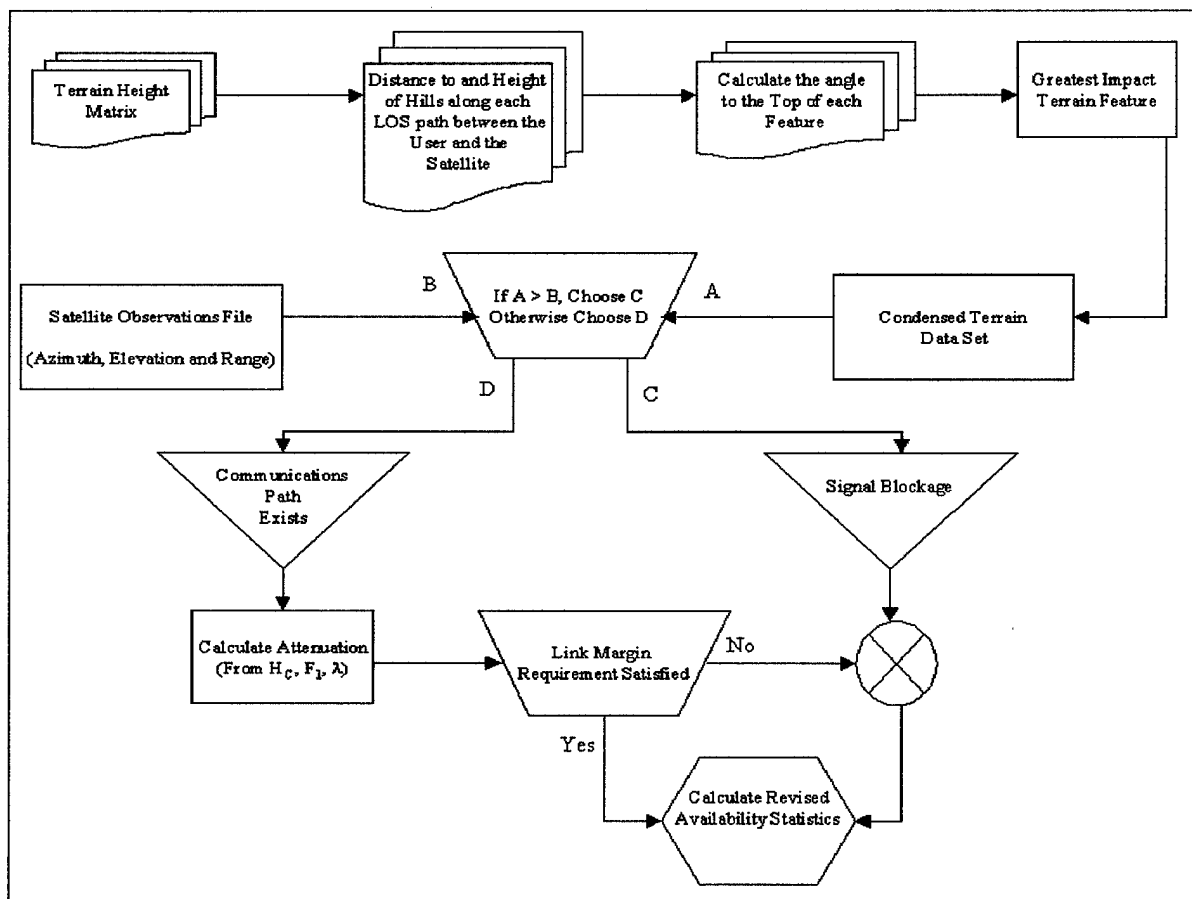
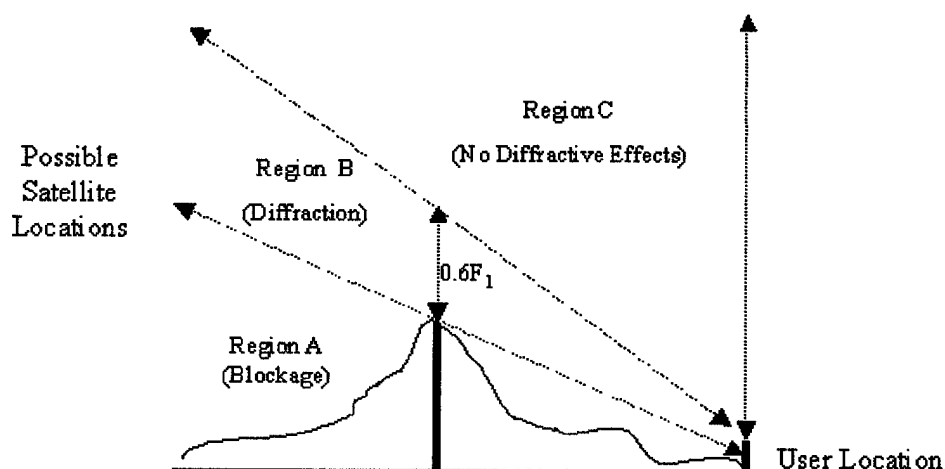


Figure 3-8: The Process Used to Model Terrain as Knife-Edge Obstacles

The MATLAB routine, 'In\_View\_Times', performs the main collation and signal path analysis functions. The routine accesses the location (azimuth and elevation) details of each satellite, for observations made over the simulation period, and compares these to the details of the dominant terrain feature along the relevant azimuth. Three categorization regions are defined depending on whether blockage, diffraction or no diffractive effects will occur. The attenuation reported is determined by the region in which an observation is made. The regions are depicted in Figure 3-9.



*Figure 3-9: Satellite Observation Categorization Regions Applied in the Model*

If the elevation angle to the peak of the dominant terrain feature is greater than the elevation angle to the satellite, the satellite is in Region A and no line-of-sight communications path exists. Under these conditions, the user is deemed to be unable to establish or maintain a communications link to the satellite in question. Such outages are not due to 'diffractive' effects, but rather a total blockage of the signal.

For those cases where a line-of-sight path does exist between the user and the satellite, the signal path clearance over the dominant peak,  $h_c$ , and the Fresnel radius



corresponding to the location of that peak,  $F_1$ , are calculated. If the clearance is less than  $0.6 (F_1)$ , the satellite is in Region B and the expected attenuation due to diffraction is calculated using the knife-edge model equations described in Chapter 2. If the resultant received signal power is less than the specified power required at the receiver, the satellite is deemed 'not in-view' at that observation time. If the clearance is greater than  $0.6 (F_1)$ , the satellite is in Region C and the model assumes that there is no diffractive attenuation effect.

The MATLAB routine 'Analyze\_Statistics' is again used to scan the modified observation data and produce reports, summarizing the performance of the constellations in the notional terrain environment. Availability statistics and other conclusions drawn from the comparisons are provided at Chapter 4.

### **3.8 Modeling Terrain Diffraction Effects with Rounded Obstacles**

The process used to model diffraction effects from terrain modeled as rounded obstacles is similar to that used in the knife-edge case. This process is described in Figure 3-10. The primary differences between the knife-edge and rounded obstacle processes are as follows:

- The curvature parameter  $\alpha$  is calculated and applied in the 'In View Times' routine.
- Another MATLAB routine, 'Curvature', is created to determine the average curvature of the top of the dominant feature. Wilson's [Wil98] cubic interpolation and the curvature equations outlined in Chapter 2 are used as the basis for determining the average curvature in the northerly and easterly directions. The larger of these values is stored in the terrain curvature matrix and used to approximate the attenuation due to diffraction, using the rounded obstacle model relationship depicted in Figure 2-3.

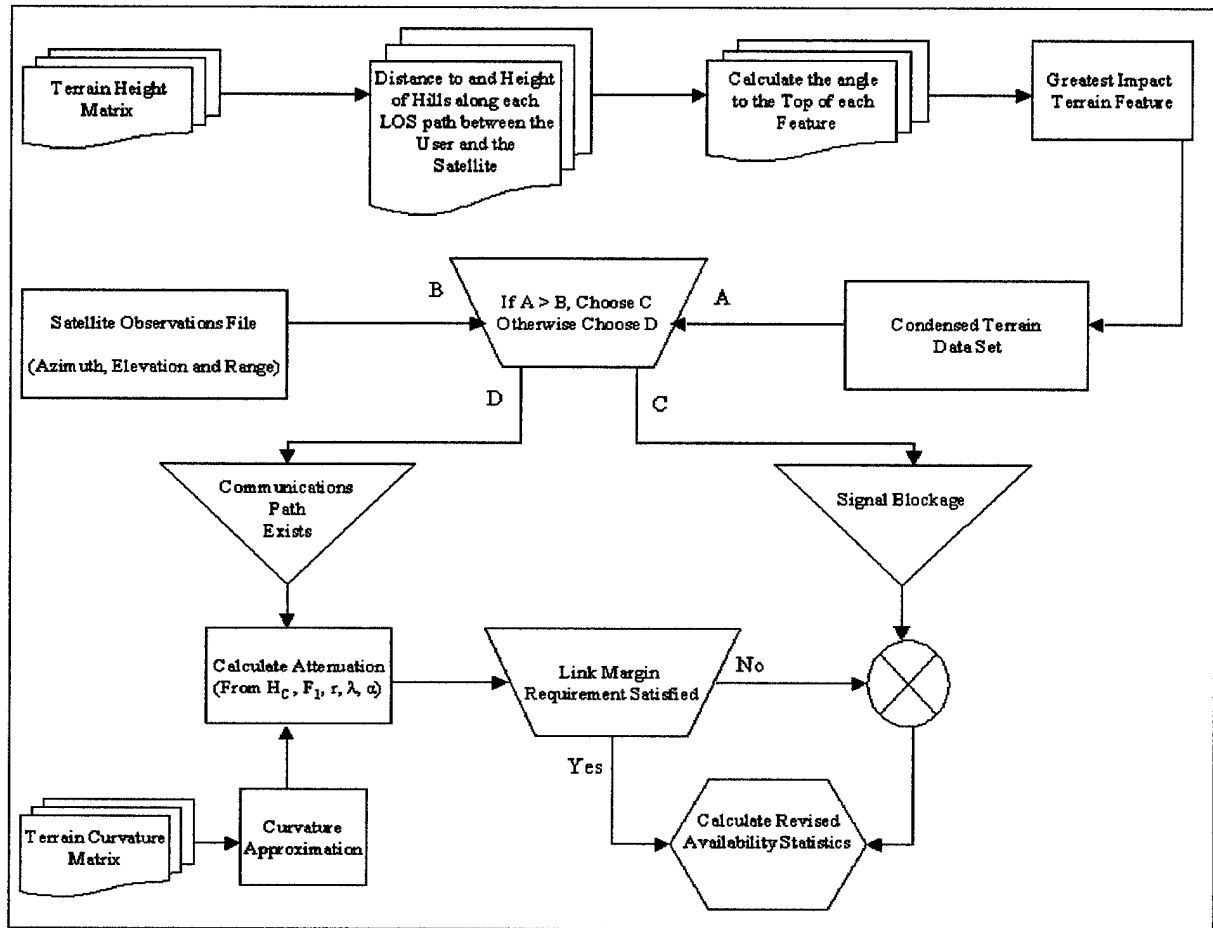


Figure 3-10: The Process Used to Model Terrain as Rounded Obstacles

Comparison of the received signal power to that specified as being required for the given constellation again determines whether a given satellite is deemed 'in-view' at each observation. The MATLAB routine, 'Analyze Statistics', is again used to scan this modified observation data and produce reports, summarizing the performance of the constellations in the notional terrain environment. Availability statistics and other conclusions drawn from the comparisons are provided at Chapter 4.

### 3.9 Verification and Validation

The majority of the theory applied in this thesis is widely accepted as being valid when applied in a ground-to-ground communications channel. Jang [Jan97] also confirmed the validity of using knife-edge obstacles to model terrain diffraction in an air-to-ground communications channel. This thesis combines the results of Jang's thesis [Jan97] with the work done by Wilson [Wil98] on terrain modeling as the basis for extrapolating the knife-edge terrain diffraction model to a space-to-ground communications channel. Expanding the analysis to include rounded obstacles does not detract from the validity of the models as the approach employed in this thesis is also widely accepted as a valid tool in the ground-to-ground communications environment as noted in Chapter 2. As such, validation of most of the processes employed has already been undertaken.

Separate or complete validation of the methods employed within this study and of the results obtained would generally require the deployment of test equipment to the user sites to record appropriate test data. The experimental results could then be compared to simulation results contained in this report to confirm the analysis and models correctly simulate the expected performance of each LEO constellation. Resource constraints prevent the application of such an approach so none of the methods applied in this analysis are subject to complete validation.

Verification processes have been conducted at nominated points to ensure each model functions as intended and that there are no coding or logic errors. Three primary means of verification have been applied:

- First, each algorithm and set of code is compared to the relevant work published by Jang, Wilson, Deygout, and Assis. Whenever possible, consistency in variable

assignments with those provided by these authors is maintained and direct importation of routines is undertaken. Appropriate acknowledgements have been made in any routine where such importations have been possible.

- Second, a known test data set is applied to each routine prior to incorporation of the routine into the models. The test data is chosen to verify the correct functioning of the routine given a variety of states and, in particular, for critical boundary states or input parameter values.
- Finally, manual calculations are undertaken to determine a known baseline for some of the parameters or output states. The results provided from the models are then inspected and tested for consistency within the entire result set and against those manual calculations performed.

There has been no attempt to verify the performance of any of the commercial packages used in the modeling process.

### **3.10 Summary**

This chapter described the objectives, methodology, processes and assumptions underlying the research. Several specialized routines have been developed to process, analyze and present the data required in the analysis. The reason these routines were required and appropriate descriptions of the functions performed by them have also been provided. Finally, the compromises and assumptions that were necessary to limit the scope of the work and the resources required to achieve the desired outcome were described. With the processes and methodology described, the results of the research can now be presented.

## **CHAPTER 4**

### **ANALYSIS AND PRESENTATION OF RESULTS**

#### **4.1 Introduction**

The purpose of this chapter is to present the results of the analyses used to characterize the performance of the three constellations in a terrain diffraction environment. The expected performance of each of the constellations, based on the theory presented in Chapter 2, is outlined. The ideal environment simulation results are then presented and compared with the expected results from the theoretical analyses. This comparison is performed to verify the performance of the constellation models and the results then used as a basis for predicting the expected performance when terrain diffraction is present on the communications path.

Further simulations are then conducted to include the effects of the notional terrain using the knife-edge and rounded obstacle models developed over the course of this investigation. The results from these simulations are then presented and compared to the performance predictions that were made and based on the ideal terrain simulation results. This approach contributes to the verification of the models.

The notional terrain landscape is also analyzed to determine the influence the landscape has on the results presented. Significant considerations in the use of the knife-edge and rounded obstacle terrain models are also highlighted. Finally, the results are summarized in a comparative analysis of the Iridium, Globalstar, and Orbcomm communication systems.

## **4.2 The Need for Defined Performance Measures and Simulations**

With 66 satellites, Iridium has a 37.5% higher satellite count than Globalstar and an 88.6% higher count than Orbcomm. In a cursory analysis, Iridium might then be considered to provide the best coverage if the assessment criteria applied is the percentage of the earth surface actually viewable by the constellation at any given point in time.

However, further analysis shows that a maximum of 51 Iridium satellites are located within the latitudes of interest for this study (approximately  $\pm 70^\circ$ ). Even so, the system still offers a considerable increase in the number of satellites able to view this portion of the earth surface over that of Orbcomm, but only a small increase over that afforded by Globalstar. However, the Iridium satellites are also at a considerably higher inclination angle than all of the Globalstar satellites and most of the Orbcomm satellites. These additional considerations show that predicting the relative performance of the three systems requires the definition of measures against which each system's performance can be evaluated. Only the performance of the individual constellations, relative to latitude rather than to each other, can be predicted from the theory without the aid of simulation.

### **4.2.1 Required Inputs to the Simulations**

Constellation design (including altitude, inclination, and the number of satellites in each plane) and communication link parameters are the primary factors used to determine the communications path characteristics in this study. Details of the constellation designs were presented in Chapter 2, as well as information relating to the communication link budgets. The ideal environment analyses have been based on these inputs.

### 4.2.2 Performance Measures

The measures applied to each of the constellations in assessing the quality of coverage provided include the average number of satellites in view, the number and duration of outages, and the overall system availability. The simulations show that these measures are latitude dependent for each of the constellations although the cause of particular variations and dependencies is not always immediately obvious.

### 4.2.3 Iridium

#### 4.2.3.1 Theoretical Performance Analysis

Iridium is a symmetric constellation of six planes containing eleven evenly spaced satellites with each plane inclined near  $90^\circ$ . Figure 4-1 illustrates the symmetric nature of the Iridium orbit paths.

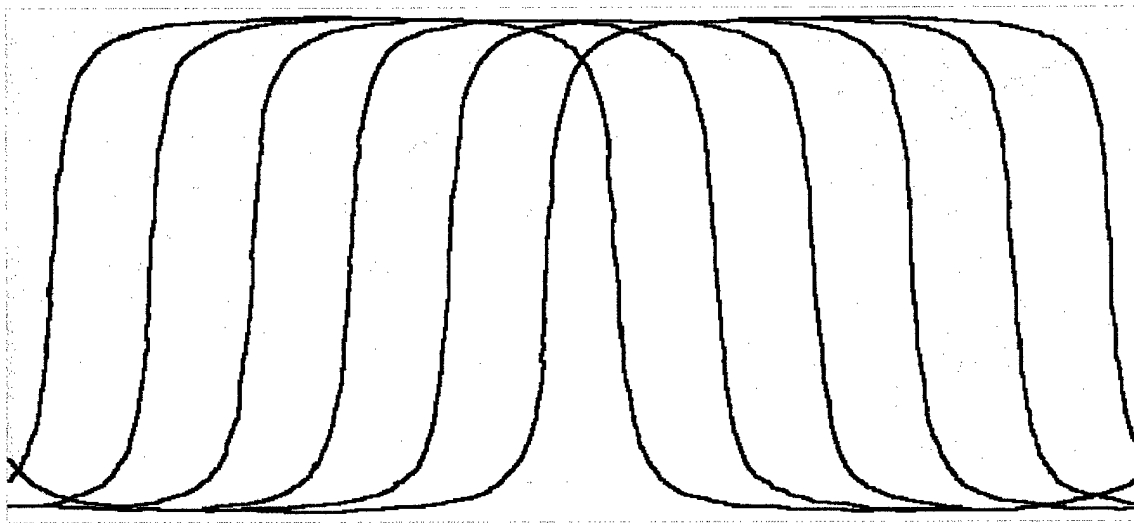


*Figure 4-1: The Iridium Orbits (Instantaneous View)*

The Iridium constellation should provide better coverage at high to middle latitudes where satellites in the constellation will be 'closer' to each other, maximizing the

communications footprint overlap. Similarly, the system should provide poorer coverage at lower latitudes, especially for users located close to the equator. The simulation of an ideal environment terrain was conducted using the SOAP and the results are summarized in Table 4-1.

*Table 4-1: Ideal Environment Simulation Results for the Iridium Constellation*

<b>Ground Station Location</b>	<b>Average Number of Satellites in View</b>	<b>Number of Outages</b>	<b>Maximum Outage Duration (s)</b>	<b>Average Outage Duration (s)</b>	<b>Availability (%)</b>
Anchorage (61°13', -149°54')	2.794	5	50	30	99.91
Killeen (31°, -97°)	1.510	14	455	275	97.77
Panama (8°58', -79°33')	1.324	17	490	333	96.72

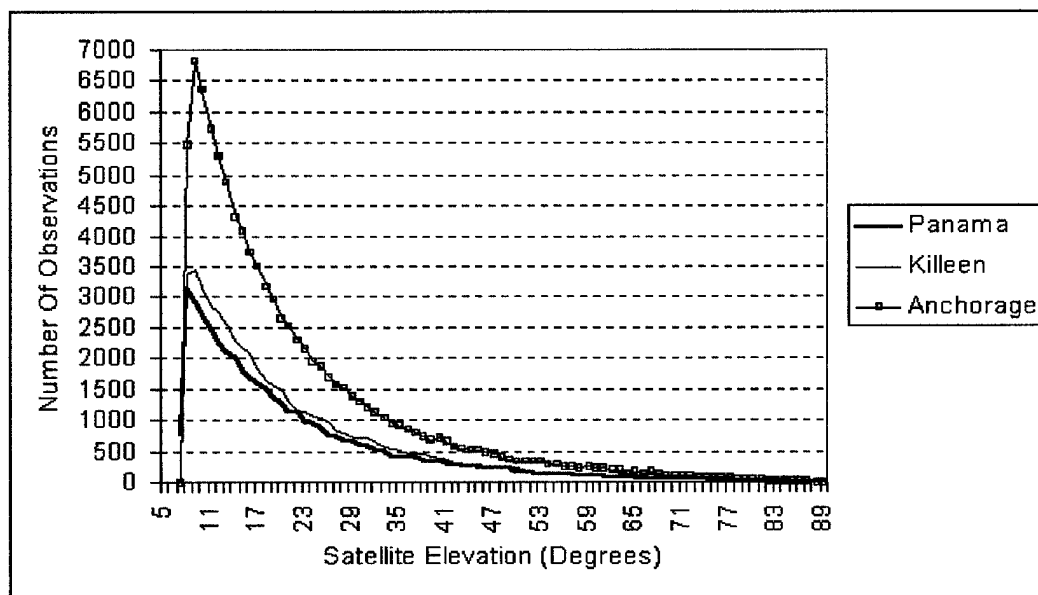
#### ***4.2.3.2 Ideal Terrain Environment Simulation Performance Analysis***

The simulation confirms the predictions of the theory-based analysis. The performance of the Iridium system improves with increasing latitude, achieving 99.91% availability and an average of 2.8 satellites in-view for users located at Anchorage. A reduction in quality of coverage is evident for users located at Panama and is best displayed by the result for system availability which falls to 96.7%, and by the average number of satellites in-view which falls to 1.3. However, the parameter that perhaps provides the most noticeable indication of Iridium's performance decline is the duration of the maximum outage, which increases from 50 seconds for users at Anchorage to approximately 8.2 minutes for users located at Panama.



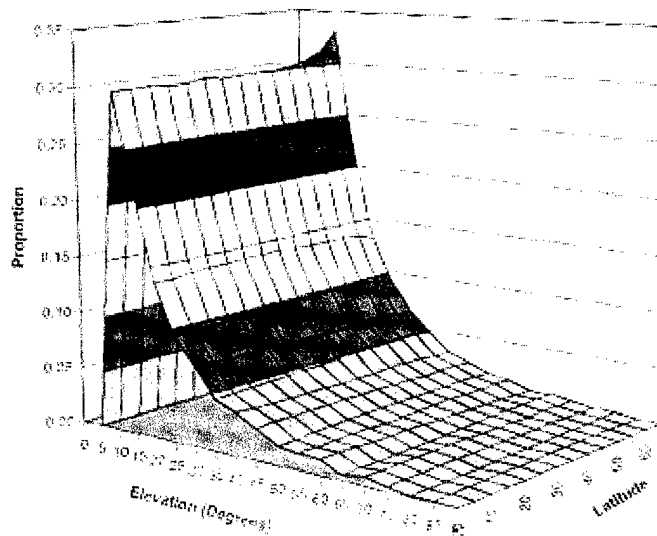
#### 4.2.3.3 Predictions Drawn From the Observation Data

Figure 4-2 shows the distribution of observations made to the Iridium satellites from each of the user sites over the two-day simulation period. The total number of observations increases as a user moves to higher latitudes and the number of higher elevation observations also improves with increasing latitude. There is also a particularly significant increase in total observations between those reported for Killen and Anchorage. This analysis suggests that users of the Iridium system situated at higher latitude locations are likely to be less affected by terrain diffraction than users situated at lower latitudes. This is to be expected since the constellation has a polar orbit, where the inter-planer satellites converge.



*Figure 4-2: Iridium Satellite Observations Made Over the Two-Day Simulation Period*

The results of the simulation closely match the detail provided in the probability density functions derived in Crowe's analysis of the Iridium system [Cro99]. This is shown in Figure 4-3 and verifies the models developed in this study function correctly.



*Figure 4-3: PDFs of Iridium Elevation Angles (Equator to 60 degrees Latitude) [Cro99]*

## **4.2.4 Globalstar**

### **4.2.4.1 Theoretical Performance Analysis**

Like Iridium, Globalstar is a symmetric constellation of eight planes inclined at  $52^\circ$ , containing six evenly spaced satellites within each plane. The inclination chosen means that the Globalstar coverage is optimized for users operating in the middle latitudes, encompassing significant population areas in the US and Europe. The constellation therefore targets users within the  $\pm 70^\circ$  latitudes and offers no potential for coverage to users above the  $80^\circ$  latitude.

At an altitude of 1410 km, each satellite provides a substantially larger footprint than those of the Iridium constellation. However, this improvement is offset to some extent by the higher free-space path losses associated with the higher altitude orbit. Figure 4-4 illustrates

the symmetric nature of the Globalstar orbital paths and the area of coverage afforded by the system.

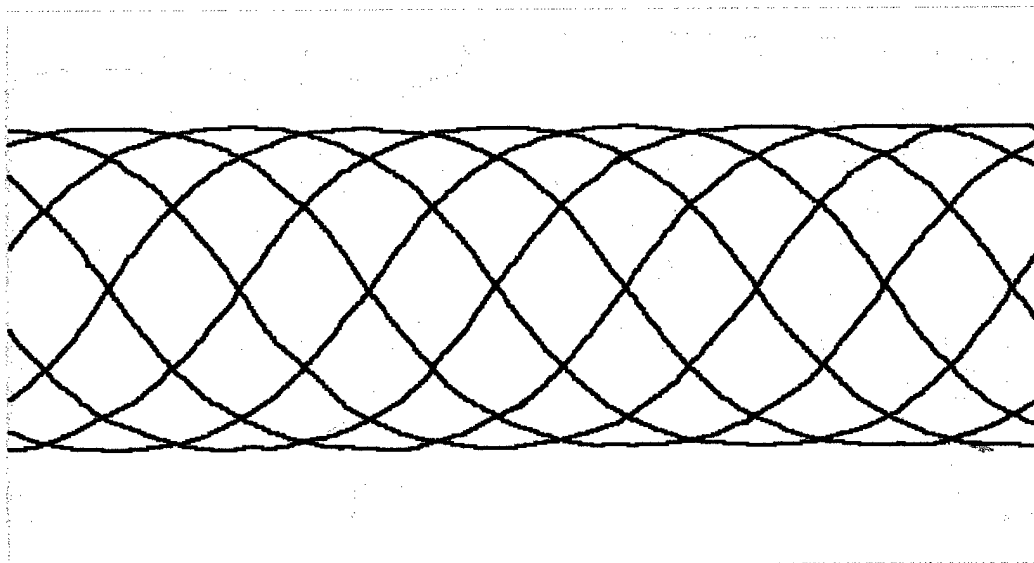


*Figure 4-4: The Globalstar Orbits (Instantaneous View)*

#### **4.2.4.2 Ideal Terrain Environment Simulation Performance Analysis**

The simulation of an ideal terrain environment was conducted using the SOAP. The results of the simulation are summarized in Table 4-2.

*Table 4-2: Ideal Environment Simulation Results for the Globalstar Constellation*

<b>Ground Station Location</b>	<b>Average Number of Satellites in View</b>	<b>Number of Outages</b>	<b>Maximum Outage Duration (s)</b>	<b>Average Outage Duration (s)</b>	<b>Availability (%)</b>
Anchorage (61°13', -149°54')	2.602	0	0	0	100
Killeen (31°, -97°)	3.601	0	0	0	100
Panama (8°58', -79°33')	2.533	0	0	0	100

The simulation again confirms the predictions of the theory-based analysis. While no outages were reported, the average number of satellites in-view peaked for users located at Killeen, the mid latitude site. Given that the number of paths between the user and the space segment increases as the number of satellites in-view increases, the probability of establishing a viable communications link at the Killeen site is higher than that of the other sites [Cro99]. This result confirms that the Globalstar system is likely to perform better at middle latitudes and poorer at the extremes of  $0^\circ$  and  $\pm 70^\circ$ .

#### ***4.2.4.3 Predictions Drawn From the Observation Data***

Figure 4-5 shows the distribution of observations made to the Globalstar satellites from each of the user sites over the two-day simulation period. The total number of observations peak for users located at middle latitudes. In this case, the middle latitudes are represented by the Killeen data.

As a user moves away from the middle latitudes the total number of observations made decreases, as does the number of higher elevation observations. This analysis suggests that users of the Globalstar system situated at middle latitude locations are likely to be less affected by terrain diffraction because more observations are made to satellites at higher elevations. The results also indicate the effect of the notional terrain is likely to be most severe at Panama which reports the lowest number of total observations and a higher proportion of these at or below  $15^\circ$  elevation.

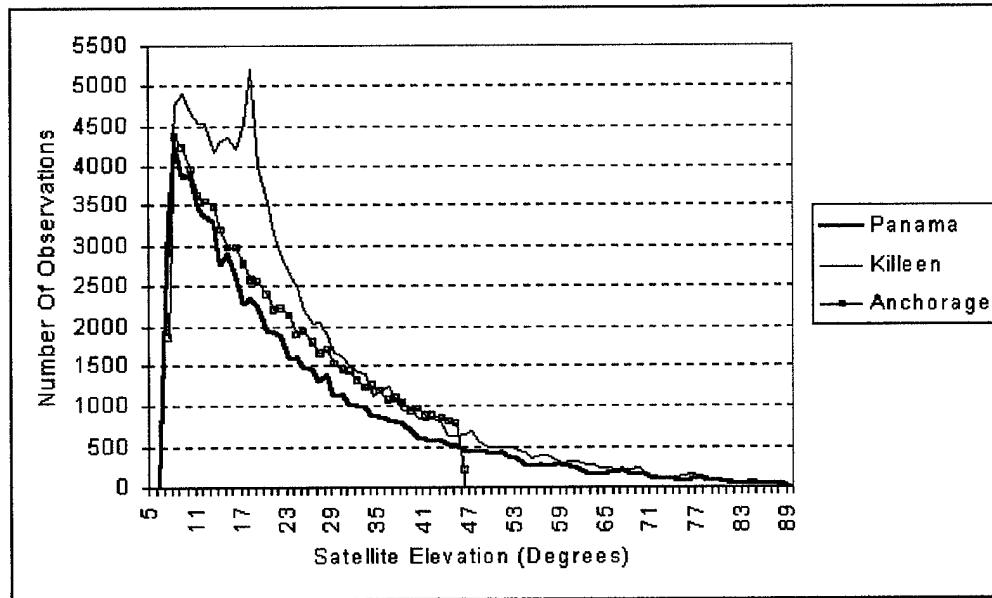


Figure 4-5: Globalstar Satellite Observations Made Over the Two-Day Simulation Period

The details provided in this analysis again correlate with those provided in the probability density functions derived in [Cro99]. This function is shown in Figure 4-6 and verifies that the Globalstar model developed in this study functions correctly.

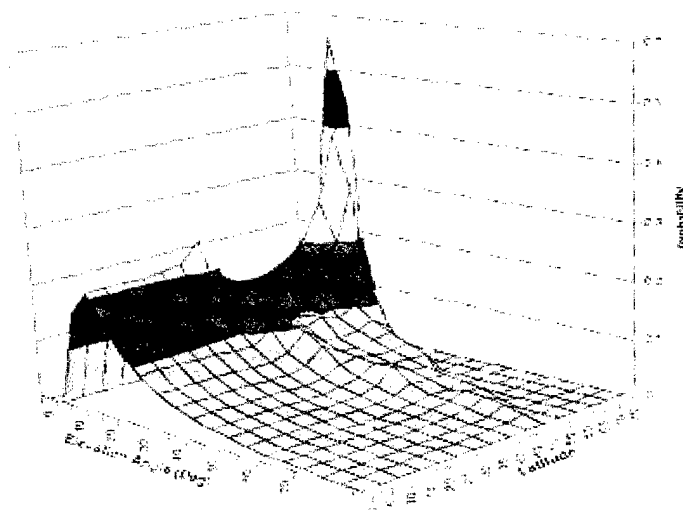


Figure 4-6: PDF of Globalstar Path Elevation Angles [Cro99]

## 4.2.5 Orbcomm

### 4.2.5.1 Theoretical Performance Analysis

The number of satellites in each Orbcomm plane varies from two to eight satellites with the intra-planar satellite spacing being non-uniform. With a total of 35 satellites located at an altitude of 775 km, the coverage provided by the system for users located between the latitudes of  $\pm 70^\circ$  might be expected to be poorer than that afforded by Iridium or Globalstar. Simply, fewer satellites are available to provide coverage to the same area of the earth's surface. However, as four of the Orbcomm planes are inclined at  $45^\circ$  the constellation might actually provide better coverage at middle to lower latitudes than either Globalstar or Iridium. Since Orbcomm also has two planes inclined near  $90^\circ$  each containing two satellites, the performance achieved at higher latitudes may be better than that of Globalstar. Figure 4-7 shows the non-uniform spacing of the satellites in the planes.

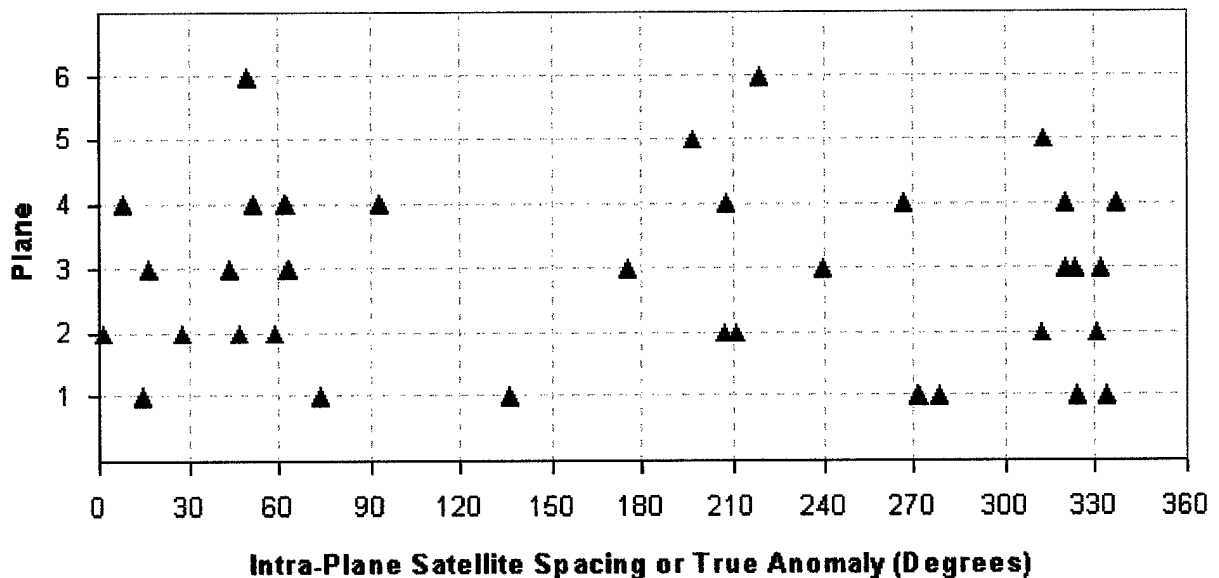
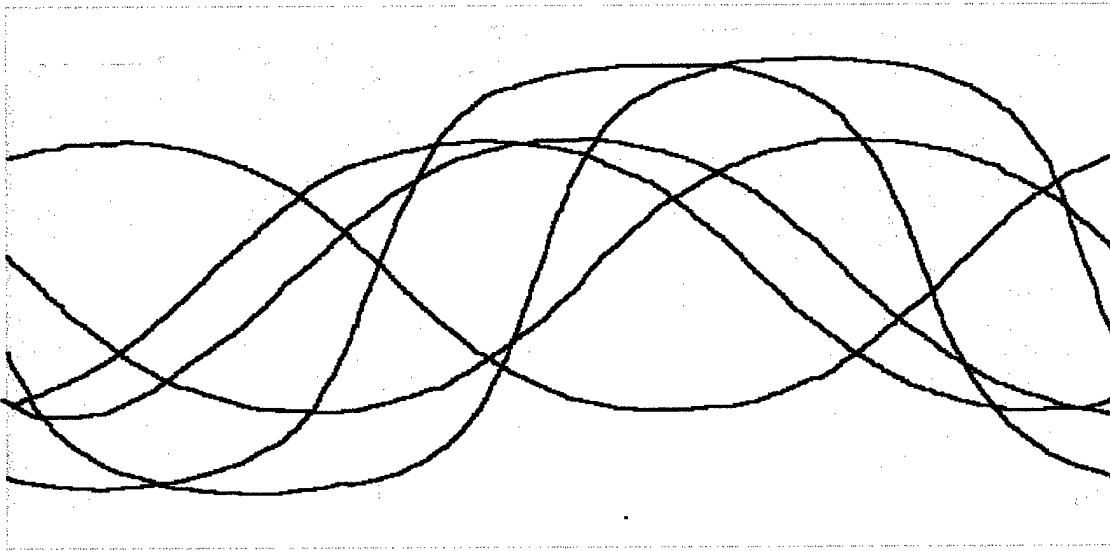


Figure 4-7: Orbcomm Satellite Spacing

Figure 4-8 shows that, unlike the Iridium and Globalstar constellation designs, the Orbcomm constellation design is not symmetrical. Additionally, the higher inclination planes are unlikely to provide significant performance improvements at the latitudes being considered in this study (e.g., Anchorage is at the highest latitude of 61° N).



*Figure 4-8: The Orbcomm Orbits (Instantaneous View)*

Orbcomm also operates at VHF frequencies rather than frequencies in the L or S-band, so the expected free-space path loss is considerably less than that specified in the Iridium and Globalstar link budget. The communications footprint achieved (equated to potential for coverage) is also substantially larger. This is partially due to the use of lower operating frequencies.

Analysis of all of these factors indicates that the Orbcomm system is optimized for middle latitude users. However, the performance achieved is not likely to be as uniform or predictable as that of the Iridium or Globalstar systems due to the more random nature of the Orbcomm constellation design.

#### 4.2.5.2 Ideal Terrain Environment Simulation Performance Analysis

The simulation again confirms the predictions of the theory-based analysis and, in particular, that Orbcomm performs better at middle to lower latitudes. Table 4-3 summarizes the simulation results obtained for the ideal environment.

*Table 4-3: Ideal Environment Simulation Results for the Orbcomm Constellation*

<b>Ground Station Location</b>	<b>Average Number of Satellites in View</b>	<b>Number of Outages</b>	<b>Maximum Outage Duration (s)</b>	<b>Average Outage Duration (s)</b>	<b>Availability (%)</b>
Anchorage (61°13', -149°54')	1.405	107	595	226	86.00
Killeen (31°, -97°)	2.463	26	260	160	97.59
Panama (8°58', -79°33')	1.912	49	845	217	93.83

Orbcomm provides best coverage at middle latitudes with an average in-view satellite count of almost 2.5 reported for Killeen. This result approaches the average count of approximately 2.8 achieved by Iridium and 2.6 achieved by Globalstar at Anchorage, for an availability of 99.91% and 100% respectively. There is, however, a 'discrepancy' in this statistic attributable to the more random nature of the Orbcomm constellation design.

There are significant periods where no satellites are in-view but this is offset by other periods where multiple satellites are in-view. Averaging the results over the entire simulation period produces a misleading statistic in the 'average number of satellites in-view' for Orbcomm. For this reason, the maximum outage duration and total number of outages reported provide better measures of the actual performance of the Orbcomm system.

The maximum outage duration for Orbcomm users at Killeen is 260 seconds. This is almost one half the maximum outage reported for Iridium users at the same location.



However, the total number of outages reported is 26. This almost doubles the number of outages reported for Iridium. The results follow a similar trend for users located at Panama, where the average number of satellites in-view is approximately 1.9. However, the maximum outage duration has increased to 14.1 minutes and the number of outages to 49. Therefore, Orbcomm users are likely to encounter more, but shorter duration, outages than Iridium users at locations in the low to middle latitudes, resulting in an overall availability of 93.8%.

Finally, the simulation verifies that low latitude users have better system coverage than those at higher latitudes. The average number of satellites in-view falls to 1.4 (almost half that reported for Killeen) and the availability falls significantly to 86%. However, the corresponding result for maximum outage duration (595 seconds / 9.9 minutes) is considerably better than the maximum reported for Panama (14.1 minutes) and again appears to contradict the overall trend of a decline in performance. The improvement can be attributed to the 'fleeting' influence of the satellites in planes five and six, which are inclined at 90°. These satellites provide brief periods of coverage at Anchorage when satellites in planes one through four provide no coverage.

The net result is a significant reduction in the maximum outage duration reported and a corresponding increase in the number of outages. Further analysis is required to determine the extent to which the coverage afforded by the satellites in planes five and six can support the connection and maintenance of a communications link for users located at Anchorage.

#### ***4.2.5.3 Predictions Drawn From the Observation Data***

Figure 4-9 shows the distribution of observations made to the Orbcomm satellites from each of the user sites over the two-day simulation period. Like Globalstar, Orbcomm shows a significant increase in the number of observations to satellites and in the number of

higher elevation observations reported for users located at the middle latitudes. This increase can be attributed to the influence of the satellites in the 45° inclined planes one through four. The significant decrease in the total number of observations from approximately 6800 for Iridium and 5700 for Globalstar to just 3600 for Orbcomm gives an additional indication that Orbcomm is not likely to perform as well as the other systems when terrain diffraction mechanisms are included in the simulation. Lower elevation satellites are more likely to be blocked from view by terrain obstacles or have their performance attenuation limited.

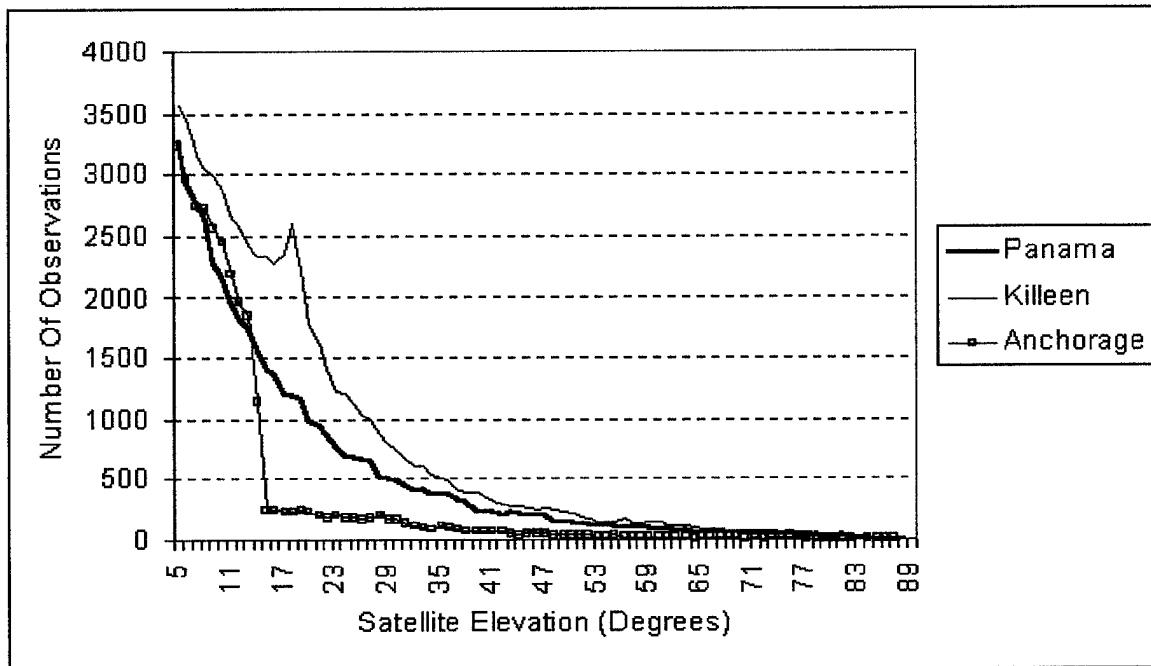


*Figure 4-9: Orbcomm Satellite Observations Made Over the Two-Day Simulation Period*

The results also indicate that the impact of terrain diffraction is most severe at Anchorage, and may be significant at Panama, especially if the terrain profile contains a large proportion of peak elevations above 13°. As Crowe did not include Orbcomm in his analysis, a comparison of the Orbcomm results is not possible.

### 4.3 The Notional Terrain Profile Applied in the Simulations

A notional terrain data set was created with the intention of ensuring that terrain diffraction is a significant consideration in the simulations. A significant proportion of observations made in the ideal terrain environment analyses are for satellites at or below elevation angles of  $20^\circ$ . The multiplication factor applied to the Killeen data set aims to produce a profile that tests to this boundary elevation condition.

Terrain profiles have been produced using multiplication factors of 10, 15, 20, 25 and 30 applied to the unclassified NIMA data set. A multiplication factor of 20 produces a terrain profile with feature peak elevations ranging between  $0^\circ$  and  $19^\circ$ , with a concentration of feature peak angles in the range of  $5^\circ$  to  $12^\circ$ . This profile is considered the most appropriate for use in the simulation given the absence of actual NIMA data for the three sites. The resultant terrain profile is shown in Figure 4-10.

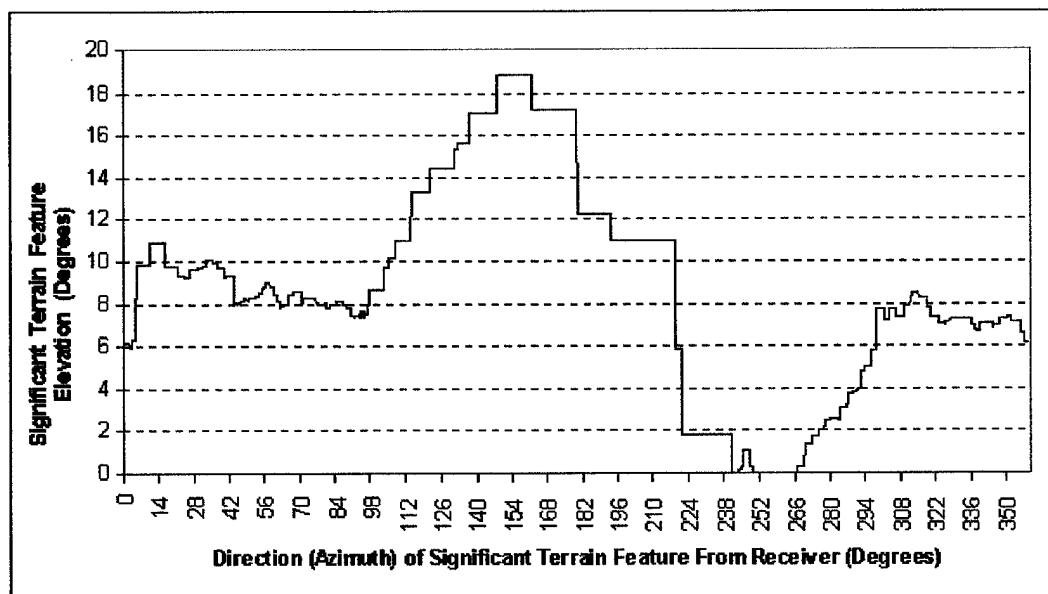


Figure 4-10: Significant Terrain Feature Elevations Profile

## **4.4 Characterizing the Transmission Paths Over the Notional Terrain**

### **4.4.1 Iridium**

The knife-edge and rounded obstacle model simulations verify the performance expectations of the Iridium system as presented in Section 4.2.3.3. The impact of the notional terrain upon the communication system performance is summarized in Table 4-4 and reflected in the following statistics:

- The average number of satellites in-view at each of the user locations is lower than that reported in the ideal terrain environment simulations. A reduction of 10.9% is reported for users located at Anchorage, 13.7% for those at Killeen, and 15.6% for users at Panama using the knife-edge approximation for diffraction. The reductions for users at these sites, based on the results from the rounded obstacle model are 11.4%, 14.3% and 16.3% respectively, only marginally poorer than those of the knife-edge model.
- Both models report approximately a seven-fold increase in the number of outages at Panama, a four-fold increase in the number of outages at Killeen and double the number of outages at Anchorage over that of the ideal terrain model.
- The maximum outage durations reported in the rounded obstacle model simulations are only five seconds greater than those reported in the knife-edge model simulations. There is little variation in the results provided by the two models.
- Both models report a significant decrease in the average outage duration. This decrease is approximately one third of the value reported in the ideal environment simulation. This statistic is misleading if analyzed without reference to the other

statistics gathered. The apparent performance improvement (i.e., a drop in the average outage duration) is actually caused by an increase in the number of shorter duration outages when the effects of terrain diffraction are included in the simulations. Therefore, this statistic does not provide a true indication of the system performance in this case.

Overall, the simulation shows that the performance of the Iridium system is most affected by terrain diffraction at lower latitudes. This effect gradually lessens as a user moves to higher latitude locations. The worst-case availability reported for Iridium in the notional terrain environment at Panama and Killeen, is approximately equal to that provided by Orbcomm in the ideal terrain environment. Additionally, the nature and duration of the outages are more predictable than those reported in the Orbcomm analysis. Given this comparison, the performance of the Iridium system should be considered better than that of Orbcomm.

*Table 4-4: Iridium Constellation Performance in a Terrain Diffraction Environment*

Ground Station Location	Average Number of Satellites in View		Number of Outages		Maximum Outage Duration (s)		Average Outage Duration (s)		Availability (%)	
	Knife-Edged Obstacles	Rounded Obstacles	Knife-Edged Obstacles	Rounded Obstacles	Knife-Edged Obstacles	Rounded Obstacles	Knife-Edged Obstacles	Rounded Obstacles	Knife-Edged Obstacles	Rounded Obstacles
Anchorage (61°13', -149°54')	2.490	2.476	11	11	120	125	49.1	51.4	99.69	99.67
Killeen (31°, -97°)	1.303	1.294	64	70	565	570	99.5	94.3	96.31	96.18
Panama (8°58', -79°33')	1.117	1.109	117	131	565	570	95.3	88.5	93.55	93.29

#### 4.4.2 Globalstar

The results produced from both the knife-edge and rounded obstacle model simulations confirm the performance predictions made at Section 4.2.4.3. A lack of variation in most of the statistics may, however, lead readers to conclude that the simulations were not implemented correctly. Especially since the results appear to indicate little impact in overall performance of the system when the effects of terrain diffraction are included in the analysis. Table 4-5 summarizes the performance of the Globalstar system when the diffractive effects of the notional terrain are included in the analysis.

*Table 4-5: Globalstar Constellation Performance in a Terrain Diffraction Environment*

Ground Station Location	Average Number of Satellites in View		Number of Outages		Maximum Outage Duration (s)		Average Outage Duration (s)		Availability (%)	
	Knife-Edged Obstacles	Rounded Obstacles	Knife-Edged Obstacles	Rounded Obstacles	Knife-Edged Obstacles	Rounded Obstacles	Knife-Edged Obstacles	Rounded Obstacles	Knife-Edged Obstacles	Rounded Obstacles
Anchorage (61°13', -149°54')	2.091	2.087	0	0	0	0	0	0	100	100
Killeen (31°, -97°)	3.209	3.207	0	0	0	0	0	0	100	100
Panama (8°58', -79°33')	2.140	2.138	2	2	15	20	10	12.5	99.99	99.98

The statistic that best defines the change in overall system performance and the impact of the notional terrain is the average number of satellites in-view. A reduction of

19.7% in the number of in-view satellites compared to the ideal terrain environment simulation is reported for users located at Anchorage using the knife-edge obstacle diffraction model. The figure falls to 10.9% for users at Killeen and 15.5% for users at Panama. Similarly, the rounded obstacle model results show reductions of 19.8%, 10.9% and 15.6% for the same sites. The trend in this statistic is for poorer satellite visibility as users move away from the middle latitudes. This result supports the earlier predictions that Globalstar performs best at the middle latitude locations for ideal environments.

Both models predict that availability remains at 100% for users at Killeen and Anchorage and falls, only slightly, to 99.99% and 99.98% for users located at Panama, depending on the model applied. The number of outages, maximum outage, and average outage durations are insignificant for each of the sites, but show initial signs of a decrease in performance in the Panama results.

The robustness of the results is explained by comparing the information presented in Figure 4-2 and Figure 4-5. Globalstar has a significantly higher number of satellites available to users at Killeen and Panama and a greater proportion of the observations made to these satellites are at higher elevation angles, relative to those of the Iridium system. For this reason, the Globalstar performance is less affected by the presence of the notional terrain and is considerably better than that of Iridium.

At Anchorage, Iridium has a higher average number of satellites in-view than Globalstar. However, a greater proportion of these observations are made to satellites at low elevations. For example, Figure 4-11 shows that Anchorage users observe approximately 6800 Iridium satellites at an elevation of  $10^{\circ}$ , decreasing to 1300 satellite observations at an elevation of  $30^{\circ}$ . The figures for Globalstar are 4300 observations to satellites at  $10^{\circ}$

elevation and 1500 observations to satellites at 30° elevation. Globalstar users make fewer overall observations at Anchorage, but more observations than Iridium users to satellites at higher elevation angles. Globalstar (with 100% availability) again outperforms the Iridium system when terrain diffraction is included in the analysis.

By any measure, the Globalstar system performance is particularly robust in the locations chosen for this analysis. The results also confirm that the system performs best at the middle latitudes with a gradual decrease in performance as users move away from these latitudes. However, the difference in performance statistics reported using the knife-edge and rounded obstacle models are insignificant.

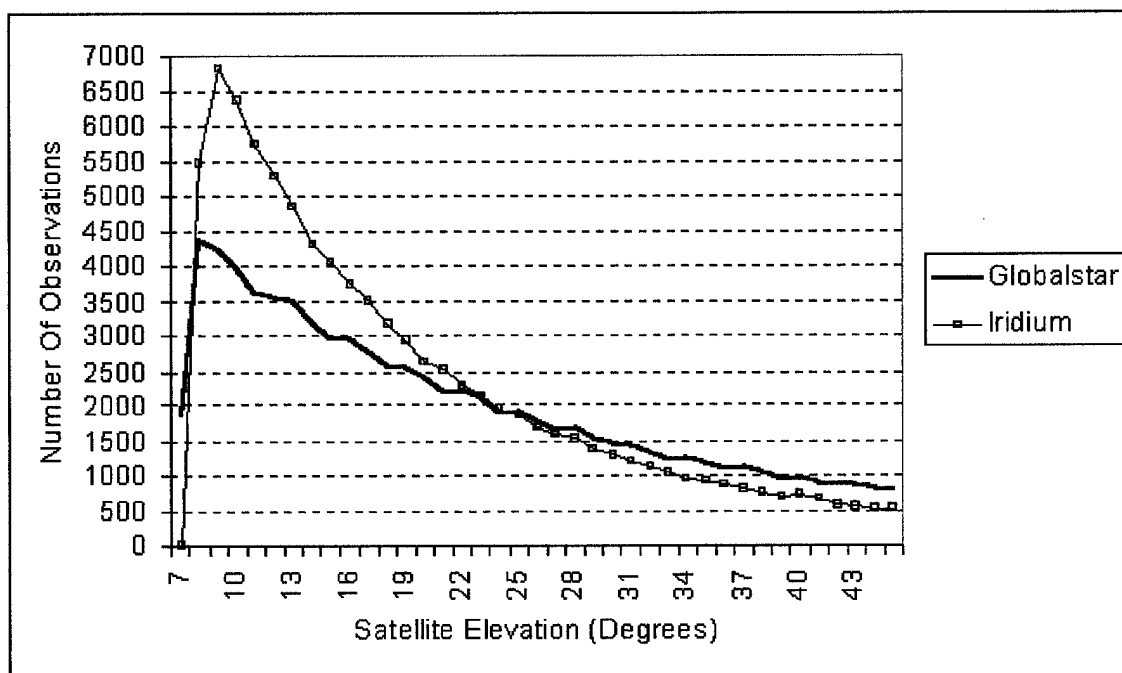


Figure 4-11: A Comparison of the Globalstar and Iridium Satellite Observations Made at Anchorage



#### 4.4.3 Orbcomm

The Orbcomm system performance in the notional terrain environment is the poorest of the three systems studied. The knife-edge and rounded obstacle model simulations very clearly reflect the performance trends presented in Section 4.2.5.3. Table 4-6 summarizes the performance of the Orbcomm system when the diffractive effects of the notional terrain are included in the analysis.

*Table 4-6: Orbcomm Constellation Performance in a Terrain Diffraction Environment*

Ground Station Location	Average Number of Satellites in View		Number of Outages		Maximum Outage Duration (s)		Average Outage Duration (s)		Availability (%)	
	Knife-Edged Obstacles	Rounded Obstacles	Knife-Edged Obstacles	Rounded Obstacles	Knife-Edged Obstacles	Rounded Obstacles	Knife-Edged Obstacles	Rounded Obstacles	Knife-Edged Obstacles	Rounded Obstacles
Anchorage (61°13', -149°54')	0.308	0.276	265	236	11955	11960	476	553	26.94	24.42
Killeen (31°, -97°)	1.430	1.406	131	131	595	605	192	199	85.42	84.90
Panama (8°58', -79°33')	0.906	0.887	224	227	4970	4995	265	269	65.61	64.67

The significant changes include the following:

- The predicted Orbcomm system performance is significantly better for users located at Killeen, the middle latitude site, with a predicted availability of approximately 85%. The results for Panama and Anchorage show the greatest impact from the inclusion of diffraction associated with the notional terrain, with availability figures of

65% and 26%. These changes represent performance reductions of 31% and 71% respectively, over that predicted in the ideal terrain environment scenario.

- The maximum outage duration increases from 14 minutes in an ideal terrain environment to 1.4 hours in the notional terrain environment at Panama and from 9.9 minutes to 3.3 hours at Anchorage.

The actual cause of the performance decline is found in the average in-view statistics. The average number of satellites in-view at each of the user locations is significantly lower than that reported in the ideal terrain environment simulations. A reduction of 41.9% is reported at Killeen, 52.6% at Panama and 78.1% at Anchorage using the knife-edge obstacle model. The reductions associated with the rounded obstacle model are, again, only marginally worse than those of the knife-edge model.

These results clearly reflect the observation data of Figure 4-9. Users at each location make fewer observations to the Orbcomm satellites and a greater proportion of these are made to satellites at lower elevation angles. The better performance of the system at Killeen results from the 45° inclination of the satellites in planes one through four. Overall, the simulations verify that the performance of the Orbcomm system is most affected by terrain diffraction at higher latitudes and at the lower extreme latitudes.

#### **4.5 Characterizing the Influence of the Notional Terrain on the Results**

Figure 4-12, Figure 4-13, and Figure 4-14 show the distribution of attenuation due to diffraction reported by each of the models for users located at Panama. Table 4-7 summarizes these results and those for each of the user locations indicating the proportion of

total observations where the rounded obstacle model reported attenuation more than 6 dB and 10 dB over that of the knife-edge model.

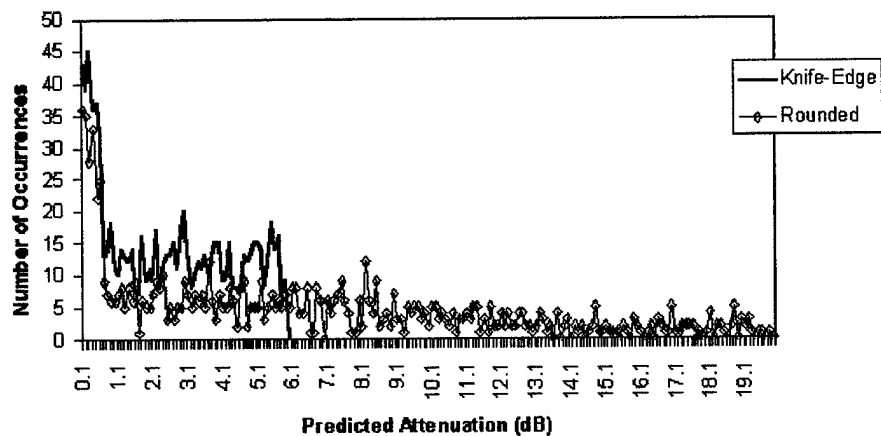


Figure 4-12: Attenuation Predictions for users of Iridium at Panama

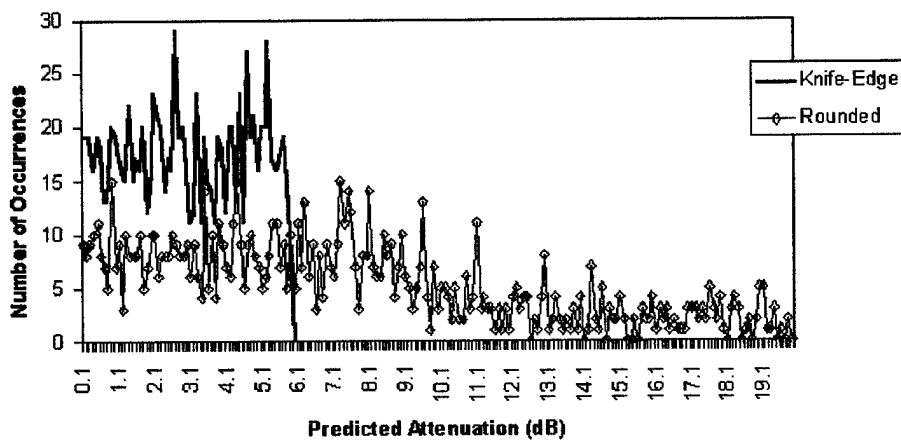


Figure 4-13: Attenuation Predictions for users of Globalstar at Panama

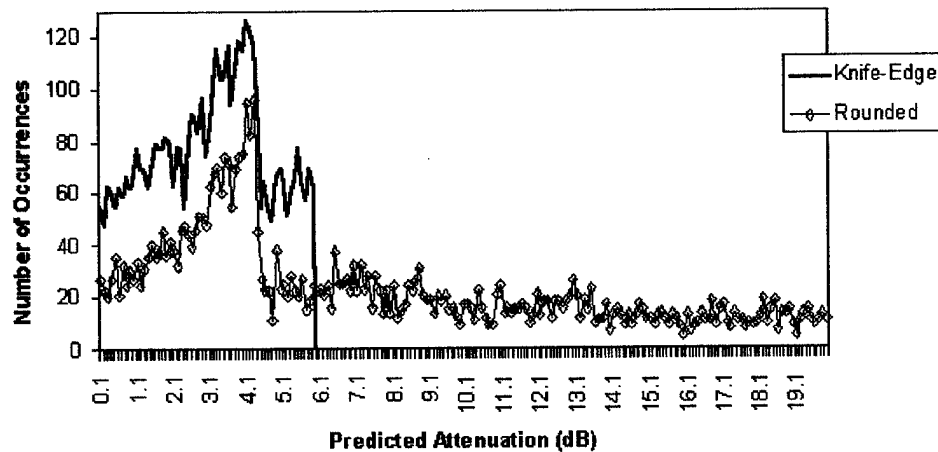


Figure 4-14: Attenuation Predictions for users of Orbcomm at Panama

Table 4-7: A Summary of the Attenuation Distributions

System	Site	Proportion of Observations Reported by the Rounded Obstacle Model showing Attenuation Greater than:	
		6 dB	10 dB
Iridium	Anchorage	42.9%	21.5%
	Killeen	42.8%	20.9%
	Panama	41.7%	21.5%
Globalstar	Anchorage	53.0%	26.2%
	Killeen	52.6%	27.5%
	Panama	52.5%	23.6%
Orbcomm	Anchorage	61.6%	42.1%
	Killeen	47.1%	29.9%
	Panama	47.0%	28.7%

The simulation results verify the prediction made in [Flo87] that up to 14 dB increase in attenuation could be observed on individual communication path links when a rounded obstacle model is applied instead of a knife-edge obstacle model. However, the overall impact of that attenuation increase does not appear to significantly influence the performance predictions made by the two models. This lack of distinction can be explained using the following reasoning:

- a. The number of observations resulting in an occurrence of ‘diffraction attenuation’ is orders of magnitude smaller than those resulting in a total blockage or shadowing of the signal. Consequently, the impact of blockage on the statistical analysis is more significant than diffraction attenuation for the notional terrain selected. A break down of the reduction in availability attributable to blockage and the diffraction attenuation reported by both models is provided in Table 4-8.

*Table 4-8: Availability Reductions Attributable to Blockage and Diffraction*

	Iridium			Globalstar			Orbcomm		
	All figures are expresses as percentages								
Anchorage (61°13', -149°54')	0.214	0.016	0.026	0	0	0	49.78	9.28	11.8
Killeen (31°, -97°)	1.368	0.089	0.223	0	0	0	10.3	1.87	2.39
Panama (8°58', -79°33')	2.992	0.179	0.437	0	0.01	0.02	24.21	4.0	4.95
	Blockage	Knife-Edge Diffraction	Rounded Obstacle Diffraction	Blockage	Knife-Edge Diffraction	Rounded Obstacle Diffraction	Blockage	Knife-Edge Diffraction	Rounded Obstacle Diffraction

- b. By applying a multiplication factor of 20 to the unclassified Killeen data set, a notional terrain consisting of sharp-edged ridges and mountains covered in a myriad of smaller conical peaks is produced. The sharpness of these terrain features is displayed in Figure 4-15, which shows a close-up view of the southwest corner of the notional terrain.

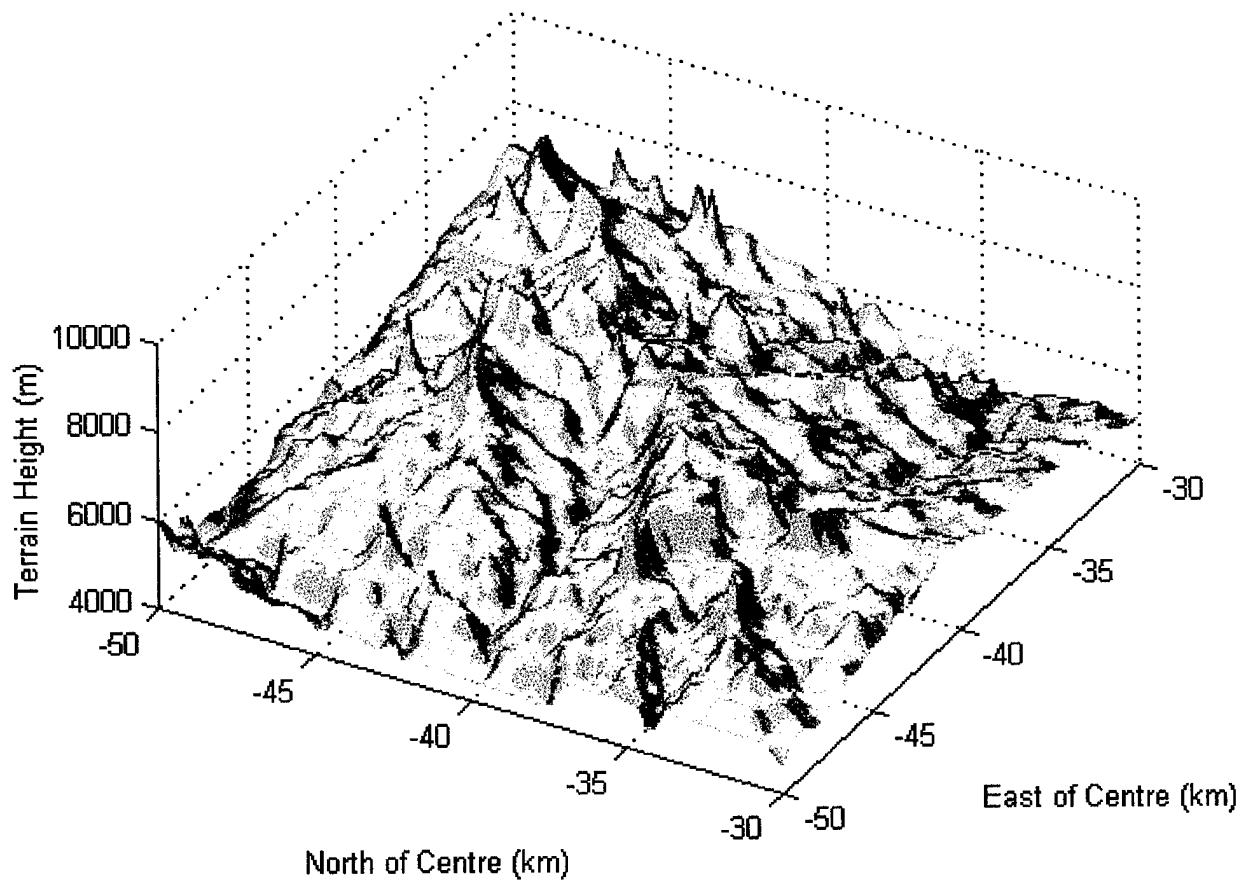


*Figure 4-15: View of the Southwest Corner of the Notional Terrain Surface*

- c. When Wilson's [Wil98] interpolation is applied to this notional terrain as the basis for calculation of the curvature of the dominant terrain feature along each azimuth, the result often approximates that provided by the knife-edge model. Approximately 51% of the dominant feature peaks have a radius of curvature of less than 10 km, resulting in the curvature distribution shown at Figure 4-16 and contributing to the lack of variance between the results obtained from both models.

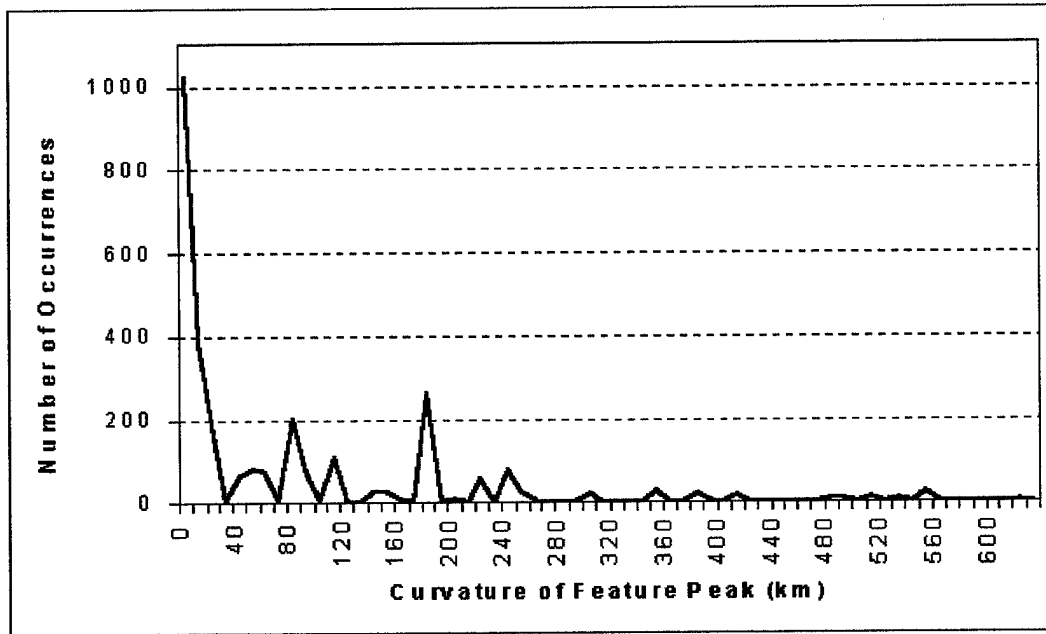


*Figure 4-16: Distribution of Dominant Feature Peak Curvature Values*

- d. A different terrain type, consisting of rolling, rather than 'peaky' hills or features with significant plateau areas at the top of each dominant feature would provide a situation that more clearly distinguishes the results obtained from both of the models.

Additionally, and as outlined in 3.5.1.3, there is an inherent difficulty in modeling the curvature of the dominant feature peaks. The distance between sample points (posts) has a significant impact on the calculated curvature of each peak. The accuracy of the rounded obstacle model varies with the sample interval selected. This is a direct result of the average curvature that is applied in the model calculations. If too small or too large a sample interval is chosen, the result may not reflect the true impact of the feature in question. The difficulty in applying a computer-based rounded obstacle may be due to this inability to effectively analyze each feature to determine the curvature of the feature peak.

## 4.6 Summary

Each step in the analysis process was designed to verify earlier predictions. The developed models and simulations provided results that are consistent with the predicted system performance.

A comparison of the three systems, within the scope of this study and the measures employed, shows that the Orbcomm communication system is most affected by terrain diffraction effects. The analyses have shown that this result is linked to the fact that there are fewer satellites in the Orbcomm constellation. More importantly, users make fewer observations to Orbcomm satellites at the sites chosen for this study. The majority of these observations are also made at elevation angles considerably lower than those made to the Iridium and Globalstar systems.

The implemented models confirm that the Iridium system performance is optimized for users located at higher latitudes, while Globalstar is optimized for users located at the middle latitudes. While both systems performed well within the latitudes of interest for the study, the Globalstar system is generally less affected by terrain diffraction. The primary reason for this is the consistently higher average number of in-view satellites available to users of the Globalstar system and a greater proportion of these to satellites at higher elevations.

Finally, the application of the notional rather than a natural terrain at the selected user sites influenced the results obtained from both diffraction models. The character of the notional terrain resembled that of the knife-edge environment and provided little differentiation between the results obtained from each model. Greater variation in the performance predicted by the two models may result from the application of a natural terrain.



## **CHAPTER 5**

### **SUMMARY AND CONCLUSIONS**

This study extended the work of Crowe [Cro99] on the performance of the Iridium and Globalstar systems. While Crowe focused on atmospheric and ionospheric impairments to the LEOSAT communications channel, this research focused on multipath communication propagation. In addition, this research developed and applied a terrain diffraction model to the space-to-ground communications channel. The analysis was also broadened to include a third LEOSAT communication system, Orbcomm.

#### **5.1 Summary**

The terrain models developed were primarily based on the results of research conducted by Jang [Jan97] and Wilson [Wil98]. Jang implemented a terrain diffraction model for use in the ground-to-ground and air-to-ground communication environments. Wilson's work provided the basis for accessing and interpreting the NIMA terrain data files and for approximating the curvature of the dominant terrain feature peaks (a requirement of the rounded obstacle terrain model).

The original goal of this research was to base the analysis around three sites for which suitable NIMA terrain data files were available. Sites were chosen based on the knowledge that NIMA terrain data has been collected for the majority of the North American continent and to ensure a reasonable spread of latitude between the sites as a means of influencing the test

results. The sites chosen were Anchorage, Killeen and Panama, to represent high, middle and low latitude site users respectively.

It was later discovered that inclusion of the actual terrain data for these sites would have necessitated a restriction be applied to the thesis distribution. Consequently, a notional terrain was created and applied throughout the analysis that was based on the unclassified Killeen data set. This approach ensured that all of the tools and models developed would comply with the NIMA data set format and could be used with actual data files should follow-on research be considered.

#### **5.1.1 Ideal Terrain Environment Performance**

The simulation confirmed the predictions of the theory-based analysis and those made by Crowe [Cro99]. The performance of the Iridium system improves with increasing latitude, achieving a maximum availability of 99.91% and an average of 2.8 satellites in-view for users located at Anchorage. While the system still provides reasonable coverage over the Panama region, system availability falls to 96.7% and the average number of satellites in-view falls to 1.3.

The analyses also confirmed that the Globalstar system is likely to perform better at middle latitude locations and poorer at the extreme latitude locations (of approximately  $0^\circ$  and  $\pm 70^\circ$ ). While no outages were reported over the duration of the simulation, the average number of satellites in-view peaked for Globalstar users at Killeen (the middle latitude site).

The analysis of the Orbcomm system was more involved as the Orbcomm constellation design, unlike Iridium and Globalstar, is not symmetrical. The system also operates at VHF

frequencies rather than frequencies in the L or S-band. Nevertheless, the simulation demonstrated that Orbcomm provides best coverage at middle latitudes with an average in-view satellite count of almost 2.5 and availability of 97.6% reported for Killeen. The availability reported for users located at Panama decreased to 93.8% and was poorest for users located at Anchorage. Anchorage users experienced only 86% availability.

### **5.1.2 Notional Terrain Environment Performance**

The analysis confirmed that the performance of the Iridium system is most affected by terrain diffraction at lower latitudes and that the effect gradually lessens as a user moves to higher latitude locations. Inclusion of the terrain models in the simulation resulted in a reduction in the average number of satellites in-view of approximately 11% for users located at Anchorage, 14% for those at Killeen, and 16% for users at Panama. Similar results were reported using both the knife-edge and rounded obstacle terrain models. Reductions in availability, to approximately 99.7%, 96.2% and 93.3%, were reported at the respective sites.

In contrast, the Globalstar system performance was particularly robust in the locations chosen for this analysis. The results also confirmed that the system performs best at the middle latitudes (as expected since the system is optimized for middle latitude coverage) with a gradual decrease in performance as users move away from Killeen. The statistic that best demonstrates a change in performance for the Globalstar system was the average number of satellites in-view. A reduction of approximately 20% in the average in-view count, over that achieved in the ideal terrain simulation, was reported for users located at Anchorage, 11% for users at Killeen, and 16% for users at Panama. Despite these decreases, both models predict that

availability will remain at 100% for users at Killeen and Anchorage and fall marginally for users located at Panama. The results demonstrate the benefit of the higher number of satellites available to Globalstar users at Killeen and Panama and of higher elevation satellites at Anchorage relative to those of the Iridium system. The analysis also confirmed the prediction made by Crowe that 'the distribution of path characteristics tends to indicate that blockage, shadowing and multipath effects will be lower for Globalstar than for Iridium' [Cro99]. However, the difference in results reported using the knife-edge and rounded obstacle terrain models were not significant.

The Orbcomm system performance in the notional terrain environment is the poorest of the three systems studied. The cause of the more significant performance decline is reflected in the average in-view statistics, where the average number of satellites in-view at each of the user locations is significantly lower than that reported in the ideal terrain environment simulations. Users at each of the locations make fewer observations to the Orbcomm satellites with a greater proportion of observations made to satellites at lower elevation angles. Overall, the simulations verified that the system performs best at Killeen as a result of the 45° inclination of planes one through four and is most affected by terrain diffraction at higher latitudes.

### **5.1.3 The Significance of the Notional Terrain Landscape**

A notional terrain data set was created with the intention of ensuring that terrain diffraction was a significant consideration in the simulations. In applying a multiplication factor of twenty to the unclassified NIMA data set, a terrain profile with a concentration of feature peak elevations in the range of 5° to 12° was produced. Most of the features of this

terrain profile were sharp-edged and the resulting feature peaks resembled upturned conical objects. The curvature of these feature peaks was not as significant as might be expected from a more rounded, and perhaps natural, terrain. While there was a reasonable variation between the models in the diffraction attenuation reported for individual observations, the occurrence of blockage was a more significant factor in the terrain environment adopted. Consequently, the results obtained from the rounded obstacle model did not differ significantly from those of the knife-edge obstacle model.

## **5.2 Conclusions**

This study verified the feasibility of applying models based on the geometric theory of diffraction rather than empirical or statistical models to approximate the effect of propagating signals over terrain in LEOSAT communications systems. While the difference in the performance predictions obtained from the knife-edge and rounded obstacle models was not significant, considerable variation was apparent in the attenuation reported for individual link observations. Both models verified that signal blockage and multipath propagation due to terrain diffraction could be significant considerations for designers and users of such systems.

The availability of a communications path between the satellite and potential users is critical to a LEOSAT communication system operation. However, predicting whether such a path exists is only one step in determining the overall performance of a system or as a basis for comparing the performance of many systems. The Iridium, Globalstar, and Orbcomm system implementations and communication architectures are fundamentally different, but each delivers particular communications services to users. Only a full requirements analysis, not

necessarily restricted to technical issues, could identify the system that provides the optimal performance for each user.

### **5.3 Recommendations**

Further research can be undertaken to combine the results of this and Crowe's study to obtain a model that addresses more of the propagation issue relevant to LEOSAT communication systems. This may be of considerable benefit to organizations requiring reliable mobile satellite communication services and in predicting the 'optimum' system, given a variety of operational requirements and practical design limitations.

Another potential area for research is the development of a 'system approach' for use as a tool in defining user requirements. Technical evaluations often focus on a narrow definition or measure of performance, rather than upon the broader requirements often stated by a user. Such a tool could then be used as the basis for making assessments of system performance and for comparing the ability of a variety of systems to meet a particular set of user requirements. Evaluation of the performance of Iridium, Globalstar, and Orbcomm in the light of such a tool, referencing all of the technical information and models available, may produce a very different set of conclusions as to systems overall performances.

## APPENDIX A: MATLAB PROGRAM LISTINGS

### Terrain\_Profile

```
function [Diffraction_Profile] = Terrain_Profile(Data_Set, Increment, File_Name)
```

```
% Written by Squadron Leader Peter Pollock, Royal Australian Air Force, AFIT student, October 1999.
```

```
% This function identifies the most significant terrain feature (based on diffractive effects) along each  
% radial, from the location of the receiver (centre of the data set) to the edge of the data set. The origin  
% or receiver location is defined to be grid square  $[n/2 + 1, m/2 + 1]$ . Zero degrees azimuth is North, 90 degrees  
% azimuth is West and so on.
```

```
% The azimuth granularity is set by the input variable 'Increment'. The user should determine the best setting for  
% Increment, based on the cell resolution at the edge of the terrain data set,  
% (ie:  $\tan(\text{Increment}) = \text{cell height} / \text{distance from Rx to edge of data set}$ )
```

```
% The input Data_Set should be a matrix of terrain elevation data of equal cell resolution in the latitude and  
% longitude directions. The post spacing (or cell dimensions) should be provided in distance units, rather than  
% angular units as in the case of raw DTED files. The files used in this thesis work were derived from  
% unclassified NIMA DTED data sets (100m post spacing) for the Killeen region in Texas. MAJ Kelce Wilson  
% (AFRL) provided the converted files. The matrix should provide an even number of rows and columns,  
% however the number of rows does not have to equal the number of columns. A further description of the  
% matrix format is given below:
```

```
% The DTED formatted data is upside down so that  $[1,1]$  is at the south west corner,  $[1,m]$  is at the south east  
% corner,  $[n,1]$  is at the north west corner and  $[n,m]$  is at the north east corner of the data set. Consequently, the  
% matrix has to be flipped prior to use. As the Killeen region is very flat, a multiplication factor of 20 was  
% applied to the height matrix to obtain features that would cause diffraction to occur. In a true analysis, with  
% actual data sets, the line marked with the asterisks *** would be deleted.
```

```
% Finally, the input variable File_Name is actually the file where the results will be stored and must be in the  
% format 'xxx.xxx'. The file is specified by the user, to avoid overwriting critical data if more than one region  
% is being evaluated at a time.
```

```
% The output, Diffraction_Profile, is the resulting significant terrain feature profile matrix and  
% is written to the file, File_Name. This file is much smaller than the data set and is used as the terrain model in  
% the communications simulation routines. Each line in this file contains six pieces of information on the  
% significant terrain feature along each azimuth radial, and is in the following format(space delimited):  
% [Azimuth(degrees),Cell Reference(eg:1 2),Distance(from origin),Height(relative to origin),Elevation of  
% feature]
```

```
% Be aware that the routine will take about 6 hours to produce a profile of a 100km x 100km region when the  
% grid (or post) spacing is 100m and Increment is set to 0.1 degrees. This assumes that the routine is run on a  
% stand-alone Pentium III 450MHz PC.
```

```
%Initialisation of local Variables  
Sample_Distance = 100;  
Range_Step = 4;  
First_Test = 1;
```

```

Data_Set = flipud(Data_Set);
[n,m] = size(Data_Set);

Data_Set = Data_Set*20;          % *** Delete this line for actual data sets

for Azimuth = 0:Increment:360-Increment
    if mod(Azimuth,100) == 0
        Azimuth
    end
    Translated_Az = Azimuth*pi/180;
    Elevation_Angle = 0;
    Significant_Cell = [0,0,0,0,0,0];

    if Translated_Az == 0
        Terrain_Vector = [0, 0];
        for Count = 1:n/2-1
            Cell = [Count, 0];
            Terrain_Vector = [Terrain_Vector; Cell];
        end
    elseif Translated_Az == pi/2
        Terrain_Vector = [0, -1];
        for Count = 2:m/2
            Cell = [0, -Count];
            Terrain_Vector = [Terrain_Vector; Cell];
        end
    elseif Translated_Az == pi
        Terrain_Vector = [-1, 0];
        for Count = 2:n/2
            Cell = [-Count, 0];
            Terrain_Vector = [Terrain_Vector; Cell];
        end
    elseif Translated_Az == 3*pi/2
        Terrain_Vector = [0, 0];
        for Count = 1:m/2-1
            Cell = [0, Count];
            Terrain_Vector = [Terrain_Vector; Cell];
        end
    elseif Translated_Az < pi/4
        Last_Visited_Cell = [0,-1];
        Terrain_Vector = Last_Visited_Cell;
        for Count = 1:(n-1)*Range_Step/2
            Y = Sample_Distance*Count/Range_Step;
            X = -Y*tan(Translated_Az);
            Cell = [floor(Y/Sample_Distance),floor(X/Sample_Distance)];
            if Cell(1) < n/2
                if Cell(2) >= -m/2
                    if ismember(Cell,Terrain_Vector)
                        else
                            Terrain_Vector = [Terrain_Vector; Cell];
                            Last_Visited_Cell = Cell;
                        end
                    end
                end
            end
        end
    end
end

```



```

end
elseif Translated_Az < pi/2
    Last_Visited_Cell=[0,-1];
    Terrain_Vector = Last_Visited_Cell;
    for Count = 1:(m-1)*Range_Step/2
        X = -Sample_Distance*Count/Range_Step;
        Y = -X*tan(pi/2-Translated_Az);
        Cell = [floor(Y/Sample_Distance),floor(X/Sample_Distance)];
        if Cell(1)>= -m/2
            if Cell(2) < n/2
                if ismember(Cell,Terrain_Vector)
                    else
                        Terrain_Vector = [Terrain_Vector; Cell];
                        Last_Visited_Cell = Cell;
                    end
                end
            end
        end
    end
elseif Translated_Az < 3*pi/4
    Last_Visited_Cell=[-1,-1];
    Terrain_Vector = Last_Visited_Cell;
    for Count = 1:m*Range_Step/2
        X = -Sample_Distance*Count/Range_Step;
        Y = X*tan(Translated_Az-pi/2);
        Cell = [floor(Y/Sample_Distance),floor(X/Sample_Distance)];
        if Cell(1)>= -m/2
            if Cell(2) >= -n/2
                if ismember(Cell,Terrain_Vector)
                    else
                        Terrain_Vector = [Terrain_Vector; Cell];
                        Last_Visited_Cell = Cell;
                    end
                end
            end
        end
    end
elseif Translated_Az < pi
    Last_Visited_Cell=[-1,-1];
    Terrain_Vector = Last_Visited_Cell;
    for Count = 1:n*Range_Step/2
        Y = -Sample_Distance*Count/Range_Step;
        X = Y*tan(pi -Translated_Az);
        Cell = [floor(Y/Sample_Distance),floor(X/Sample_Distance)];
        if Cell(1)>= -n/2
            if Cell(2) >= -m/2
                if ismember(Cell,Terrain_Vector)
                    else
                        Terrain_Vector = [Terrain_Vector; Cell];
                        Last_Visited_Cell = Cell;
                    end
                end
            end
        end
    end
elseif Translated_Az < 5*pi/4

```

```

Last_Visited_Cell = [-1,0];
Terrain_Vector = Last_Visited_Cell;
for Count = 1:n*Range_Step/2
    Y = -Sample_Distance*Count/Range_Step;
    X = -Y*tan(Translated_Az-pi);
    Cell = [floor(Y/Sample_Distance),floor(X/Sample_Distance)];
    if Cell(1) >= -n/2
        if Cell(2) < m/2
            if ismember(Cell,Terrain_Vector)
            else
                Terrain_Vector = [Terrain_Vector; Cell];
                Last_Visited_Cell = Cell;
            end
        end
    end
end
elseif Translated_Az < 3*pi/2
    Last_Visited_Cell = [-1,0];
    Terrain_Vector = Last_Visited_Cell;
    for Count = 1:(m-1)*Range_Step/2
        X = Sample_Distance*Count/Range_Step;
        Y = -X*tan(3*pi/2-Translated_Az);
        Cell = [floor(Y/Sample_Distance),floor(X/Sample_Distance)];
        if Cell(1) < m/2
            if Cell(2) >= -n/2
                if ismember(Cell,Terrain_Vector)
                else
                    Terrain_Vector = [Terrain_Vector; Cell];
                    Last_Visited_Cell = Cell;
                end
            end
        end
    end
end
elseif Translated_Az < 7*pi/4
    Last_Visited_Cell = [0,0];
    Terrain_Vector = Last_Visited_Cell;
    for Count = 1:(m-1)*Range_Step/2
        X = Sample_Distance*Count/Range_Step;
        Y = X*tan(Translated_Az-3*pi/2);
        Cell = [floor(Y/Sample_Distance),floor(X/Sample_Distance)];
        if Cell(1) < m/2
            if Cell(2) < n/2
                if ismember(Cell,Terrain_Vector)
                else
                    Terrain_Vector = [Terrain_Vector; Cell];
                    Last_Visited_Cell = Cell;
                end
            end
        end
    end
end
elseif Translated_Az < 2*pi
    Last_Visited_Cell = [0,0];
    Terrain_Vector = Last_Visited_Cell;

```

```

for Count = 1:(n-1)*Range_Step/2
    Y = Sample_Distance*Count/Range_Step;
    X = Y*tan(2*pi-Translated_Az);
    Cell = [floor(Y/Sample_Distance),floor(X/Sample_Distance)];
    if Cell(1)< n/2
        if Cell(2) < m/2
            if ismember(Cell,Terrain_Vector)
            else
                Terrain_Vector = [Terrain_Vector; Cell];
                Last_Visited_Cell = Cell;
            end
        end
    end
end
end
end

[a,b] = size(Terrain_Vector);
for Count_1 = 1:a
    Terrain_Vector(Count_1, 1) = Terrain_Vector(Count_1, 1) + (1+n/2);
    Terrain_Vector(Count_1, 2) = Terrain_Vector(Count_1, 2) + (1+m/2);
end
Origin_Height = Data_Set(Terrain_Vector(1,1),Terrain_Vector(1,2));
for Count = 1:a
    Cell_Distance = Sample_Distance*sqrt((Terrain_Vector(Count,1)-
        (1+n/2))^2+(Terrain_Vector(Count,2)-(1+m/2))^2);
    if Cell_Distance == 0
        Cell_Distance = 0.5*sqrt(2*(Sample_Distance)^2);
    end
    Cell_Height = Data_Set(Terrain_Vector(Count,1),Terrain_Vector(Count,2));
    Relative_Height = Cell_Height - Origin_Height;
    Cell_Elevation_Angle = 180 * atan(Relative_Height / Cell_Distance) / pi;
    if Cell_Elevation_Angle > Elevation_Angle
        Significant_Cell =
            [Azimuth,Terrain_Vector(Count,1),Terrain_Vector(Count,2),Cell_Distance,
            Relative_Height, Cell_Elevation_Angle];
        Elevation_Angle = Cell_Elevation_Angle;
    elseif Count == a
        if Significant_Cell == [0,0,0,0,0,0]
            Significant_Cell = [Azimuth,0,0,1, 0, 0];
        end
    end
end
end

if First_Test == 1
    Diffraction_Profile = Significant_Cell;
    First_Test = 0;
else
    Diffraction_Profile = [Diffraction_Profile; Significant_Cell];
end
end

dlmwrite(File_Name,Diffraction_Profile,');

```

### Soap\_Dump\_Strip

```
function [Final_Matrix] = Soap_Dump_Strip(Input_File, Output_File, Satellites_Per_Plane);
```

```
% Written by Squadron Leader Peter Pollock, Royal Australian Air Force, AFIT student, October 1999.
```

```
% This routine strips unnecessary information from the SOAP output files, which contain the visibility times  
% for each satellite in a given plane within the constellation over a two day period. The routine produces files  
% that are much smaller (reduced from 11+Mb to around 500Kb) and as such makes the files much easier and  
% quicker to handle in later routines.
```

```
% The input parameters are:
```

```
% a. Input_File: specifies the name of the file containing the Excel modified SOAP output file for each of the
```

```
% Iridium planes, eg: Plane_0.csv
```

```
% b. Output_File: specifies the name and location of the file used to store the stripped file output,
```

```
% eg: Iridium_5.txt
```

```
% c. Satellites_Per_Plane: specifies the number of satellites in the plane from the SOAP data. This
```

```
% is required to set the counters to determine which data to strip from the file.
```

```
% The output parameter, Final_Matrix, is a matrix containing the in view characteristics (stripped version)
```

```
% for the satellites in a given Iridium Plane. The matrix is completed and written to the output file in
```

```
% the final lines of the routine.
```

```
% The purpose of the variable called Store_1 is to store half of the final matrix, Soap_Output, while the
```

```
% routine is executing. I found that this helped the PC I was using cope with the memory allocation
```

```
% requirements for such large input files.
```

```
Plane = dlmread(Input_File,');  
[a,b] = size(Plane)
```

```
Store_1 = 'Store_1.csv';  
Pointer = 1;
```

```
Time_Snap_Pointer = 1;  
First = 1;
```

```
for Time = 0:5:172800
```

```
    if mod(Time,10000) == 0
```

```
        Time
```

```
    end
```

```
    Sat_In_View = 0;
```

```
    if Pointer <= a
```

```
        for Count_3 = 2:4:(Satellites_Per_Plane * 4 - 2)
```

```
            Sat_In_View = Sat_In_View + Plane(Pointer,Count_3);
```

```
        end
```

```
        if Sat_In_View > 0
```

```
            Time_Snap(Time_Snap_Pointer, 1) = Time;
```

```
            Count_2 = 2;
```

```
            for Count_1 = 2:4:(Satellites_Per_Plane * 4 - 2)
```

```
                if Plane(Pointer,Count_1) == 1
```

```
                    Time_Snap(Time_Snap_Pointer, Count_2) = Plane(Pointer, Count_1+1);
```

```
                    Time_Snap(Time_Snap_Pointer, Count_2+1) = Plane(Pointer, Count_1+2);
```

```

        Time_Snap(Time_Snap_Pointer, Count_2+2) = Plane(Pointer, Count_1+3);
        Count_2 = Count_2 + 3;
    else
        Time_Snap(Time_Snap_Pointer, Count_2) = 0;
        Time_Snap(Time_Snap_Pointer, Count_2+1) = 0;
        Time_Snap(Time_Snap_Pointer, Count_2+2) = 0;
        Count_2 = Count_2 + 3;
    end
end
Time_Snap_Pointer = Time_Snap_Pointer + 1;
end
Pointer = Pointer + 1;
end
if Time == 86395
    if Pointer ~= 1
        dlmwrite(Store_1, Time_Snap, ',');
        clear Time_Snap;
        Time_Snap_Pointer = 1;
    end
end
end

clear Plane;
disp('reading first half back in...');
Final_Matrix = dlmread(Store_1, ',');
disp('Combining the matrices...');
Final_Matrix = [Final_Matrix; Time_Snap];
disp('Dumping to Output file...');
dlmwrite(Output_File, Final_Matrix, ',');

```

### In\_View\_Times

```

function [In_View_Profile] = In_View_Times(Terrain_File, Curvature_File, Increment, Output_File,
Constellation);

```

% Written by Squadron Leader Peter Pollock, Royal Australian Air Force, AFIT student, October 1999.

% This routine determines the number of Iridium satellites in view of the Rx at each 5 second time increment over a two day analysis period. The analysis report includes the expected number of satellites in view when the analysis is based on:

- % a. The SOAP analysis, which assumes a smooth earth model.
- % b. The effect of terrain blockage is combined with the output of the SOAP analysis.
- % c. The effects of Knife edge diffraction and terrain blockage are combined with the output of the SOAP analysis.
- % d. The effects of Rounded Obstacle diffraction and terrain blockage are combined with the output of the SOAP analysis.

% The results of the analysis are stored in a matrix called In\_View\_Profile. The matrix is stored in the output file at the conclusion of the routine.

```
% The required inputs are:
% a. Terrain_File: The file used to store the profile produced using the Terrain_Profile routine.
% b. Increment: The azimuth increment used to create the terrain profile.
% c. Output_File: The name of the file that will be used to store the results of this analysis. The file name must be
%    in the format of an input string, ie: in single quotation marks('xxx.xxx').

% The SOAP analysis for Iridium is stored in six files, representing the in view results for each of the planes
% in the constellation. These files have been stored as Irium_0 through Iridium_5 and are loaded directly from
% within the routine.

% One additional input is loaded directly within the routine. The curvature matrix, produced in the routine called
% Determine_Curvature, is used to approximate the curvature of the top of the terrain feature in the rounded
% obstacle diffraction model.
```

```
global Pointer_0 Pointer_1 Pointer_2 Pointer_3 Pointer_4 Pointer_5 Pointer_6 Pointer_7
global Time First In_View Blocked Knife_Edge_Limited Rounded_Limited
global Terrain a_T Curvature
```

```
disp('Loading Files...');
```

```
if Constellation == 'Iridium'
    Iridium_0 = dlmread('C:\My Documents\Peter\AFIT\EENG799\Thesis\Analysis Work\Iridium\Killeen\Plane
        0\Iridium 0.csv','');
    [a_0,b_0] = size(Iridium_0);
    Iridium_1 = dlmread('C:\My Documents\Peter\AFIT\EENG799\Thesis\Analysis Work\Iridium\Killeen\Plane
        1\Iridium 1.csv','');
    [a_1,b_1] = size(Iridium_1);
    Iridium_2 = dlmread('C:\My Documents\Peter\AFIT\EENG799\Thesis\Analysis Work\Iridium\Killeen\Plane
        2\Iridium 2.csv','');
    [a_2,b_2] = size(Iridium_2);
    Iridium_3 = dlmread('C:\My Documents\Peter\AFIT\EENG799\Thesis\Analysis Work\Iridium\Killeen\Plane
        3\Iridium 3.csv','');
    [a_3,b_3] = size(Iridium_3);
    Iridium_4 = dlmread('C:\My Documents\Peter\AFIT\EENG799\Thesis\Analysis Work\Iridium\Killeen\Plane
        4\Iridium 4.csv','');
    [a_4,b_4] = size(Iridium_4);
    Iridium_5 = dlmread('C:\My Documents\Peter\AFIT\EENG799\Thesis\Analysis Work\Iridium\Killeen\Plane
        5\Iridium 5.csv','');
    [a_5,b_5] = size(Iridium_5);
    Pointer_0 = 1;
    Pointer_1 = 1;
    Pointer_2 = 1;
    Pointer_3 = 1;
    Pointer_4 = 1;
    Pointer_5 = 1;
elseif Constellation == 'Gblstar'
    Globalstar_0 = dlmread('C:\My Documents\Peter\AFIT\EENG799\Thesis\Analysis
        Work\Globalstar\Anchorage\Plane 0\Global 0.csv','');
    [a_0,b_0] = size(Globalstar_0);
    Globalstar_1 = dlmread('C:\My Documents\Peter\AFIT\EENG799\Thesis\Analysis
        Work\Globalstar\Anchorage\Plane 1\Global 1.csv','');
```

```

[a_1,b_1] = size(Globalstar_1);
Globalstar_2 = dlmread('C:\My Documents\Peter\AFIT\EENG799\Thesis\Analysis
    Work\Globalstar\Anchorage\Plane 2\Global 2.csv','');
[a_2,b_2] = size(Globalstar_2);
Globalstar_3 = dlmread('C:\My Documents\Peter\AFIT\EENG799\Thesis\Analysis
    Work\Globalstar\Anchorage\Plane 3\Global 3.csv','');
[a_3,b_3] = size(Globalstar_3);
Globalstar_4 = dlmread('C:\My Documents\Peter\AFIT\EENG799\Thesis\Analysis
    Work\Globalstar\Anchorage\Plane 4\Global 4.csv','');
[a_4,b_4] = size(Globalstar_4);
Globalstar_5 = dlmread('C:\My Documents\Peter\AFIT\EENG799\Thesis\Analysis
    Work\Globalstar\Anchorage\Plane 5\Global 5.csv','');
[a_5,b_5] = size(Globalstar_5);
Globalstar_6 = dlmread('C:\My Documents\Peter\AFIT\EENG799\Thesis\Analysis
    Work\Globalstar\Anchorage\Plane 6\Global 6.csv','');
[a_6,b_6] = size(Globalstar_6);
Globalstar_7 = dlmread('C:\My Documents\Peter\AFIT\EENG799\Thesis\Analysis
    Work\Globalstar\Anchorage\Plane 7\Global 7.csv','');
[a_7,b_7] = size(Globalstar_7);
Pointer_0 = 1;
Pointer_1 = 1;
Pointer_2 = 1;
Pointer_3 = 1;
Pointer_4 = 1;
Pointer_5 = 1;
Pointer_6 = 1;
Pointer_7 = 1;
elseif Constellation == 'Orbcomm'
    Orbcomm_0 = dlmread('C:\My Documents\Peter\AFIT\EENG799\Thesis\Analysis
        Work\Orbcomm\Killeen\Plane 0\Orbcomm 0.csv','');
    [a_0,b_0] = size(Orbcomm_0);
    Orbcomm_1 = dlmread('C:\My Documents\Peter\AFIT\EENG799\Thesis\Analysis
        Work\Orbcomm\Killeen\Plane 1\Orbcomm 1.csv','');
    [a_1,b_1] = size(Orbcomm_1);
    Orbcomm_2 = dlmread('C:\My Documents\Peter\AFIT\EENG799\Thesis\Analysis
        Work\Orbcomm\Killeen\Plane 2\Orbcomm 2.csv','');
    [a_2,b_2] = size(Orbcomm_2);
    Orbcomm_3 = dlmread('C:\My Documents\Peter\AFIT\EENG799\Thesis\Analysis
        Work\Orbcomm\Killeen\Plane 3\Orbcomm 3.csv','');
    [a_3,b_3] = size(Orbcomm_3);
    Orbcomm_4 = dlmread('C:\My Documents\Peter\AFIT\EENG799\Thesis\Analysis
        Work\Orbcomm\Killeen\Plane 4\Orbcomm 4.csv','');
    [a_4,b_4] = size(Orbcomm_4);
    Orbcomm_5 = dlmread('C:\My Documents\Peter\AFIT\EENG799\Thesis\Analysis
        Work\Orbcomm\Killeen\Plane 5\Orbcomm 5.csv','');
    [a_5,b_5] = size(Orbcomm_5);
    Pointer_0 = 1;
    Pointer_1 = 1;
    Pointer_2 = 1;
    Pointer_3 = 1;
    Pointer_4 = 1;
    Pointer_5 = 1;
end

```

```

Curvature = dlmread(Curvature_File,');
[a_c,b_c] = size(Curvature);

Terrain = dlmread(Terrain_File,');
[a_T,b_T] = size(Terrain);

disp('Done');

First = 1;

for Time = 0:5:172800
    if mod(Time,80000) == 0
        Time
    end
    In_View = 0;
    Blocked = 0;
    Knife_Edge_Limited = 0;
    Rounded_Limited = 0;
    if Constellation == 'Iridium'
        Pointer_0 = Determine_Terrain_Effect(Iridium_0, a_0, 11, Pointer_0, Increment, 'Iridium');
        Pointer_1 = Determine_Terrain_Effect(Iridium_1, a_1, 11, Pointer_1, Increment, 'Iridium');
        Pointer_2 = Determine_Terrain_Effect(Iridium_2, a_2, 11, Pointer_2, Increment, 'Iridium');
        Pointer_3 = Determine_Terrain_Effect(Iridium_3, a_3, 11, Pointer_3, Increment, 'Iridium');
        Pointer_4 = Determine_Terrain_Effect(Iridium_4, a_4, 11, Pointer_4, Increment, 'Iridium');
        Pointer_5 = Determine_Terrain_Effect(Iridium_5, a_5, 11, Pointer_5, Increment, 'Iridium');
    elseif Constellation == 'Gblstar'
        Pointer_0 = Determine_Terrain_Effect(Globalstar_0, a_0, 6, Pointer_0, Increment, 'Gblstar');
        Pointer_1 = Determine_Terrain_Effect(Globalstar_1, a_1, 6, Pointer_1, Increment, 'Gblstar');
        Pointer_2 = Determine_Terrain_Effect(Globalstar_2, a_2, 6, Pointer_2, Increment, 'Gblstar');
        Pointer_3 = Determine_Terrain_Effect(Globalstar_3, a_3, 6, Pointer_3, Increment, 'Gblstar');
        Pointer_4 = Determine_Terrain_Effect(Globalstar_4, a_4, 6, Pointer_4, Increment, 'Gblstar');
        Pointer_5 = Determine_Terrain_Effect(Globalstar_5, a_5, 6, Pointer_5, Increment, 'Gblstar');
        Pointer_6 = Determine_Terrain_Effect(Globalstar_6, a_6, 6, Pointer_6, Increment, 'Gblstar');
        Pointer_7 = Determine_Terrain_Effect(Globalstar_7, a_7, 6, Pointer_7, Increment, 'Gblstar');
    elseif Constellation == 'Orbcomm'
        Pointer_0 = Determine_Terrain_Effect(Orbcomm_0, a_0, 7, Pointer_0, Increment, 'Orbcomm');
        Pointer_1 = Determine_Terrain_Effect(Orbcomm_1, a_1, 8, Pointer_1, Increment, 'Orbcomm');
        Pointer_2 = Determine_Terrain_Effect(Orbcomm_2, a_2, 8, Pointer_2, Increment, 'Orbcomm');
        Pointer_3 = Determine_Terrain_Effect(Orbcomm_3, a_3, 8, Pointer_3, Increment, 'Orbcomm');
        Pointer_4 = Determine_Terrain_Effect(Orbcomm_4, a_4, 2, Pointer_4, Increment, 'Orbcomm');
        Pointer_5 = Determine_Terrain_Effect(Orbcomm_5, a_5, 2, Pointer_5, Increment, 'Orbcomm');
    end
    Blocked_Stat = In_View - Blocked;
    Knife_Edge_Stat = In_View - Blocked - Knife_Edge_Limited;
    Rounded_Stat = In_View - Blocked - Rounded_Limited;
    %if In_View == 0
    if First == 1
        In_View_Profile = [Time, In_View, Blocked_Stat, Knife_Edge_Stat, Rounded_Stat];
        First = 0;
    else
        Next_Time_Snap = [Time, In_View, Blocked_Stat, Knife_Edge_Stat, Rounded_Stat];
        In_View_Profile = [In_View_Profile; Next_Time_Snap];
    end
end

```



```

    end
end
dlmwrite(Output_File, In_View_Profile, '');

function [Update_Pointer] = Determine_Terrain_Effect(Plane, a_Plane, Satellites_Per_Plane, Pointer, Increment,
                                                    Constellation);

global Pointer_0 Pointer_1 Pointer_2 Pointer_3 Pointer_4 Pointer_5 Pointer_6 Pointer_7
global Time First_In_View Blocked Knife_Edge_Limited Rounded_Limited
global Terrain a_T Curvature

if Pointer <= a_Plane
    if Plane(Pointer, 1) == Time
        for Count = 2:3:(Satellites_Per_Plane * 3 - 1)
            if Plane(Pointer, Count) ~= 0
                In_View = In_View + 1;
                Ref = round(Plane(Pointer, Count)/Increment + 1);
                if Ref <= a_T
                    Sat_El = Plane(Pointer, Count+1);
                    Sat_Range = Plane(Pointer, Count+2);
                    if Sat_El < Terrain(Ref, 6)
                        Blocked = Blocked + 1;
                    else
                        Margin = Calculate_Power_Rx(Terrain(Ref, 4), Terrain(Ref, 5), Sat_El, Sat_Range, 0, 0, Constellation);
                        if Margin < 0
                            Knife_Edge_Limited = Knife_Edge_Limited + 1;
                        end
                        Radius = Curvature(Ref, 2);
                        Margin = Calculate_Power_Rx(Terrain(Ref, 4), Terrain(Ref, 5), Sat_El, Sat_Range, Radius, 1,
                                                    Constellation);
                        if Margin < 0
                            Rounded_Limited = Rounded_Limited + 1;
                        end
                    end
                end
            end
        end
        Pointer = Pointer + 1;
    end
end
Update_Pointer = Pointer;

```

### Calculate\_Power\_Received

```
function [Attenuation] = Calculate_Power_Rx(Distance, Height, Sat_Elevation, Sat_Range, Curvature_Radius,  
Type, Constellation)
```

% Written by Squadron Leader Peter Pollock, Royal Australian Air Force, AFIT student, October 1999.

% This function calculates the expected power received from the specified satellite, based on the input  
% parameters specified:  
% System: specifies the constellation being studied (Globalstar or Iridium). This is used to determine the Tx  
% EIRP and the power required at the receiver to establish an effective communications link.  
% Distance: specifies the distance between the significant terrain feature and the receiver.  
% Height: specifies the height of the significant terrain feature.  
% Sat\_Elevation: specifies the elevation of the satellite wrt the receiver (smooth earth).  
% Sat\_Range: specifies the distance from the Rx to the satellite in view.  
% Curvature\_Radius: specifies the curvature radius of the significant terrain feature at this azimuth.  
% Type: specifies which diffraction model to use (Knife edge = 0, Rounded = 1).

% The output parameter, Link\_Margin, approximates the received power, based on the knife edge and  
% rounded obstacle model parameters.

% Please note that this routine will have to be modified to incorporate the globalstar parameters.

```
if Constellation == 'Iridium'  
    Frequency = 1.6E+9;  
    Wavelength = 3E+8/Frequency;  
    Required_Rx_Power = -151.5;  
    Rx_Gain = 1;  
    System_Losses = 0.7;  
    if Sat_Elevation <= 20.8  
        Tx_EIRP = 15.7;  
    elseif Sat_Elevation <= 33.2  
        Tx_EIRP = 12.5;  
    elseif Sat_Elevation <= 51.9  
        Tx_EIRP = 10;  
    else  
        Tx_EIRP = 7.5;  
    end  
elseif Constellation == 'Gblstar'  
    Frequency = 2.46E+9;  
    Wavelength = 3E+8/Frequency;  
    Required_Rx_Power = -171.4;  
    System_Losses = 3.5;  
    if Sat_Elevation <= 25  
        Tx_EIRP = 2.8;  
        Rx_Gain = 1;  
    elseif Sat_Elevation <= 50  
        Tx_EIRP = -0.4;  
        Rx_Gain = 2.6;  
    else  
        Tx_EIRP = 0.1;  
        Rx_Gain = 2.6;
```

```

end
elseif Constellation == 'Orbcomm'
    Frequency = 137.5E+6;
    Wavelength = 3E+8/Frequency;
    Required_Rx_Power = -143.8;
    Rx_Gain = 0;
    System_Losses = 11.3;
    Tx_EIRP = 12.5;
end

Radians = Sat_Elevation*pi/180;
LOS_Height = Distance * tan(Radians);
Clearance_Height = LOS_Height - Height;

Fresnel_Radius = sqrt(Wavelength * Distance);
Free_Space_Loss = 20*log10(4*pi*Sat_Range*1000/Wavelength);

if Type == 0
    Knife_Edge_Loss = 6 - (Clearance_Height / Fresnel_Radius) * 6 / 0.6;
    if Knife_Edge_Loss < 0
        Knife_Edge_Loss = 0;
    else
        Knife_Edge_Loss = Knife_Edge_Loss;
    end
    Rx_Power = Tx_EIRP + Rx_Gain - Free_Space_Loss - System_Losses - Knife_Edge_Loss;
    Attenuation = Knife_Edge_Loss;
elseif Type == 1
    Alpha = (Wavelength^(2/3)) * (Curvature_Radius^(1/3))/Fresnel_Radius;
    if Alpha == 0
        Maximum_Loss = 6;
    elseif Alpha <= 0.1
        Maximum_Loss = 6.5;
    elseif Alpha <= 0.2
        Maximum_Loss = 7.2;
    elseif Alpha <= 0.3
        Maximum_Loss = 7.8;
    elseif Alpha <= 0.4
        Maximum_Loss = 8.3;
    elseif Alpha <= 0.5
        Maximum_Loss = 9;
    elseif Alpha <= 0.6
        Maximum_Loss = 9.7;
    elseif Alpha <= 0.7
        Maximum_Loss = 10.6;
    elseif Alpha <= 0.8
        Maximum_Loss = 11.4;
    elseif Alpha <= 0.9
        Maximum_Loss = 12.2;
    elseif Alpha <= 1
        Maximum_Loss = 13.3;
    elseif Alpha <= 1.1
        Maximum_Loss = 14.4;
    elseif Alpha <= 1.2

```

```

    Maximum_Loss = 15.2;
elseif Alpha <= 1.3
    Maximum_Loss = 16.4;
elseif Alpha <= 1.4
    Maximum_Loss = 17.8;
elseif Alpha <= 1.5
    Maximum_Loss = 20;
else
    Maximum_Loss = 20;
end
Rounded_Loss = Maximum_Loss - (Clearance_Height / Fresnel_Radius) * Maximum_Loss / 0.6;
if Rounded_Loss < 0
    Rounded_Loss = 0;
else
    Rounded_Loss = Rounded_Loss;
end
Rx_Power = Tx_EIRP + Rx_Gain - Free_Space_Loss - System_Losses - Rounded_Loss;
Attenuation = Rounded_Loss;
end

Link_Margin = Rx_Power - Required_Rx_Power;
if Link_Margin < 0
    if Type == 0
        disp('Knife_Edge outage occurred');
    else
        disp('Rounded outage occurred');
    end
end
end

```

### **Determine\_Curvature**

```
function [Curvature] = Determine_Curvature(Raw_Data, Increment, Post_Spacing, Input_File, Output_File);
```

```

% This routine approximates the curvature of the top of each significant terrain feature. The routine
% (SurfaceDerivatives) used to approximate the cubic spline coefficients for each of the Data_Set cells,
% in the easterly and northerly directions, was provided by Major Kelce Wilson of AFRL. These coefficients
% are used to determine the required coefficients in the generalised curvature equation:

```

```
% The radius of curvature is then calculated as  $|1/k|$ .
```

```
% The input parameters are:
```

```
% a. Data_Set is the DTED terrain matrix for the site in question.
```

```
% b. Increment is the azimuth resolution / sample angle used to create the terrain profile from the data set.
```

```
% c. Input_File is the file containing the terrain profile data and is entered as a string ('xxx.xxx').
```

```
% d. Output_File is used to store the curvature data on completion of the routine.
```

```

% The output is a matrix of curvature values for the significant terrain feature along each radial from
% the receiver to the edge of the data set.

```

```

disp('Loading data...');
Data_Set = dlmread(Raw_Data, ' ');
Data_Set = Data_Set * 20; %*** This line should be deleted if a real data set (not the notional set) were used
disp('Done');

```

```

disp('Calculating Surface Derivatives...');
[Latitude, Longitude] = SurfaceDerivatives(Data_Set);
[a_Lat,b_Lat,c_Lat] = size(Latitude);
[a_Long,b_Long,c_Long] = size(Longitude);
disp('Done...');

```

```

clear Data_Set;
Terrain = dlmread(Input_File, ' ');
[a_T,b_T] = size(Terrain);
First = 1;
for Count = 0:Increment:360-Increment
    if mod(Count,100) == 0
        Count
    end
    Ref = round(Count/Increment + 1);
    if Terrain(Ref,2) ~= 0
        X_Vector = [Count,Longitude(Terrain(Ref,2),Terrain(Ref,3),1),Longitude(Terrain(Ref,2),Terrain(Ref,3),2)];
        Y_Vector = [Count,Latitude(Terrain(Ref,2),Terrain(Ref,3),1),Latitude(Terrain(Ref,2),Terrain(Ref,3),2)];
        X_Curvature = [2*X_Vector(3)/((1+X_Vector(2)^2)^(3/2))];
        X_Radius = [Count,round(Post_Spacing/abs(X_Curvature))];
        Y_Curvature = [2*Y_Vector(3)/((1+Y_Vector(2)^2)^(3/2))];
        Y_Radius = [Count,round(Post_Spacing/abs(Y_Curvature))];
        if First == 1
            X_Matrix = X_Radius;
            Y_Matrix = Y_Radius;
            First = 0;
        else
            X_Matrix = [X_Matrix;X_Radius];
            Y_Matrix = [Y_Matrix;Y_Radius];
        end
    else
        X_Vector = [Count,0,0];
        Y_Vector = [Count,0,0];
        if First == 1
            X_Matrix = [Count,0];
            Y_Matrix = [Count,0];
            First = 0;
        else
            X_Radius = [Count,0];
            Y_Radius = [Count,0];
            X_Matrix = [X_Matrix;X_Radius];
            Y_Matrix = [Y_Matrix;Y_Radius];
        end
    end
end
end
end

```

```

clear Terrain Latitude Longitude;

disp('Writing derivatives to file...');
dlmwrite('Longitude.txt', X_Matrix,');
dlmwrite('Latitude.txt', Y_Matrix,');
disp('done...');

for Count = 0:Increment:360-Increment
    Ref = round(Count/Increment + 1);
    if Count == 0
        if X_Matrix(Ref,2) > Y_Matrix(Ref,2)
            Curvature = X_Matrix(Ref,:);
        else
            Curvature = Y_Matrix(Ref,:);
        end
    elseif X_Matrix(Ref,2) > Y_Matrix(Ref,2)
        Curvature = [Curvature; X_Matrix(Ref,:)];
    else
        Curvature = [Curvature; Y_Matrix(Ref,:)];
    end
end

dlmwrite(Output_File, Curvature,');

```

### Surface\_Derivatives

```

function [UpDown,LeftRight] = SurfaceDerivatives(surface_matrix)

% [UpDown,LeftRight] = SurfaceDerivatives(surface_matrix)
%
% Finds approximations to the first, second, and third directional derivatives
% for a normalized-dimension matrix. That is, all horizontal distances between
% adjacent columns and rows are set to 1.0 for the calculations.
% input:      surface - 2D matrix of floating point values
% output:     UpDown - 3D matrix of derivatives going from row 1 toward row M
%             LeftRight - 3D matrix of derivatives going from row 1 toward row N
% Output matrices are of dimension MxNx3 for an input matrix of size MxN.
% Elements [(:,1)] are the first derivatives (B), [(:,2)] are the second (C),
% and [(:,3)] are the third (D). The initial surface matrix values correspond
% to A in the standard cubic spline equation:
%
% 
$$S_n(x) = A_n + B_n(X-X_n) + C_n(X-X_n)^2 + D_n(X-X_n)^3$$

%
% written by Kelce Wilson, AFRL/SNAS, Oct 2000

[M,N]=size(surface_matrix);
UpDown=zeros(M,N,3);
LeftRight=zeros(M,N,3);
for I=1:M

```

```

    Sabcd=splcoefs(surface_matrix(I,:),1:N);
    LeftRight(I,1)=Sabcd(2,:);
    LeftRight(I,2)=Sabcd(3,:);
    LeftRight(I,3)=Sabcd(4,:);
end
for J=1:N
    Sabcd=splcoefs((surface_matrix(:,J))',1:M);
    UpDown(:,J,1)=Sabcd(2,:);
    UpDown(:,J,2)=Sabcd(3,:);
    UpDown(:,J,3)=Sabcd(4,:);
end
return

function [Sabcd] = splcoefs(points,xi)
%
% [Sabcd] = splcoefs(points,xi)
%
% Finds coefficient vectors for cubic spline interpolation
%
%  $S_n(x) = a_n + b_n(x-x_n) + c_n(x-x_n)^2 + d_n(x-x_n)^3$ 
%
% Vectors are stored in the S matrix, a is Sabcd(1,:),
% b is Sabcd(2,:), ...
%
% Points is a vector containing points sampled at xi

n=length(points);
a=points;
b=zeros(size(a));
c=b;
d=b;
L=b;
u=b;
z=b;
x=xi;
h=x(2:n)-x(1:n-1);
for I=2:n-1
    alph(I)=(3/h(I))*(a(I+1)-a(I))-(3/h(I-1))*(a(I)-a(I-1));
end
L(1)=0;
u(1)=0;
z(1)=0;
for I=2:n-1
    L(I)=2*(x(I+1)-x(I-1))-h(I-1)*u(I-1);
    u(I)=h(I)/L(I);
    z(I)=(alph(I)-h(I-1)*z(I-1))/L(I);
end
L(n)=1;
z(n)=0;
c(n)=0;
for I=n-1:-1:1
    c(I)=z(I)-u(I)*c(I+1);
    b(I)=(a(I+1)-a(I))/h(I)-h(I)*(c(I+1)+2*c(I))/3;

```

```

    d(I)=(c(I+1)-c(I))/(3*h(I));
end
Sabcd(1,:)=a;
Sabcd(2,:)=b(1:n-1) 0;
Sabcd(3,:)=c(1:n-1) 0;
Sabcd(4,:)=d(1:n-1) 0;
return

```

### Analyse\_Statistics

```
function [Best] = Analyse_Statistics(Input_File);
```

% Written by Squadron Leader Peter Pollock, Royal Australian Air Force, AFIT student, October 1999.

% The purpose of this routine is to analyse the in view data calculated in the routine Iridium\_In\_View.  
 % The output should be a meaningful interpretation of the effect of terrain diffraction on the availability  
 % of the communications system as a whole. The primary statistical parameters of interest are:  
 % a. The maximum outage time.  
 % b. The number of outages expected to equal or exceed 5 seconds in duration.  
 % c. The average number of satellites in view.  
 % d. The overall system availability.

% The results are stored in several forms

```

Matrix = dlmread(Input_File,');
[a,b] = size(Matrix);

```

```

SOAP_Average = sum(Matrix(:,2))/a;
Blocked_Average = sum(Matrix(:,3))/a;
Knife_Average = sum(Matrix(:,4))/a;
Rounded_Average = sum(Matrix(:,5))/a;
Average_No_In_View = [SOAP_Average,Blocked_Average,Knife_Average,Rounded_Average]
Outage_Matrix = [0,0,0,0];
Averages_Matrix = zeros(2,4);
Store = [0];
for Count_1 = 2:b
    Started = 0;
    Max_Duration = 0;
    Outage_Duration = 0;
    First = 1;
    for Count_2 = 1:a
        if Matrix(Count_2,Count_1) == 0
            if Started == 0
                Start_Time = Matrix(Count_2,1);
                Started = 1;
            end
        else
            if Started == 1

```



```

Stop_Time = Matrix(Count_2,1);
Outage_Duration = Stop_Time - Start_Time;
if Outage_Duration > Max_Duration
    Max_Duration = Outage_Duration;
    Outage_Matrix(Count_1-1) = Max_Duration;
end
if First == 1
    Store = [Outage_Duration];
    First = 0;
else
    Store = [Store;Outage_Duration];
end
Started = 0;
end
end
end
Averages_Matrix(1,Count_1-1) = length(Store);
Averages_Matrix(2,Count_1-1) = sum(Store)/length(Store);
end

```

```

SOAP_Availability = 100 * (172800 - Averages_Matrix(1,1)*Averages_Matrix(2,1)) / 172800;
Blocked_Availability = 100 * (172800 - Averages_Matrix(1,2)*Averages_Matrix(2,2)) / 172800;
Knife_Availability = 100 * (172800 - Averages_Matrix(1,3)*Averages_Matrix(2,3)) / 172800;
Rounded_Availability = 100 * (172800 - Averages_Matrix(1,4)*Averages_Matrix(2,4)) / 172800;

```

```

Maximum_Outage = Outage_Matrix
Average_Outages = Averages_Matrix
Availability_Matrix = [SOAP_Availability,Blocked_Availability,Knife_Availability,Rounded_Availability]

```

### **Plot\_Attenuation\_Data**

```

function Plot_Attenuation_Data;

Edges = 0:0.1:20;

load 'A_KE_G_Profile.csv'
KE = A_KE_G_Profile;
KE_Losses = histc(KE,Edges);
[a,b] = size(KE)
Min_KE = min(KE)
Max_KE = max(KE)
dlmwrite('C:\My Documents\Peter\AFIT\EENG799\Thesis\Analysis
Work\Terrain\KE_Attenuation.csv',KE_Losses,');

load 'A_R_G_Profile.csv'
Rounded = A_R_G_Profile;
Rounded_Losses = histc(Rounded,Edges);
[a,b] = size(Rounded)
Min_Rounded = min(Rounded)

```

```

Max_Rounded = max(Rounded)
dlmwrite('C:\My Documents\Peter\AFIT\EENG799\Thesis\Analysis
Work\Terrain\Rounded_Attenuation.csv',Rounded_Losses,',' );

```

### **Plot\_Curvature\_Data**

```

function Plot_Curvature_Data;

Edges = 0:10000:637800;

Curvature = dlmread('Curvature_File.csv',',' );
Terrain = histc(Curvature,Edges);
[a,b] = size(Terrain)
Min_Terrain = min(Terrain)
Max_Terrain = max(Terrain)
dlmwrite('C:\My Documents\Peter\AFIT\EENG799\Thesis\Analysis
Work\Terrain\Curvature_Profile.csv',Terrain,',' );

```

### **Plot\_Elevation\_Data**

```

function Plot_Elevation_Data;

Edges = 5:1:90;

P_I = dlmread('C:\My Documents\Peter\AFIT\EENG799\Thesis\Analysis Work\Iridium\Panama\P_Elevation
Samples',',' );
Iridium = histc(P_I,Edges);
Min_P_I = min(P_I)
Max_P_I = max(P_I)
K_I = dlmread('C:\My Documents\Peter\AFIT\EENG799\Thesis\Analysis Work\Iridium\Killeen\K_Elevation
Samples',',' );
Iridium = [Iridium;histc(K_I,Edges)];
Min_K_I = min(K_I)
Max_K_I = max(K_I)
A_I = dlmread('C:\My Documents\Peter\AFIT\EENG799\Thesis\Analysis Work\Iridium\Anchorage\A_Elevation
Samples',',' );
Iridium = [Iridium;histc(A_I,Edges)];
Min_A_I = min(A_I)
Max_A_I = max(A_I)
Iridium = reshape(Iridium,86,3);
[a,b] = size(Iridium)
dlmwrite('C:\My Documents\Peter\AFIT\EENG799\Thesis\Analysis Work\Iridium\I_Histogram.csv',Iridium,',' );

P_G = dlmread('C:\My Documents\Peter\AFIT\EENG799\Thesis\Analysis Work\Globalstar\Panama\P_Elevation
Samples',',' );

```

```

Globalstar = histc(P_G,Edges);
Min_P_G = min(P_G)
Max_P_G = max(P_G)
K_G = dlmread('C:\My Documents\Peter\AFIT\EENG799\Thesis\Analysis Work\Globalstar\Killeen\K_Elevation
Samples',' ');
Globalstar = [Globalstar;histc(K_G,Edges)];
Min_K_G = min(K_G)
Max_K_G = max(K_G)
A_G = dlmread('C:\My Documents\Peter\AFIT\EENG799\Thesis\Analysis
Work\Globalstar\Anchorage\A_Elevation Samples',' ');
Globalstar = [Globalstar;histc(A_G,Edges)];
Min_A_G = min(A_G)
Max_A_G = max(A_G)
[a,b] = size(Globalstar)
Globalstar = reshape(Globalstar,86,3);
[a,b] = size(Globalstar)
dlmwrite('C:\My Documents\Peter\AFIT\EENG799\Thesis\Analysis
Work\Globalstar\G_Histogram.csv',Globalstar,',');

P_O = dlmread('C:\My Documents\Peter\AFIT\EENG799\Thesis\Analysis Work\Orbcomm\Panama\P_Elevation
Samples',' ');
Orbcomm = histc(P_O,Edges);
Min_P_O = min(P_O)
Max_P_O = max(P_O)
K_O = dlmread('C:\My Documents\Peter\AFIT\EENG799\Thesis\Analysis Work\Orbcomm\Killeen\K_Elevation
Samples',' ');
Orbcomm = [Orbcomm;histc(K_O,Edges)];
Min_K_O = min(K_O)
Max_K_O = max(K_O)
A_O = dlmread('C:\My Documents\Peter\AFIT\EENG799\Thesis\Analysis
Work\Orbcomm\Anchorage\A_Elevation Samples',' ');
Orbcomm = [Orbcomm;histc(A_O,Edges)];
Min_A_O = min(A_O)
Max_A_O = max(A_O)
[a,b] = size(Orbcomm)
Orbcomm = reshape(Orbcomm,86,3);
[a,b] = size(Orbcomm)
dlmwrite('C:\My Documents\Peter\AFIT\EENG799\Thesis\Analysis
Work\Orbcomm\O_Histogram.csv',Orbcomm,',');

```

### **Terrain\_Plot**

```

function Terrain_Plot(Terrain_Matrix);
a=1:1:944;
b=1:1:1110;
contour(Terrain_Matrix)
%mesh(a,b,Terrain_Matrix)
title('Notional Terrain Contour Map')
xlabel('West To East Grid Squares')

```

```
ylabel('South To North Grid Squares')
xlabel('Terrain Height (m)')
grid
colormap(gray)
colorbar
%surface(a,b,Terrain_Matrix)
```

## BIBLIOGRAPHY

- [All89] J E Allnutt, *Satellite to Ground Radiowave Propagation*, Peter Peregrinus, 1989
- [Ass71] Assis, *A Simplified Solution to the Problem of Multiple Diffraction Over Rounded Obstacles*, IEEE Transactions on Propagation and Antennas, pp 292-295, March 1971
- [Ayr99] Ayers and Mendelson, *Calculus*, Schaum's Outline Series, 1999, pp 343
- [Cro99] Crowe, *Thesis – A Comparative Analysis of the Iridium and Globalstar Satellite Transmission Paths*, US Department of the Air Force, Air University, AFIT, March 1999
- [Dey66] Deygout, *Multiple Knife-Edge Diffraction of Microwaves*, IEEE Transactions on Propagation and Antennas, Vol AP-14, No 4, pp 480-489, July 1966
- [Flo87] Flock, *Propagation Effects on Satellite Systems at Frequencies Below 10 GHz*, NASA Reference Publication 1108(02), 1987
- [Glo01] Globalstar Federal Communications Commission Filings, 19-DSS-P-91 (48) and CSS-91-014, 15 September 1995
- [Gol92] Goldhirsh and Vogel, *Propagation Effects for Land Mobile Satellite Systems*, NASA Reference Publication 1274, 1992
- [Ipp86] Ippolito, *Radiowave Propagation in Satellite Communications*, Van Nostrand Reinhold, 1986
- [Jan97] Jang, *Thesis – Diffraction Analysis and Tactical Applications of Signal Propagation Over Rough Terrain*, US Department of the Air Force, Air University, AFIT, June 1997
- [Llo00] Lloyd, *The Big LEO Tables*,  
<http://www.ee.surrey.ac.uk/Personal/L.Wood/constellations/tables/index.html>
- [Nim01] National Imagery and Mapping Agency Home Page, <http://www.nima.mil>
- [Nor00] North American Aerospace Defense Command (NORAD) Home Page,  
<http://www.ee.surrey.ac.uk/Personal/L.Wood/constellations/tables/index.html>
- [Pol99] Polychronos, Hippenstiel and Ha, *Performance Analysis of Non-coherent BPSK Using First, Second and Third Order Selection Combining in a Nakagami Fading Channel*, MILCOM 1999 Vol 1 pp65-69

- [Pri93] Prichard, Suyderhoud and Nelson, *Satellite Communications Systems Engineering*, Prentice-Hall, 1993
- [Pro95] John Proakis, *Digital Communications*, Third Edition, McGraw-Hill, 1995
- [Rap96] Theodore Rappaport, *Wireless Communications Principles and Practice*, Prentice-Hall, 1996
- [Rod96] Dennis Roddy, *Satellite Communications*, McGraw-Hill, 1996
- [Tas94] Tascione, *Introduction to the Space Environment*, Orbit, 1994
- [Tir98] Tirkas, Wangsvick and Balanis, *IEEE Antennas and Propagation*, 1998, pp 991-5
- [Tow89] A A R Townsend, *Digital Line-of-sight Radio Links*, Prentice-Hall, 1988
- [Wer99] Wertz and Larson, *Space Mission Analysis and Design*, Third Edition, The Space Technology Library, 1999
- [Wil98] Wilson K.S., *Dissertation – Effects of Clutter Height Distribution on Adaptive Clutter Erasure Performance*, US Department of the Air Force, Air University, AFIT, June 1998

## **VITA**

Squadron Leader Peter Pollock was born in Sydney, Australia. He joined the Royal Australian Air Force as an Engineering Cadet in January 1984 and graduated from the Royal Melbourne Institute of Technology in the state of Victoria, Australia in 1987 with a Bachelor Degree in Communication Engineering. From 1988 to 1999 he occupied a series of positions relating to engineering development and management within the Australian air defense, tactical communication and strategic communication environments. In July 1999, he entered the Graduate School of Engineering at the Air Force Institute of Technology.

REPORT DOCUMENTATION PAGE				Form Approved OMB No. 074-0188	
<p>The public reporting burden for this collection of information is estimated to average 1 hour per response, including the time for reviewing instructions, searching existing data sources, gathering and maintaining the data needed, and completing and reviewing the collection of information. Send comments regarding this burden estimate or any other aspect of the collection of information, including suggestions for reducing this burden to Department of Defense, Washington Headquarters Services, Directorate for Information Operations and Reports (0704-0188), 1215 Jefferson Davis Highway, Suite 1204, Arlington, VA 22202-4302. Respondents should be aware that notwithstanding any other provision of law, no person shall be subject to a penalty for failing to comply with a collection of information if it does not display a currently valid OMB control number.</p> <p><b>PLEASE DO NOT RETURN YOUR FORM TO THE ABOVE ADDRESS.</b></p>					
1. REPORT DATE (DD-MM-YYYY) 21-02-2001		2. REPORT TYPE Master's Thesis		3. DATES COVERED (From - To) Jun 2000 - Feb 2001	
4. TITLE AND SUBTITLE  A Model to Predict Diffraction Attenuation Resulting From Signal Propagation Over Terrain in Low Earth Orbit Satellite Systems				5a. CONTRACT NUMBER	
				5b. GRANT NUMBER	
				5c. PROGRAM ELEMENT NUMBER	
6. AUTHOR(S)  Pollock, Peter R., Squadron Leader, Royal Australian Air Force				5d. PROJECT NUMBER	
				5e. TASK NUMBER	
				5f. WORK UNIT NUMBER	
7. PERFORMING ORGANIZATION NAMES(S) AND ADDRESS(S)  Air Force Institute of Technology Graduate School of Engineering and Management (AFIT/EN) 2950 P Street, Building 640 WPAFB OH 45433-7765				8. PERFORMING ORGANIZATION REPORT NUMBER  AFIT/GSO/ENG/01M-01	
9. SPONSORING/MONITORING AGENCY NAME(S) AND ADDRESS(ES)  N/A				10. SPONSOR/MONITOR'S ACRONYM(S)	
				11. SPONSOR/MONITOR'S REPORT NUMBER(S)	
12. DISTRIBUTION/AVAILABILITY STATEMENT  Approved For Public Release; Distribution Unlimited.					
13. SUPPLEMENTARY NOTES  N/A					
14. ABSTRACT  This study focused on multipath communication propagation impairments to the LEOSAT communications channel. Two terrain diffraction models, based on the geometric theory of diffraction (GTD), were developed and applied to the space-to-ground communications channel. These models were used to predict the impact of terrain on the performance of three LEOSAT communication systems with designs based on the Iridium, Globalstar and Orbcomm implementations. The study verified the feasibility of applying models based on the GTD rather than empirical or statistical models, to approximate the effect of propagating signals over terrain. Both models confirm that signal blockage and multipath propagation, due to terrain diffraction, can be significant considerations for designers and users of such systems.					
15. SUBJECT TERMS  Low earth Orbit, Satellite, Signal propagation, Terrain, Diffraction, Iridium, Globalstar, Orbcomm					
16. SECURITY CLASSIFICATION OF:			17. LIMITATION OF ABSTRACT  UU	18. NUMBER OF PAGES  128	19a. NAME OF RESPONSIBLE PERSON Major Richard A. Raines, ENG
a. REPORT  U	b. ABSTRACT  U	c. THIS PAGE  U			19b. TELEPHONE NUMBER (Include area code) (937) 255-3636, ext 4715